

**Springer Theses**

Recognizing Outstanding Ph.D. Research

Christopher Schirwitz

# Purification of Peptides in High- Complexity Arrays

A New Method for the Specific  
Surface Exchange and Purification  
of Entire Peptide Libraries

 Springer

# **Springer Theses**

Recognizing Outstanding Ph.D. Research

For further volumes:  
<http://www.springer.com/series/8790>

## **Aims and Scope**

The series “Springer Theses” brings together a selection of the very best Ph.D. theses from around the world and across the physical sciences. Nominated and endorsed by two recognized specialists, each published volume has been selected for its scientific excellence and the high impact of its contents for the pertinent field of research. For greater accessibility to non-specialists, the published versions include an extended introduction, as well as a foreword by the student’s supervisor explaining the special relevance of the work for the field. As a whole, the series will provide a valuable resource both for newcomers to the research fields described, and for other scientists seeking detailed background information on special questions. Finally, it provides an accredited documentation of the valuable contributions made by today’s younger generation of scientists.

### **Theses are accepted into the series by invited nomination only and must fulfill all of the following criteria**

- They must be written in good English.
- The topic should fall within the confines of Chemistry, Physics, Earth Sciences, Engineering and related interdisciplinary fields such as Materials, Nanoscience, Chemical Engineering, Complex Systems and Biophysics.
- The work reported in the thesis must represent a significant scientific advance.
- If the thesis includes previously published material, permission to reproduce this must be gained from the respective copyright holder.
- They must have been examined and passed during the 12 months prior to nomination.
- Each thesis should include a foreword by the supervisor outlining the significance of its content.
- The theses should have a clearly defined structure including an introduction accessible to scientists not expert in that particular field.

Christopher Schirwitz

# Purification of Peptides in High-Complexity Arrays

A New Method for the Specific  
Surface Exchange and Purification  
of Entire Peptide Libraries

Doctoral Thesis accepted by  
the University of Heidelberg and the German Cancer  
Research Center (DKFZ), Germany

 Springer

*Author*

Dr. Christopher Schirwitz  
Functional Genome Analysis/  
Chip-based Peptide Libraries  
German Cancer Research Center  
Heidelberg  
Germany

*Supervisor*

Prof. (apl.) Dr. Reiner Dahint  
Applied Physical Chemistry  
University of Heidelberg  
Heidelberg  
Germany

ISSN 2190-5053

ISBN 978-3-319-00806-6

DOI 10.1007/978-3-319-00807-3

Springer Cham Heidelberg New York Dordrecht London

ISSN 2190-5061 (electronic)

ISBN 978-3-319-00807-3 (eBook)

Library of Congress Control Number: 2013942482

© Springer International Publishing Switzerland 2013

This work is subject to copyright. All rights are reserved by the Publisher, whether the whole or part of the material is concerned, specifically the rights of translation, reprinting, reuse of illustrations, recitation, broadcasting, reproduction on microfilms or in any other physical way, and transmission or information storage and retrieval, electronic adaptation, computer software, or by similar or dissimilar methodology now known or hereafter developed. Exempted from this legal reservation are brief excerpts in connection with reviews or scholarly analysis or material supplied specifically for the purpose of being entered and executed on a computer system, for exclusive use by the purchaser of the work. Duplication of this publication or parts thereof is permitted only under the provisions of the Copyright Law of the Publisher's location, in its current version, and permission for use must always be obtained from Springer. Permissions for use may be obtained through RightsLink at the Copyright Clearance Center. Violations are liable to prosecution under the respective Copyright Law. The use of general descriptive names, registered names, trademarks, service marks, etc. in this publication does not imply, even in the absence of a specific statement, that such names are exempt from the relevant protective laws and regulations and therefore free for general use.

While the advice and information in this book are believed to be true and accurate at the date of publication, neither the authors nor the editors nor the publisher can accept any legal responsibility for any errors or omissions that may be made. The publisher makes no warranty, express or implied, with respect to the material contained herein.

Printed on acid-free paper

Springer is part of Springer Science+Business Media ([www.springer.com](http://www.springer.com))

**Parts of this thesis have been published in:**

C. Schirwitz, F. F. Löffler, T. Felgenhauer, V. Stadler, A. Nesterov-Müller, R. Dahint, F. Breitling, and F. R. Bischoff, Purification of High-complexity Peptide Microarrays by Spatially Resolved Array Transfer to Gold-coated Membranes, *Advanced Materials* **2013**, 25, 1598–1602.

# Supervisor's Foreword

Compared to the human genome which is formed by approximately 25,000 genes, the human proteome with over a million functional proteins represents a much higher diversity. Although genetic research provides valuable information on the proteins which can be translated, a great task in the future will be the exploration of the entire protein interaction network. Understanding the set of protein interactions will greatly help to identify the mechanisms behind fatal diseases such as cancer, AIDS, or tuberculosis and, hopefully, provide new cures. Hence, micro arrays containing proteins or small protein fragments in the form of peptides have become of great interest in proteomic research. Using these microarrays, a large number of potential target molecules can be screened for interaction with a probe in a short time frame.

However, protein and peptide micro arrays are still lacking behind oligonucleotide arrays in terms of density, quality, and manufacturing costs. A new approach developed at the German Cancer Research Center (DKFZ) has solved the problems in synthesizing high-density peptide arrays. The current technology is capable of producing arrays with up to 40,000 different peptides per  $\text{cm}^2$  by means of a micro particle-based solid-phase peptide synthesis. Similar to Ronald Frank's Spot synthesis, the peptides are combinatorially synthesized directly on a solid support, whereby the exact location of each peptide is known.

However, the in situ synthesis bears a conceptual disadvantage: The quality of the peptides is dependent on the efficiency of the synthesis so that peptide fragments are present in the resulting array among the desired full length peptides. In peptide-protein interaction studies such peptide fragments can, for example, cause unwanted side reactions and display false binding events. In his Ph.D. thesis, Christopher Schirwitz presents an innovative approach to improve the quality of in situ synthesized high-complexity peptide micro arrays. The central achievement is a new method allowing for the fast one-step purification of entire arrays without loss of resolution or spatial information.

Meanwhile, effort is put into the development of label-free detection techniques to screen for interactions in such purified peptide arrays without the need of fluorescent labels. As current biosensors allow for the label-free readout of

binding events with high sensitivity and lateral resolution, substantial progress is expected towards the development of a fully integrated, easy-to-use detection system for in situ high-throughput screening of biomolecular interactions in high-density peptide arrays. Most likely, other interesting applications will follow.

Heidelberg, June 2013

Prof. Dr. Dahint Reiner



# Acknowledgments

I would like to thank PD Dr. F. Ralf Bischoff (DKFZ), Prof. (apl.) Dr. Reiner Dahint, and Prof. Michael Grunze (Applied Physical Chemistry, University of Heidelberg) for supervising and supporting my work as my *Thesis Advisory Committee* (TAC) in the *International Ph.D. Program* of the DKFZ. This thesis would not have been possible without funding and support by the DKFZ, the *Helmholtz International School for Cancer Research*, the *Max-Buchner* research foundation, the *Baden–Württemberg Stiftung*, and the federal state of Baden–Württemberg. I am obliged to my colleagues in the group *Chip-based Peptide Libraries* at the DKFZ, the spin-off company *PEPperPRINT GmbH*, and the “new” department of *Peptide Arrays and Antibody Libraries* at the *Karlsruhe Institute for Technology* (KIT), who brought the project into being and contributed to its success. Namely: PD Dr. Frank Breitling, PD Dr. F. Ralf Bischoff, Dr. Volker Stadler, PD Dr. Alexander Nesterov-Müller, Dr. Thomas Felgenhauer, Dr. Felix Löffler, Jürgen Kretschmer, Daniela Rambow, Klaus Leibe, Jochen Stortz, Michelle Leuenberger, Frieder Märkle, Sebastian Schillo, Jakob Striffler, Bastian Münster, Yun–Chien Cheng, Lothar Hahn and Fanny Liu. I would also like to thank our alumni, first and foremost Dr. Mario Beyer, Dr. Simon Fernandez, Dr. Kai König and Dr. Ines Block.

For the excellent collaboration and scientific support I am truly thankful to my group at the department of Applied Physical Chemistry, University of Heidelberg: Prof. (apl.) Dr. Reiner Dahint, Anna Grab, Franziska Schenk, Dr. Noha Waly, Dr. Andrea Seehuber, Hacı Osman Güvenç, and Mustafa Sayin. I would also like to show my gratitude to the groups of Prof. (apl.) Dr. Michael Zharnikov (in particular Dr. Nikolaus Meyerbröker for maintaining the *MAX 200*), Prof. Dr. Axel Rosenhahn and all other colleagues at the department of Applied Physical Chemistry under the direction of Prof. Dr. Michael Grunze for their support and valuable scientific discussions.

Furthermore, I am obliged to many of my colleagues at the DKFZ, particularly the groups of PD Dr. Stefan Wiemann (DKFZ) and Prof. Dr. Holger Sültmann, first and foremost Johanna Sonntag, Christian Schmidt, and Mark Laible. I would also like to thank the group of Prof. Dr. Joachim Spatz (University of Heidelberg), in particular Dr. Nadine Perschmann, Theresa Pohl, and Dr. Marcus Abel, for

technical and scientific support. I owe sincere and earnest thankfulness to our collaboration partners: PD Dr. Peter Findeisen and Dr. Diego Yepes (Institute for Clinical Chemistry, University of Mannheim). Moreover, it is a great pleasure to thank everyone who helped me write my dissertation successfully, first and foremost Hacı Osman Güvenc and Michelle Leuenberger.

I am truly indebted and thankful to my wife, my parents, my sister, my grand parents, and the rest of my family for inspiring and supporting me in every situation.

# Contents

<b>1</b>	<b>Introduction</b>	1
1.1	General Introduction	1
1.1.1	Proteins and Peptides	1
1.1.2	Peptide Arrays	2
1.1.3	Solid Phase Peptide Synthesis	3
1.1.4	Activation of Amino Acids	6
1.1.5	Protecting Groups	8
1.1.6	Combinatorial Synthesis	10
1.2	High-Density Peptide Arrays	11
1.2.1	Amino Acid Particles	11
1.2.2	Laser Printer	12
1.2.3	Chip-Based Synthesis	15
1.2.4	Peptide Synthesis with Micro Particles	15
1.2.5	Motivation: Purification of Peptide Arrays	17
	References	19
<b>2</b>	<b>Concept and State-of-the-Art</b>	23
2.1	Purification Concept	23
2.2	Synthesis Surfaces	23
2.2.1	Cleaning and Activation	25
2.2.2	Surface-Initiated ATRP	25
2.2.3	Cleavable Linkers	26
2.3	Introduction to Surface Analytical Techniques	28
2.3.1	UV/Vis Photospectrometry	28
2.3.2	Spectroscopic Ellipsometry	30
2.3.3	Scanning Electron Microscopy	33
2.3.4	X-ray Photoelectron Spectroscopy	35
	References	40
<b>3</b>	<b>Results and Discussion</b>	43
3.1	Surface Chemistry A: Synthesis Surfaces	43
3.1.1	Improved Cleaning and Activation	43
3.1.2	Silanization for siATRP	44

3.1.3	Improved siATRP for Synthesis Coatings . . . . .	46
3.1.4	SAMs for the Peptide Array Synthesis . . . . .	50
3.2	Cleavable Linkers . . . . .	60
3.2.1	Choice of Cleavable Linkers . . . . .	60
3.2.2	Coupling of Cleavable Linkers . . . . .	61
3.2.3	Cleavage Efficiency of the HBA Linker . . . . .	64
3.3	Surface Chemistry B: Receptor Surfaces . . . . .	76
3.3.1	Membranes as Receptor Surface . . . . .	76
3.3.2	Sputter Coating . . . . .	79
3.4	Peptide Transfer and Purification. . . . .	82
3.4.1	Synthesis of Model Peptide Arrays with the Laser Printer. . . . .	82
3.4.2	Setup in the Peptide Array Purification . . . . .	82
3.4.3	Specific Transfer of Model Peptides . . . . .	83
3.4.4	Specific Transfer of Model Peptides in High-Resolution. . . . .	89
3.4.5	Purification of in situ Synthesized Peptide Arrays . . . . .	93
3.5	Important Parameters in the Transfer . . . . .	96
3.5.1	Blocking Agents . . . . .	96
3.5.2	Gold Thickness and Fluorescent Labels . . . . .	99
	References . . . . .	101
<b>4</b>	<b>Conclusion</b> . . . . .	105
4.1	Conclusion . . . . .	105
4.2	Outlook . . . . .	106
<b>5</b>	<b>Materials and Methods</b> . . . . .	107
5.1	Devices and Measuring Parameters . . . . .	107
5.1.1	UV/Vis Spectrometry . . . . .	107
5.1.2	Ellipsometry . . . . .	107
5.1.3	Scanning Electron Microscopy . . . . .	108
5.1.4	X-ray Photoelectron Spectroscopy . . . . .	108
5.1.5	Sputter Coating . . . . .	109
5.1.6	Fluorescence Scans . . . . .	109
5.1.7	Spotting Robot . . . . .	110
5.1.8	Equipment for the Micro Chip-Based Synthesis . . . . .	110
5.2	Materials . . . . .	111
5.2.1	Chemicals and Solvents . . . . .	111
5.2.2	Micro Chips . . . . .	111
5.2.3	Amino Acid Micro Particles . . . . .	112
5.2.4	Pre-synthesized Peptides. . . . .	112
5.2.5	Buffers and Antibodies. . . . .	112

5.3	Methods . . . . .	113
5.3.1	Preparation of Synthesis Surfaces . . . . .	113
5.3.2	Coupling of Cleavable Linkers . . . . .	116
5.3.3	Coupling of SMCC and Spotting . . . . .	117
5.3.4	Cleavage of the HBA Linker . . . . .	117
5.3.5	Micro Particle-Based Peptide Synthesis . . . . .	118
5.3.6	Coupling of Peptides from Solution . . . . .	119
5.3.7	Peptide Array Transfer and Purification . . . . .	119
5.3.8	Blocking with EG <sub>7</sub> -SH and PEG-SH . . . . .	120
5.3.9	Blocking Before Immunostaining . . . . .	120
5.3.10	Immunostaining . . . . .	120
5.3.11	Staining with the Biotin/Streptavidin System . . . . .	120
	References . . . . .	121
	<b>Appendix: Abbreviations . . . . .</b>	<b>123</b>
	<b>Amino Acid Codes . . . . .</b>	<b>127</b>
	<b>Funding . . . . .</b>	<b>129</b>
	<b>Curriculum Vitae . . . . .</b>	<b>131</b>

# Chapter 1

## Introduction

### 1.1 General Introduction

#### 1.1.1 Proteins and Peptides

Besides polysaccharides, lipids, and nucleic acids, proteins are the major players in organisms. They are essential building blocks and take on structural, mechanical, and informational functions in virtually every cell of a living system. In general, proteins are formed of amino acids connected by amide (*peptide*) bonds. The term *protein* usually refers to polypeptides built of more than 50 amino acids, whereby the exact sequence of amino acids is called *primary structure*. Due to formation of internal hydrogen bonds, proteins show a typical spatial arrangement of their amino acid residues which is referred to as *secondary structure*. Regular forms of *secondary structure* are  $\beta$ -sheet and  $\alpha$ -helix. The spatial arrangement of the entire polypeptide chain which is dominated by alterations of the *secondary structure* as well as orientation of the side-chain residues of the amino acids is called *tertiary structure* or *protein folding*. The *tertiary structure* strongly depends on the conditions the protein is exposed to. For example, a protein with hydrophobic and hydrophilic domains tends to rearrange in aqueous media to minimize energetically unfavorable conformations. Polar side-chains will be exposed to the aqueous medium, whereas nonpolar residues will be gathered together in a hydrophobic core. The term *quaternary structure* describes the arrangement of structures formed by several “independent” protein subunits. *Quaternary structures* can, for example, be stabilized by hydrogen bonds or disulfide bridges between the protein subunits.

Non-covalent interaction of two or more proteins via electrostatic forces, VAN-DEER-WAALS forces and hydrogen bonds enables the dynamic and reversible processes necessary for life. Hence, protein–protein or protein–peptide interaction is essential for almost every biological function such as enzyme activity, signal transduction and cell mechanics. Studying the set of expressed proteins and their interaction in a defined compartment of an organism, which is referred to as *proteomics*, has become a major field of modern biology. Especially in cancer

research where many crucial interactions happen beyond the genetic level detailed understanding of processes in the human proteome would lead to immense progress. With an estimated number of 650,000 possible interactions just for the human proteome [1] and an even larger number of involved proteins, the demand for tools to study proteomics in high-throughput is apparent.

### 1.1.2 Peptide Arrays

Traditional molecular biology techniques provide valuable information, but they are often tedious and time-consuming: the more complex the investigated living system, the higher the demand for studies in a high-throughput format. In genomic research, this demand has led to the development of oligonucleotide micro arrays (or DNA arrays), which are, at present, routinely applied to screen thousands of molecules for specific interaction with a sample in parallel. Furthermore, oligonucleotide arrays are the most prominent example of how modern array technologies have helped to advance an entire sub-field of molecular biology. The arrays are synthesized by means of lithographic [2], electrolytic [3], or electrophoretic [4] techniques. Photolithographic methods are capable of producing highly ordered arrays with >250,000 oligonucleotides per  $\text{cm}^2$  [5]. Furthermore, randomly ordered bead arrays reach densities of >1 million features per  $\text{cm}^2$ —combined with nucleic acid decoding strategies they are applied in whole-genome genotyping [6–9].

However, in humans most of the crucial interaction beyond gene expression happens on the protein level. Compared to the genome, the human proteome reaches a much higher complexity of biological functions. To enable screening for interactions within a reasonable time and at reasonable cost, great research effort is put into the development of high-throughput approaches. However, compared to oligonucleotide arrays the assembly of synthetic proteins and peptides in the form of high-density arrays is considerably more challenging. In a human being, the genetic code specifies 20 different *proteinogenic* amino acids, whereas only 4 nucleotides are involved in DNA. This means the combinatorial diversity must be much higher for synthesizing protein arrays than for oligonucleotide arrays (see 1.1.6). Moreover, the length of functional proteins reaches from several hundred to thousands of amino acid residues which can each contribute to the molecule's three-dimensional structure and its function in the living system. Since the first protein array synthesis was demonstrated by MACBEATH and co-workers in 2000, conservation of the native folding and site-specific immobilization on a support have remained critical parameters [10, 11].

In contrast, synthesis and site-specific immobilization of peptides, which represent subunits of functional proteins rather than entire proteins, are more easily performed. Although peptide arrays cannot detect interactions which are supported by an extended region of a protein or a complex folding (i.e. *conformational binders*), there are plenty of applications in which peptide arrays help to improve

and accelerate research in proteomics. For instance, many protein interactions are mediated by *peptide recognition modules*: domains which incorporate peptides in their binding pockets such as the SH2, SH3, PH, EVH1, PDZ or WW domain [12]. Whenever a short amino acid sequence is essential for protein interaction, peptide arrays can be applied to explore the properties of the so-called *epitope*, e.g. to search for potential binders. Hence, peptide arrays play an important role in the characterization of antibodies (epitope mapping, serological tests), in the profiling of enzymes, in the screening for new protein biomarkers, and in the development of peptide-based drugs and vaccines.

This Ph.D. thesis dealt with the development of a purification method to improve the quality of peptide arrays. Particularly, the focus was placed on the purification of high-density arrays to pave the way for more efficient screenings and, thus, more challenging applications.

### 1.1.3 Solid Phase Peptide Synthesis

In the early 1960s Bruce MERRIFIELD revolutionized the field of peptide synthesis by inventing the solid phase technique [13–15]. Based on his solid phase peptide synthesis (SPPS) almost every peptide consisting of 30–40 amino acids can today be routinely assembled [16, 17]. Short proteins (>50 amino acids) are obtained by special protocols or chemical ligation of peptide segments [17]. Synthetic peptides are usually produced in so-called “peptide synthesizers”. Synthesizers are machines which automate the required coupling and washing cycles. They are loaded with a resin in the form of small polymer beads. These beads bear functional groups to which amino acids can be coupled from solution. The peptide chain is, thus, anchored on the surface of the beads and subsequently elongated with amino acids from solution. After the last amino acid has been added to the growing chain, a cleavable linker attached between bead surface and peptides allows for the cleavage of the crude product. Peptides are then purified by routine techniques such as gel filtration, affinity chromatography, and high-performance liquid chromatography (HPLC). Although this process seems simple, a profound strategy is necessary to avoid formation of false peptides. Amino acids usually bear more than one reactive site which is why Merrifield invented an ingenious protecting group strategy to exclusively synthesize one sequence of amino acids. His protecting group strategy is referred to as the “orthogonal principle” because the technique makes use of different types of protecting groups which are cleaved under different conditions. Figure 1.1 schematically shows the MERRIFIELD principle in SPPS: Starting from a functionalized polystyrene (PS) bead, an amino acid is activated at its carboxylic end. Its N-terminus is protected with a protecting group (PG, *red*) which is different from the PG (*yellow*) used for the side-chain residue (R). When the amino acid has been coupled to the PS bead (Fig. 1.1b), first all unreacted functional groups are capped to avoid formation of incorrect sequences. Then, only the N-terminal PG (*red*) is cleaved, whereas the side-chain



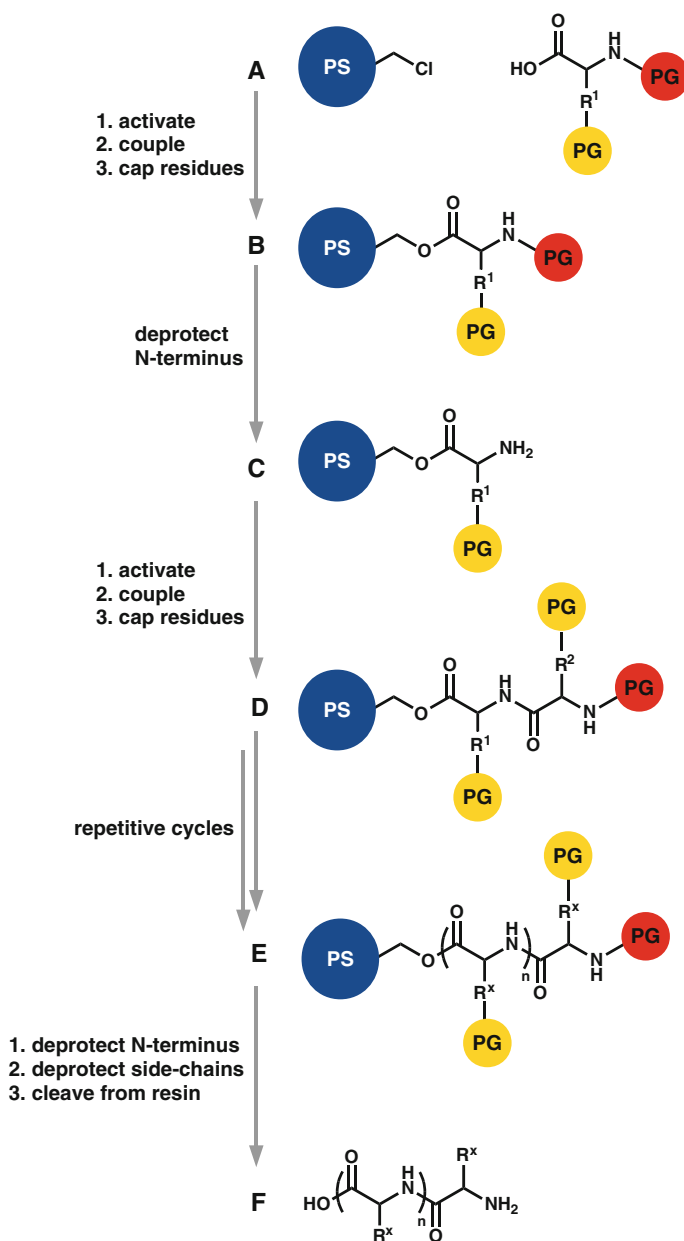


**Fig. 1.1** Schematic: Protecting group strategy in MERRIFIELD'S SPPS (washing steps are not shown)

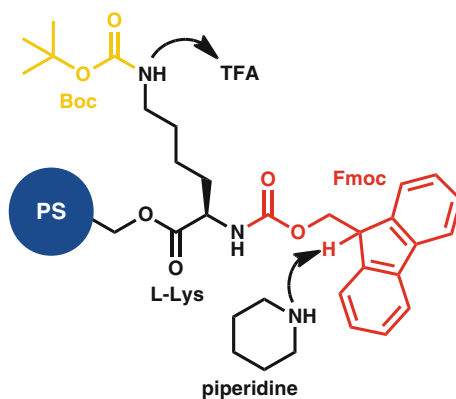
remains protected (Fig. 1.1c). The reaction is followed by another cycle to couple the next amino acid (Fig. 1.1d). The cycle is repeated until the desired peptide sequence is reached (Fig. 1.1e). After final deprotection of the N-terminal end, the side-chains are deprotected and the peptides are cleaved from the PS bead (Fig. 1.1f).

At present, mainly two orthogonal protecting group strategies are applied: The Boc/Bn (Boc = *tert*butoxycarbonyl, Bn = benzyl) strategy which is based on a gradual acid lability, and the Fmoc/*t*Bu (Fmoc = 9-fluorenylmethoxycarbonyl, *t*Bu = *tert*butyl) strategy which employs acid/base-labile protecting groups (see 1.1.5) [18, 19].

In both strategies, the peptide is synthesized from the C-terminal to N-terminal end with the C-terminus anchored to the solid support (e.g. the polymer beads). The Boc/Bn strategy is based on MERRIFIELD's first procedures on SPPS, whereby Boc is used to protect the amino end of the peptide and Bn protecting groups [20] are attached to the side-chains. The invention of the Fmoc protecting group by the CARPINO and HAN paved the way for another strategy, which is now a common way to produce synthetic peptides [21, 22].

Figure 1.2 schematically shows an orthogonal protected L-Lys linked to a PS bead. The N-terminal end can be deprotected with the comparatively mild base piperidine, whereas the side-chain protecting group Boc is only susceptible to acidic cleavage media such as trifluoroacetic acid (TFA). MERRIFIELD's principle of SPPS and his orthogonal protection group strategy were first considered to be inferior to synthesis in solution because intermediates cannot be isolated, but this opinion expeditiously changed once the merit of MERRIFIELD's invention was realized [23]. In conjunction with the invention of high performance liquid chromatography (HPLC) [24] by HORVÁTH and LIPSKI, which allows for both analytical and preparative purification of the crude product, SPPS soon became *the* method of producing peptides for multiple applications [23, 25, 26]. Today, not only peptides, but various molecules such as synthetic DNA or oligosaccharides are produced by solid phase techniques in industrial scale.

**Fig. 1.2 Schematic:** Orthogonal protecting group strategy in SPPS. Fmoc-L-Lys(Boc)-OH anchored to a PS bead: The Fmoc protecting group is labile to piperidine, whereas the Boc protecting group can be cleaved with trifluoroacetic acid (TFA)



### 1.1.4 Activation of Amino Acids

Along with the rapid progress in SPPS, new activation reagents and protecting groups have been developed to yield higher coupling efficiencies and to minimize side reactions. In general, the longer the desired peptides, the lower the expected total yield and the greater the likelihood of unwanted reactions. Therefore, SPPS usually requires an excess of the protected amino acid and a potent coupling reagent for each synthesis step. Today's routine couplings mostly involve benzotriazole- and carbodiimide-based reagents. However, a variety of "special" compounds exist, especially for difficult couplings. There are several detailed reviews summarizing the progress in activation strategies over the last years [18, 25, 27–31]. The following is a brief overview of important coupling reagents and protecting groups.

In a typical peptide coupling reaction in SPPS, the carboxylic acid moiety of the amino acid is activated using a coupling reagent. It is then reacted with the amino group of the amino acid immobilized on the solid support (see Fig. 1.1). The right choice of coupling reagent is the key to efficiently activating the carboxyl group without promoting enolate formation which results in the loss of important chiral information. Figure 1.3 shows a selection of common coupling reagents in peptide synthesis.

Acyl halides, acyl azides and mixed anhydrides (Fig. 1.3a–c) have a long history in classic peptide synthesis [29]. In general, acyl halides are most reactive but due to side reactions, e.g. loss of configuration or formation of hydrogen halides, they are not regularly applied. However, acyl fluorides are a useful tool in sterically challenging couplings [29] because they are more stable to moisture than chlorides or bromides and can easily be prepared with cyanuric fluoride [33]. Reagents also exist to form acyl fluorides in situ such as 1,1,3,3-tetramethylfluoroformamidinium hexafluorophosphate (TFFH), an air-stable non-hygroscopic salt [33, 34].

Another major group is the active esters (Fig. 1.3d, e): nitrophenyl, pentafluorophenyl (Opfp), and *N*-hydroxysuccinimide derivatives of amino acids are prepared in industrial scale because they can be stored in the form of crystalline powders. Opfp esters take on an important role in SPPS and, more importantly in the context of this work, in the production of amino acid micro particles (see 1.2.1).

To activate amino acids in situ, carbodiimides (Fig. 1.3g, h) such as *N,N'*-diisopropyl- (DIC) and *N,N'*-dicyclohexylcarbodiimide (DCC) are widely used. These reagents are comparatively cheap and show high reactivity in most applications. The drawbacks are their toxicity, incidental rearrangement from *O*-acylurea to *N*-acylurea, and rarely, racemization of the activated amino acid. However, side reactions can be suppressed by additives and the use of solvents of low dielectric constant [28, 29]. Using carbodiimides in combination with hydroxylamines such as 1-hydroxybenzotriazol (HOBt, Fig. 1.3i) and 1-hydroxy-7-aza-benzotriazol (HOAt, not shown) has proven to be an excellent activation strategy in SPPS. In addition, storable active esters are standardly produced with the aid of carbodiimides.

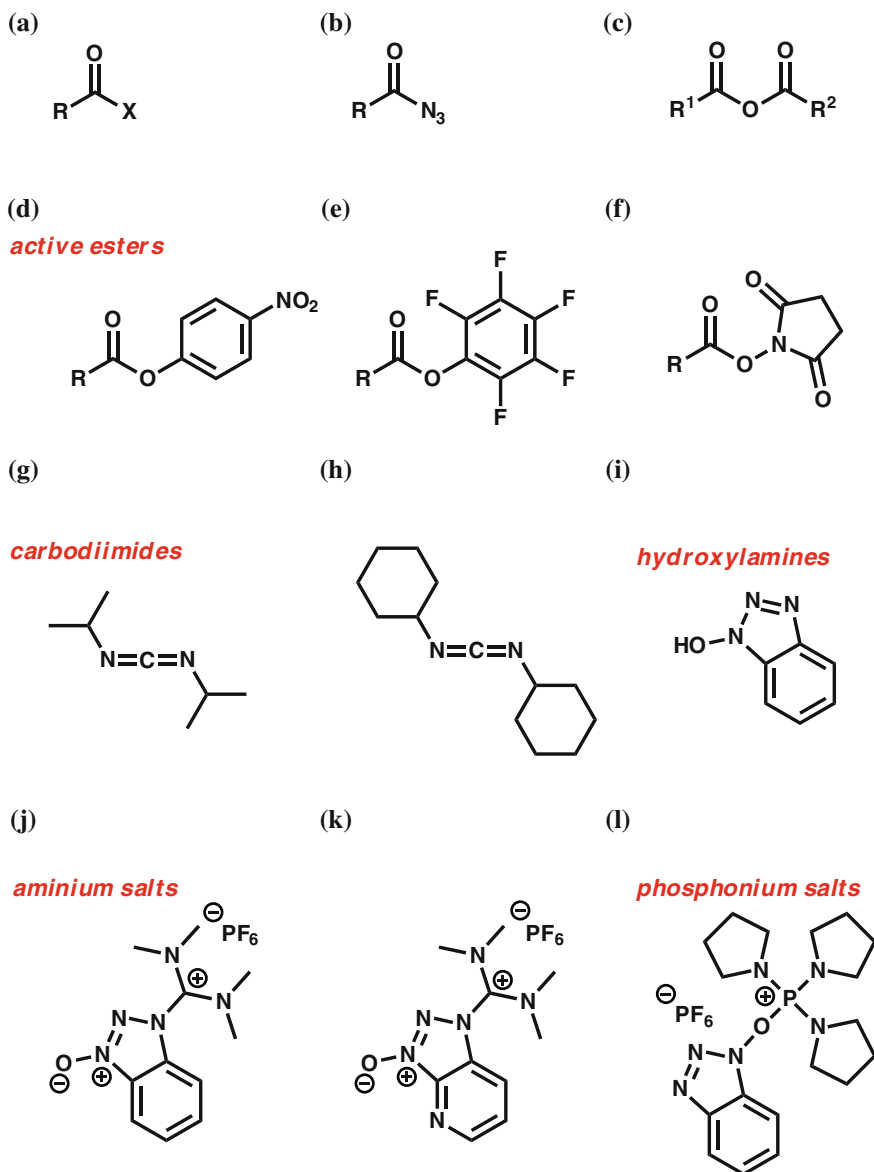


**Fig. 1.3** Common activation strategies in peptide synthesis. Selection of coupling reagents that are routinely applied in the activation of the carboxylic moiety (HBTU and HATU are depicted in the *guanidinium* form [32])

Aminium and the corresponding phosphonium salts are classes of expensive, but excellent coupling reagents. Compounds such as 2-(1H-benzotriazole-1-yl)-1,1,3,3-tetramethyluronium hexafluorophosphate (HBTU, Fig. 1.3j), 2-(7-Aza-1H-

benzotriazole-1-yl)-1,1,3,3-tetramethyluronium hexafluorophosphate (HATU, Fig. 1.3k), and benzotriazole-1-yl-oxy-tripyrrolidinophosphonium hexafluorophosphate (PyBOP, Fig. 1.3l) are useful for the activation of sterically hindered carboxylic components [28]. Although HBTU and HATU were historically named *uronium* salts, the reagents were recently reported to crystallize in the *guanidinium N-oxide* form [30, 32].

Furthermore, many variations of the discussed coupling reagents exist which differ slightly in terms of reactivity and designated use. For further details reference is made to the review articles [18, 25, 27–31].

### 1.1.5 Protecting Groups

In addition to sophisticated activation strategies, the choice of protecting groups plays an important role in today's SPPS. As mentioned above (see 1.1.3), a fundamental aspect of MERRIFIELD's procedure was the principle of orthogonality which he enhanced together with BARANY to yield protecting groups cleaved by completely different mechanisms [35, 36].

In general, orthogonality refers to a set of different classes of protecting groups which can each be selectively removed in the presence of the other classes. In SPPS two strategies have become state-of-the-art: The Boc/Bn strategy and the Fmoc/*t*Bu strategy. The Boc/Bn strategy typically works with a gradual acid lability of  $N^z$ -amino and side-chain protecting groups, whereas the Fmoc/*t*Bu strategy is also mechanistically orthogonal because it uses acid- and base-labile protecting groups. In our micro particle-based peptide array synthesis solely the Fmoc/*t*Bu strategy is applied. Hence, the following paragraph gives a brief overview of important protecting groups in the context of this work. For a more detailed approach to protecting groups in SPPS reference is made to the literature [19].

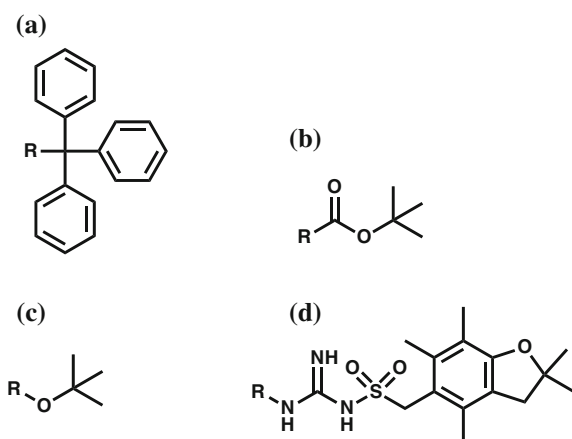
To avoid polymerization of activated amino acids,  $N^z$ -protection is mandatory. Furthermore, the choice of the  $N^z$ -protecting group determines the entire synthesis strategy, i.e. the side-chain protecting groups which may be used. Fmoc is typically removed under basic conditions using 20 % (v/v) piperidine in *N,N*-dimethylformamide (DMF) [37]. In contrast, acid-labile protecting groups are applied to the peptide side-chains which remain unaffected by alkaline treatment. Table 1.1 provides a list of the standard acid-labile protecting groups for  $N^z$ -Fmoc O<sub>2</sub>C-esters.

A big advantage of the Fmoc-strategy is obvious: Ala, Gly, Ile, Leu, Met, Phe, Pro, and Val do not require side-chain protection because their side-chain residues are not prone to undergo side-reactions. Asn, Cys, Gln, and His are commonly protected with a Trt group (Fig. 1.4a). In case of Cys a protecting group is mandatory because the free thiol is very susceptible to acylation, oxidation, or alkylation. Even with a protecting group, Cys is prone to  $\beta$ -elimination and formation of piperidyl alanine in the  $N^z$ -Fmoc strategy. Asn and Gln are more stable to side-reactions, but a Trt group helps to avoid possible dehydration in the presence of bases.

**Table 1.1** List of the standard side-chain protecting groups for Fmoc-protected and Opfp-activated amino acids (EDTA = ethylenediaminetetraacetic acid)

Amino acid derivative	Side-chain protecting group	Molecular weight (g.mol <sup>-1</sup> )	Recommended TFA concentration for cleavage [19]
Fmoc-Ala-Opfp	(none)	477.38	(none)
Fmoc-Arg-Opfp	Pbf	814.82	90 % (v/v), scavengers
Fmoc-Asn-Opfp	Trt	762.72	90 % (v/v), H <sub>2</sub> O, EDTA
Fmoc-Asp-Opfp	<i>Or</i> Bu	577.50	90 % (v/v)
Fmoc-Cys-Opfp	Trt	751.76	95 % (v/v), scavengers
Fmoc-Glu-Opfp	<i>Or</i> Bu	591.52	90 % (v/v)
Fmoc-Gln-Opfp	Trt	776.75	90 % (v/v), H <sub>2</sub> O, EDTA
Fmoc-Gly-Opfp	(none)	463.35	(none)
Fmoc-His-Opfp	Trt	785.77	95 % (v/v)
Fmoc-Ile-Opfp	(none)	519.46	(none)
Fmoc-Leu-Opfp	(none)	519.46	(none)
Fmoc-Lys-Opfp	Boc	634.59	25–50 % (v/v)
Fmoc-Met-Opfp	(none)	537.50	(none)
Fmoc-Phe-Opfp	(none)	553.48	(none)
Fmoc-Pro-Opfp	(none)	503.42	(none)
Fmoc-Ser-Opfp	<i>t</i> Bu	549.49	90 % (v/v)
Fmoc-Thr-Opfp	<i>t</i> Bu	563.51	90 % (v/v)
Fmoc-Trp-Opfp	Boc	692.63	95 % (v/v)
Fmoc-Tyr-Opfp	<i>t</i> Bu	625.58	35 % (v/v)
Fmoc-Val-Opfp	(none)	505.43	(none)

**Fig. 1.4** Standard acid-labile protecting groups in the N<sup>z</sup>-Fmoc strategy. **a** Trityl is applied to Asn, Cys, Gln, and His. **b** Lys and Trp are protected with Boc. **c** A *t*Bu is attached to the acidic amino acids Asp and Glu; the hydroxy groups of Ser, Thr, and Tyr are also protected with a *t*Bu moiety. **d** Arg requires a special protecting group: Pbf is applied to suppress deguanidination and  $\delta$ -lactam formation



A *t*Bu is attached to Asp and Glu (Fig. 1.4c) to prevent their side-chains from being activated in the course of the coupling reaction which would lead to branched peptides or intramolecular cyclization. Ser, Thr, and Tyr are protected likewise to avoid *O*-acylation or dehydration. In the case of Tyr, the acidity of the phenol ring, however, makes the alkyl protecting group less stable (see Table 1.1).

Lys and Trp are protected with a Boc moiety (Fig. 1.4b) to avoid acylation or formation of branched peptides. Arg requires a special protecting group: 2,2,4,6,7-Pentamethyl-2,3-dihydrobenzofuran-5-sulfonyl (Pbf, Fig. 1.4d) is used to avoid deguanidination and to minimize  $\delta$ -lactam formation. Pbf is currently the best protecting group for Arg, but  $\delta$ -lactam formation is still not completely suppressed. Moreover, in peptides with several Arg residues the high acid-stability of Pbf constrains the deprotection reaction.

Some deprotection reactions require additional scavengers which prevent the protecting group from rebinding to the amino acid side-chain. For example, *triisobutylsilane* (TIBS) or *triethylsilane* (TES) are commonly used as scavengers in peptide deprotection solutions.

### 1.1.6 Combinatorial Synthesis

Compared to oligonucleotide arrays, the combinatorial synthesis of peptide arrays is more difficult: Instead of only 4 monomers which are each based on the same phosphorylated saccharide, a minimum of 20 different proteinogenic amino acids bearing a variety of functional groups is required implying a much higher combinatorial diversity. In general, two approaches are used to produce peptide arrays: Either, the peptides can be synthesized by standard SPPS and then immobilized on a solid support in the desired array pattern or the peptides are combinatorially synthesized on the support. The former is tedious and cost-intensive while the latter requires high repetitive coupling efficiencies and a deliberate synthesis strategy.

The *in situ* synthesis of peptide arrays by lithographic methods [38, 39] as in oligonucleotide synthesis is not marketable due to expensive equipment, non-standard building blocks, labor-intensive protocols, and low synthesis efficiencies [40]. Therefore, peptide arrays are still lagging behind DNA arrays in terms of complexity and density. However, the first fully combinatorial approach by Ronald FRANK published in 1992 was a milestone in the development of the field. His SPOT synthesis is based on a spatially resolved spotting technique which uses the same principles as MERRIFIELD'S SPPS [41]. C-terminally pre-activated and N-terminally protected amino acids are applied to a pre-modified cellulose sheet in a distinct pattern. In the first run, the amino acids readily couple to functional groups embedded in the cellulose sheet. In the following steps the peptide sequences are elongated the same manner as in SPPS. Different amino acid solutions can be applied to any position of the array in the same run so that the peptide array is synthesized layer by layer instead of peptide by peptide [42, 43]. Orthogonal protection of the amino acids ensures that only the amino end is reacted with the next building block, while the side chains remain protected until the final deprotecting step. There are numerous publications on applications of peptide arrays synthesized by the SPOT technique [12, 44], but such peptide arrays are still costly and limited in density due to the following disadvantages: Using a solvent leads to

spreading and evaporation of the droplets on the solid support. Thus, commercial peptide arrays produced in situ by the SPOT synthesis only reach resolutions of 25 peptides per  $\text{cm}^2$  (with up to 15 amino acid residues) at a price of 7–14€ per peptide [44], which is quite inferior to the economic efficiency of DNA arrays.

## 1.2 High-Density Peptide Arrays

A new approach developed in our research group “Chip-based Peptide Libraries” has solved the problems in synthesizing high density peptide micro arrays by using solid amino acid toner particles. These micro particles can be addressed onto a solid support either using a custom-built laser printer [45] or a micro chip equipped with an array of pixel electrodes [46]. Peptide synthesis is initiated by melting the particle matrix and the resulting peptide quality is equivalent to standard synthesis from solution. Strictly following MERRIFIELD’s principle of orthogonal synthesis up to 280,000 individual peptides can be arrayed on a single solid support ( $22 \times 21 \text{ cm}^2$ , synthesis area  $19.1 \times 19.1 \text{ cm}^2$ ). Moreover, an areal density of up to 40,000 peptides per  $\text{cm}^2$  can be achieved via the micro chip approach [46]. The laser printer technology has already been commercialized in the company *PEP-perPRINT GmbH* (Heidelberg/Germany), offering customized high-density peptide arrays with 700–800 different peptides per  $\text{cm}^2$  (dependent on the size and layout of the array).

### 1.2.1 Amino Acid Particles

Amino acid micro particles have been the key invention towards the synthesis of highly resolved peptide arrays. The particles can be exactly addressed onto a solid support in high density, whereby adhesion forces between surface and particle make the particles “stick” at the target location. In contrast to the SPOT synthesis, which is limited in resolution due to evaporation and spreading of the solvent, the micro particle-based method allows for a spatial and temporal separation of deposition and coupling reaction.

The amino acid micro particles have been developed on the basis of one-component powder toners, a common class of toner particles in xerography. One-component toners consist of particles, around 5–10  $\mu\text{m}$  in size, which are comprised of approximately 90 % (m/m) of a resin (e.g. polystyrene-*n*-butylacrylate copolymers, polyester- or epoxy resins), 5 % (m/m) (in)organic pigments, 3 % (m/m) charge control agents (CCAs, e.g. azo complexes), and the remaining portion of additional additives [47, 48]. The resin is important for the chargeability: Dependent on its position in the “triboelectric series”, a polymer can be negatively or positively charged by friction [49]. Charge control agents are added to stabilize these triboelectric charges which are applied to the particles in the



printing process (see 1.2.2 and 1.2.3) [50]. Although they account for only 5 % of the particle mass, additives such as pigments can have a big impact on the position in the triboelectric series [51]. Therefore, every toner has not only to be optimized in terms of color, but also in terms of electric charge properties.

Whereas pigments are the most important additive in standard toners, the most important “additive” in the micro particles used for peptide synthesis is the amino acid. The different amino acid toners used in the peptide array production mainly consist of a commercial styrene acrylic copolymer (e.g. SLEC PLT 7552, *Sekisui Chemical GmbH*, Düsseldorf/Germany), containing approximately 10 % (m/m) of an Fmoc-protected and Opfp-activated amino acid (see 1.1.4) [45]. Dependent on the type of amino acid comprised and the particle diameter, the micro particles show different charge to mass ratios (q/m-values) which have to be measured and optimized by adapting the particle composition to fit the requirements of combinatorial synthesis (see 1.1.6 and 1.2.4) [52–54]. Other additives are CCAs (e.g. Fe<sub>3</sub> + or Al<sub>3</sub> + naphthol complexes) and small amounts of a pigment (e.g. pyrazolone orange, *ABCR GmbH*, Karlsruhe/Germany) to stabilize the triboelectrical charge and make the particles easy to detect. To reduce agglomeration, the micro particles are coated with *Aerosil* silica nano particles (e.g. *Aerosil 812*, hydrophobic, *Evonik Degussa GmbH*, Essen/Germany). Most importantly, the resin used in the particle production has to be meltable at temperatures around 90 °C to give a highly viscous, but fluid reaction sphere. Currently, toner particles for all 20 proteinogenic amino acids are routinely used in the peptide array production. The amino acids embedded in the particles show low decay rates of less than 1 % per month (except arginine with 5 % per month) and coupling efficiencies similar to standard SPPS from solution [45, 46]. Furthermore, no racemization from L- to D-configuration is observed even if the amino acid toners are heated to 90 °C for 90 min.

The main focus in particle production lies on the size distribution of the micro particles. Because standard toner production techniques such as dispersing and extruding [47] are not feasible with labile amino acids, a new procedure has been developed. The components are mixed in solution and only briefly heated to give a homogenous matrix. The solvent is subsequently removed under reduced pressure. Throughout numerous milling and sieving steps the size distribution of the micro particle fraction is adapted to perfectly fit the designated use. As recently shown, the mean diameter influences the q/m-values and thus has a major impact on the quality of the deposition pattern (see 1.2.4) [55]. In general, the highest densities in a peptide array can only be achieved with particles smaller than the desired feature size.

## 1.2.2 Laser Printer

Similar to a standard color laser printer with 4 cartridges (CMYK: cyan, magenta, yellow, black) the prototype of the peptide laser printer was equipped with 20 cartridges, one for each of the 20 proteinogenic amino acids. The first laser printer

was constructed in 2003 on the basis of an *OKI C7400* (*OKI Systems GmbH*, Düsseldorf/Germany) color laser printer which was enhanced with a linear stage drive and 16 additional cartridges (Fig. 1.5). The cartridges had to be aligned “inline” which resulted in a device length of 3.2 m. As nearly all commercial laser printers, the *OKI C7400* is, in fact, an LED (light emitting diode) printer. The LED technique is superior to the laser technique because it is precise, compact, and works without movable parts or mirrors. However, the term “laser printer” today refers to both building classes. The most critical parameters in a printer with 20 cartridges are the positioning mechanism and the driving software which are mainly responsible for the maximum resolution of the device. The first prototype constructed in cooperation with the group “Rapid Product Development” at the *Fraunhofer Institute for Manufacturing Engineering and Automation* (IPA, Stuttgart/Germany) reached a resolution of 400 spots per  $\text{cm}^2$  which was already higher than the peptide density provided by means of the SPOT synthesis [45].

The second generation laser printer (Fig. 1.6) built for the company *PEPPER-PRINT GmbH* (Heidelberg/Germany) was constructed as a joint project involving IPA (see above), *KMS Automation GmbH* (Schramberg-Waldmössingen/Germany), the *Technical University of Varna* (Department of Physics, Varna/Bulgaria), and *Mikrosistemi* (Varna/Bulgaria). Compared to the first prototype, the second generation printer has been improved in several key aspects. To summarize, the cartridges were arranged to be movable in the z-direction so that only the currently “active” cartridge is in contact with the solid support. Moreover, the number of cartridges has been increased to 24 and each cartridge has been equipped with a separate motor. The driver software and the positioning mechanics were improved. An automated offtake for particle dust has been added to extract excessive particles which could cause contaminations. In addition, print job management and positioning processes have been automated based on barcodes and marks “written” in the synthesis glass slide with a laser. With the new features, the second laser printer already reaches a resolution of 700–800 spots per  $\text{cm}^2$ . The LED rows, in principle, should be capable of producing 1600 spots per  $\text{cm}^2$  after further improvement of the device.

The printing principle in both printers is the same: An organic photoconductor (OPC) drum is evenly charged by a primary charge roller (PCR, Fig. 1.7a). An LED row then “writes” the electrostatic printing pattern onto the OPC drum



**Fig. 1.5** Prototype of the peptide laser printer. **a** *OKI C7400* laser printer; **b** Peptide laser printer (closed); **c** Printing track without cartridges

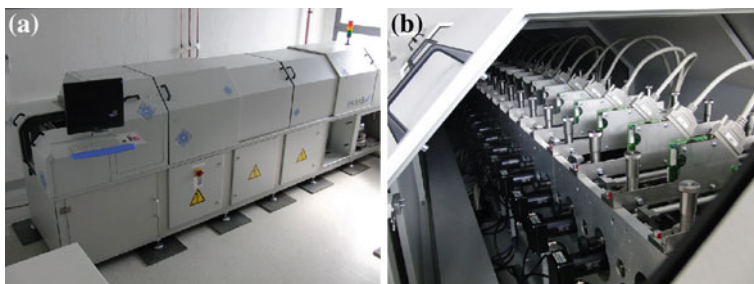


**Fig. 1.6** Second generation laser printer. **a** Closed printer with control center. **b** Printing track with 24 movable cartridges, each driven by a separate motor

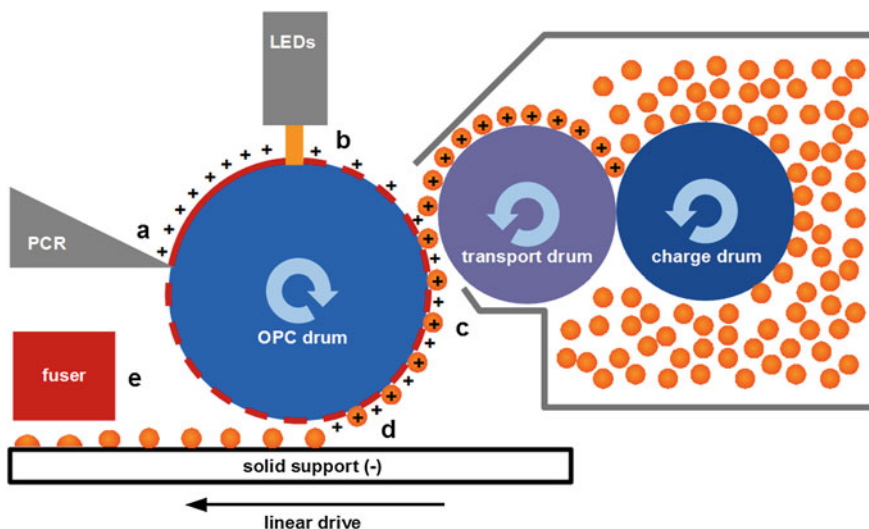


**Fig. 1.7** Schematic of a laser printer. **a** A primary charge roller (PCR) evenly charges an organic photoconductor (OPC) drum. **b** LED rows generate a charge pattern on the OPC drum by discharging upon illumination. **c** Particles with the same charge as present on the OPC (here negatively charged) are only transferred to illuminated/discharged areas. The charge pattern is translated into a particle pattern. **d** The particles are printed by rolling the OPC drum over a solid support. A counter voltage can be applied to the support to overcome adhesion forces. **e** A fuser melts the particles and secures the printing pattern

(Fig. 1.7b). The drum coating, which is insulating in the dark, becomes conductive upon light exposure: Illuminated areas on the drum are neutralized by grounding. Particles with the same charge as present on the OPC drum are selectively transferred to discharged areas (Fig. 1.7c). For this purpose particles are previously charged by friction and then transported from the reservoir to the OPC drum by two additional drums. The electrostatic pattern on the OPC drum is, thus, translated into the corresponding particle pattern. This pattern is subsequently

printed onto a solid support by rolling the OPC drum over the surface and applying a counter voltage to the support (Fig. 1.7d). Other setups involve oppositely charged particles and OPC drums. In this case, the pattern written by the LED rows is a negative of the printing pattern because particles are transferred to remaining charged areas on the drum. In terms of charges, setups with both negatively and positively charged particles are possible [47].

### ***1.2.3 Chip-Based Synthesis***

In parallel to the laser printer technique, a method to generate high-density peptide arrays on complementary metal oxide semiconductor (CMOS) chips has been developed [46, 56–60]. In general, amino acid micro particles are triboelectrically charged in custom-built aerosol chambers and, then, transported to the surface of a semiconductor chip. The chip surface is equipped with a defined grid of aluminum pixel electrodes which can be selectively energized. This way, potentials can be applied to specific pixels, whereas all other pixels remain switched off. By the generated electrical fields particles are attracted from the aerosol to the energized pixels and, thus, deposited in a defined pattern. Strong adhesion forces make the particles “stick” to the pixels even if the voltage is switched off after deposition [56].

Based on the data from simulations, the quality of the particle deposition has recently been enhanced by using a smaller fraction of amino acid micro particles (mean diameter: 2–3  $\mu\text{m}$ ) for the aerosol [55]. Furthermore, the setup of the aerosol generator has been simplified and supplemented by inserting a sieve to prevent large particle agglomerates from reaching the chip surface. Currently, an aerosol generator with 20 reservoir units is used to generate high-precision deposition patterns for all 20 types of amino acid toners (see Fig. 1.8).

### ***1.2.4 Peptide Synthesis with Micro Particles***

Laser printer and chip-based synthesis both make use of the same coupling principle: After a particle pattern has been addressed to the surface, the particles are melted at temperatures around 90 °C and allowed to couple for 60–90 min (Fig. 1.9a, b). The melting step gives highly viscous reaction spheres which are not larger than the corresponding particle cluster. An entire deposition pattern can thus contain any of the 20 different monomers because there is no danger of mixing of the reaction spheres. In these well-defined spheres, the coupling reaction between surface-bound amino groups and carboxyl-activated amino acids delivered from the particle takes place. After cooling to room temperature, unreacted amino acids and particle residues are washed away. Unreacted amino groups at the surface are subsequently “capped” by acylation with acetic anhydride ( $\text{Ac}_2\text{O}$ ) to avoid formation of wrong peptide sequences (Fig. 1.9c). Only after this step, the N-terminal

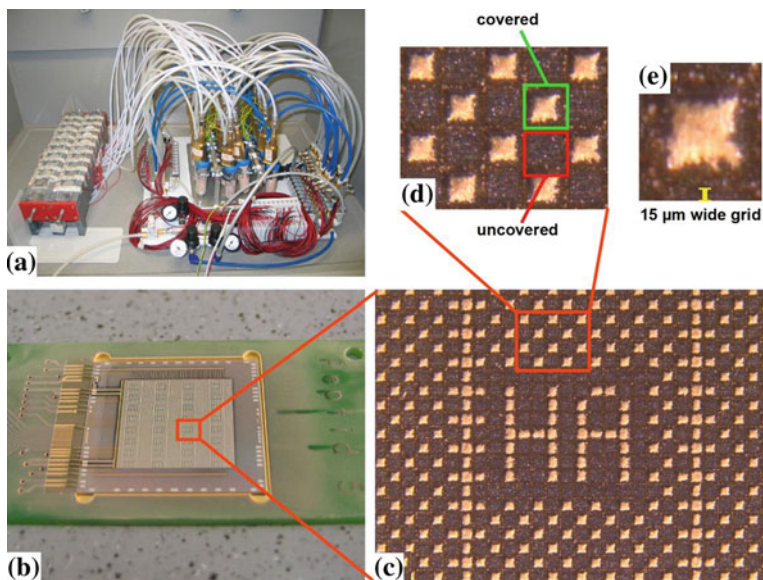


**Fig. 1.8** Aerosol generator and particle deposition on the micro chip. **a** Setup of the aerosol generator with 20 particle units. **b** Deposition pattern on a micro chip. **c** Magnification of the deposition pattern. Each pixel electrode has a dimension of  $84 \times 84 \mu\text{m}^2$ . **d** Particle covered (green) and uncovered (red) pixel electrodes. **e** A  $15 \mu\text{m}$  wide grid separates the pixels (yellow) [55]

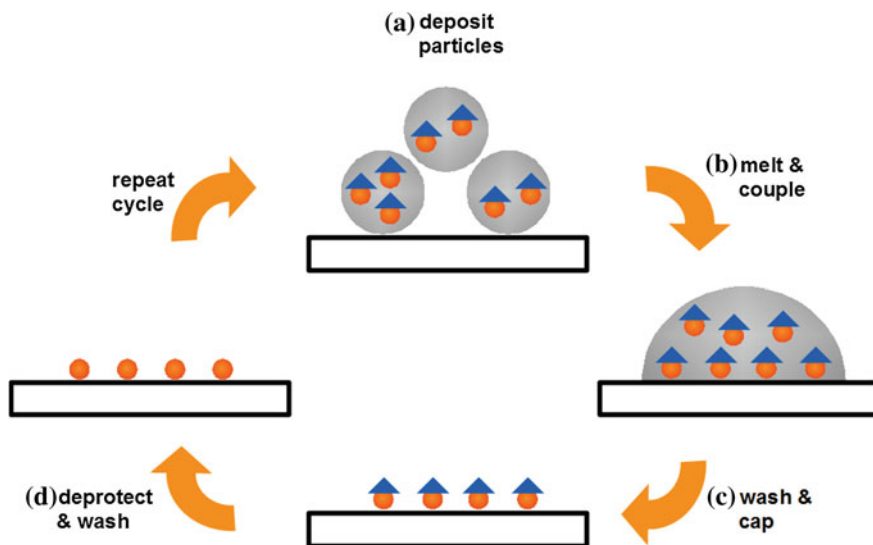


**Fig. 1.9** Coupling cycle in micro particle-based SPPS. **a** Clusters of micro particles are deposited on a desired spot or pixel electrode. **b** Melting gives well-defined reaction spheres in which the coupling reaction takes place. **c** Washing steps remove particle residues; unreacted amino groups on the surface are subsequently “capped” by acylation. **d** The amino group of the lastly coupled amino acid is deprotected before the coupling cycle starts over with a new deposition step

protecting group, e.g. Fmoc, is cleaved from the newly added amino acids (Fig. 1.9d) and the deposition and coupling cycle can start anew.

### 1.2.5 Motivation: Purification of Peptide Arrays

The amount of peptide synthesized at each position of the array strongly depends on the coupling efficiency and on the length of the peptide. As mentioned before, the repetitive yield of each coupling step determines the overall yield of peptide. The longer the peptides become, the more fragments are produced among the full-length peptides. For example, in the synthesis of a 20 meric peptide only 36 % full-length peptides can be expected if the repetitive coupling efficiency is 95 % (see Fig. 1.10).

Thanks to MERRIFIELD's protecting group strategy, the fragments can be efficiently capped by acylation with highly reactive  $\text{Ac}_2\text{O}$  in each coupling cycle. Capping avoids formation of peptides with incorrect amino acid sequences (see Fig. 1.11), but nevertheless, the acylated fragments diminish array quality and can lead to false-positive or false-negative results in subsequent assays.

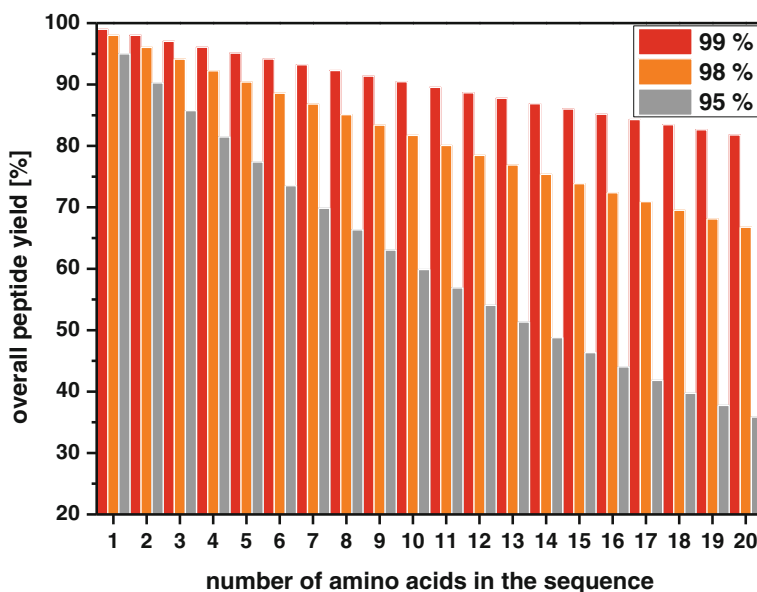
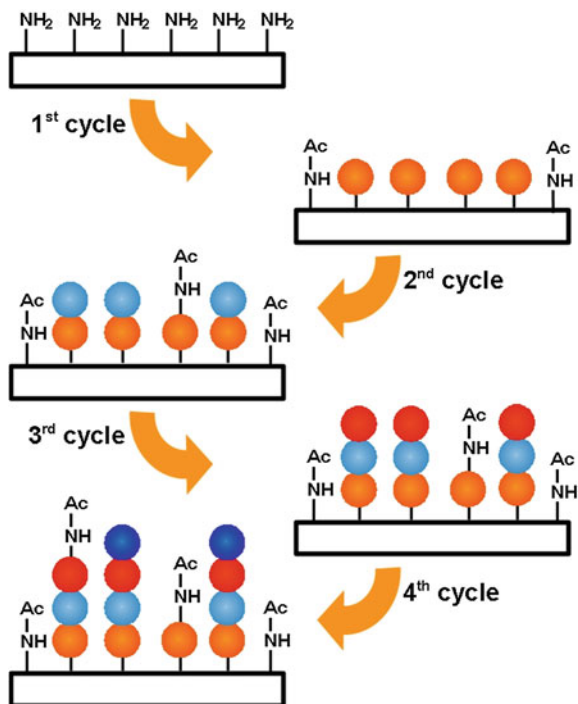


**Fig. 1.10** Peptide yield in SPPS dependent on the repetitive coupling efficiency. With a repetitive coupling efficiency of 99 % per amino acid, 82 % of full-length peptides can be expected synthesizing a 20 meric peptide. With a repetitive coupling efficiency of 98 % per amino acid, the total yield already decreases to 67 %. When only 95 % coupling efficiency per step is reached, the synthesis yields only 36 % of full-length peptides

**Fig. 1.11** Formation of fragments in the course of SPPS. Inefficient coupling produces peptide fragments. These fragments are routinely capped by acylation to avoid formation of peptides with incorrect amino acid sequences



In 2000, WENSCHUH et al. reported the synthesis efficiency of SPOT synthesis to be comparable to the efficiency of standard SPPS [61]. However, these results were obtained for 15 meric peptides synthesized with a resolution of maximum 15 spots per  $\text{cm}^2$  and it was noted that longer peptides resulted in a lower quality. Similar studies on peptides synthesized by the SPOT technique stated efficiencies ranging from below 40 % to more than 92 % which clearly indicates that the total yield per spot strongly depends on synthesis protocol as well as length and amino acid sequence of the respective peptides [62–65]. As a consequence, results obtained from in situ synthesized peptide arrays usually have to be further verified using HPLC purified peptides produced by standard SPPS. The only existing technique to purify peptide arrays produced by the SPOT synthesis is tedious and expensive: The peptides are synthesized on a cellulose sheet in large-scale spots and cleaved by dry aminolysis [66, 67]. The spots are subsequently stamped out and each product is externally purified by HPLC [12]. Thus, each spot yields a reservoir of purified peptide which can be re-spotted, e.g. on a modified glass slide, in higher resolution than originally achieved by the in situ SPOT synthesis. Additionally, also re-spotting of dissolved cellulose-peptide conjugates without previous aminolysis is a common technique to produce peptide micro arrays on glass supports [68].

In spite of the fact that the purified peptides may suffice for several array replicas, re-spotting is extremely cost-intensive and diminishes the benefits from

combinatorial synthesis. Moreover, external purification of the array members is not feasible for high-complexity peptide arrays as produced by the micro particle-based method (see 1.2.4). Hence, this work presents a new method allowing for the fast one-step purification of such high-resolution peptide arrays which is currently capable of purifying arrays with up to 10,000 peptides per cm<sup>2</sup>. An additional advantage of the method is the transfer to a new support which has not undergone a complete synthesis and, thus, has not been stressed by the numerous coupling and washing cycles.

## References

1. M.P.H. Stumpf, T. Thorne, E. De Silva, R. Stewart, J.A. Hyeong, M. Lappe, C. Wiuf, Proc. Natl. Acad. Sci. U.S.A. **105**, 6959–6964 (2008)
2. S.P.A. Fodor, J.L. Read, M.C. Pirrung, L. Stryer, A.T. Lu, D. Solas, Science **251**, 767–773 (1991)
3. R.D. Egeland, E. M. Southern, Nucleic Acids Res. **33**, (2005)
4. M.J. Heller, A.H. Forster, E. Tu, Electrophoresis **21**, 157–164 (2000)
5. E. Southern, K. Mir, M. Shchepinov, Nat. Genet. **21**, 5–9 (1999)
6. F.J. Steemers, J.A. Ferguson, D.R. Walt, Nat. Biotechnol. **18**, 91–94 (2000)
7. F.J. Steemers, K.L. Gunderson, Biotechnol. J. **2**, 41–49 (2007)
8. C.N. LaFratta, D.R. Walt, Chem. Rev. **108**, 614–637 (2008)
9. K.L. Gunderson, *Methods in Molecular Biology*, vol. 529, (Clifton, New Jersey, 2009), pp. 197–213
10. G. MacBeath, S.L. Schreiber, Science **289**, 1760–1763 (2000)
11. L. Berrade, A.E. Garcia, J.A. Camarero, Pharm. Res. **28**, 1480–1499 (2011)
12. R. Volkmer, ChemBioChem **10**, 1431–1442 (2009)
13. R.B. Merrifield, J. Am. Chem. Soc. **85**, 2149–2154 (1963)
14. R.B. Merrifield, Science **150**, 178–184 (1965)
15. R.B. Merrifield, J.M. Stewart, Nature **207**, 522–523 (1965)
16. F. Albericio, Curr. Opin. Chem. Biol. **8**, 211–221 (2004)
17. B.L. Nilsson, M.B. Soellner, R.T. Raines, Annu. Rev. Biophys. Biomol. Struct. **34**, 91–118 (2005)
18. K.-H. Altmann, M. Mutter, Chem. unserer Zeit **27**, 274–286 (1993)
19. A. Isidro-Llobet, M. Álvarez, F. Albericio, Chem. Rev. **109**, 2455–2504 (2009)
20. B.W. Erickson, R.B. Merrifield, J. Am. Chem. Soc. **95**, 3750–3756 (1973)
21. L.A. Carpino, G.Y. Han, J. Am. Chem. Soc. **92**, 5748–5749 (1970)
22. L.A. Carpino, G.Y. Han, J. Org. Chem. **37**, 3404–3409 (1972)
23. M. Verlander, Int. J. Pept. Res. Ther. **13**, 75–82 (2007)
24. C. Horvath, S.R. Lipsky, Anal. Chem. **41**, 1227–1234 (1969)
25. B.L. Bray, Nat. Rev. Drug Discovery **2**, 587–593 (2003)
26. A. Ganesan, Mini-Rev. Med. Chem. **6**, 3–10 (2006)
27. J.M. Humphrey, A.R. Chamberlin, Chem. Rev. **97**, 2243–2266 (1997)
28. O. Marder, F. Albericio, Chim. Oggi **21**, 35–40 (2003)
29. S.Y. Han, Y.A. Kim, Tetrahedron **60**, 2447–2467 (2004)
30. T.I. Al-Warhi, H.M.A. Al-Hazimi, A. El-Faham, Recent development in peptide coupling reagents. J. Saudi Chem. Soc. **16**(2), 97–116 (2012)
31. F. Albericio, R. Chinchilla, D.J. Dodsworth, C. Nájera, Org. Prep. Proced. Int. **33**, 203–303 (2001)



32. L.A. Carpino, H. Imazumi, A. El-Faham, F.J. Ferrer, C. Zhang, Y. Lee, B.M. Foxman, P. Henklein, C. Hanay, C. Mügge, H. Wenschuh, J. Klose, M. Beyermann, M. Bienert, *Angew. Chem. Int. Ed.* **41**, 441–445 (2002)
33. A. El-Faham, S.N. Khattab, *Synlett*, 886–904 (2009)
34. L.A. Carpino, A. El-Faham, *J. Am. Chem. Soc.* **117**, 5401–5402 (1995)
35. G. Barany, R.B. Merrifield, *J. Am. Chem. Soc.* **99**, 7363–7365 (1977)
36. G. Barany, F. Albericio, *J. Am. Chem. Soc.* **107**, 4936–4942 (1985)
37. E. Atherton, H. Fox, D. Harkiss, C.J. Logan, R.C. Sheppard, B.J. Williams, *J. Chem. Soc. Chem. Commun.* 537–539, (1978)
38. C.Y. Cho, E.J. Moran, S.R. Cherry, J.C. Stephans, S.P.A. Fodor, C.L. Adams, A. Sundaram, J.W. Jacobs, P.G. Schultz, *Science* **261**, 1303–1305 (1993)
39. J.P. Pellois, X. Zhou, O. Srivannavit, T. Zhou, E. Gulari, X. Gao, *Nat. Biotechnol.* **20**, 922–926 (2002)
40. X. Gao, J.P. Pellois, Y. Na, Y. Kim, E. Gulari, X. Zhou, *Mol. Diversity* **8**, 177–187 (2004)
41. R. Frank, *Tetrahedron* **48**, 9217–9232 (1992)
42. R. Frank, *J. Immunol. Methods* **267**, 13–26 (2002)
43. R. Frank, *Comb. Chem. High Throughput Screening* **5**, 429–440 (2002)
44. F. Breitling, A. Nesterov, V. Stadler, T. Felgenhauer, F.R. Bischoff, *Mol. BioSyst.* **5**, 224–234 (2009)
45. V. Stadler, T. Felgenhauer, M. Beyer, S. Fernandez, K. Leibe, S. Güttler, M. Gröning, K. König, G. Torralba, M. Hausmann, V. Lindenstruth, A. Nesterov, I. Block, R. Pipkorn, A. Poustka, F.R. Bischoff, F. Breitling, *Angew. Chem. Int. Ed.* **47**, 7132–7135 (2008)
46. M. Beyer, A. Nesterov, I. Block, K. König, T. Felgenhauer, S. Fernandez, K. Leibe, G. Torralba, M. Hausmann, U. Trunk, V. Lindenstruth, F.R. Bischoff, V. Stadler, F. Breitling, *Sci.* **318**, 1888 (2007)
47. H.-T. Macholdt, *Chem. unserer Zeit* **24**, 176–181 (1990)
48. Y. Hoshino, S. Kiatkamjornwong, *Part. Sci. Technol.* **25**, 147–162 (2007)
49. C.C. Ku, R. Liepins, *Electrical Properties of Polymers: Chemical Principles* (Hanser Publishers, Munich, 1987)
50. E. Michel, R. Baur, H.T. Macholdt, *J. Electrostat.* **51–52**, 91–96 (2001)
51. M.W. Williams, *J. Macromol. Sci. Part C: Polym. Rev.* **14**, 251–265 (1976)
52. A. Nesterov, F. Löffler, K. König, U. Trunk, K. Leibe, T. Felgenhauer, F. R. Bischoff, F. Breitling, V. Lindenstruth, V. Stadler, M. Hausmann, *J. Phys. D: Appl. Phys.* **40**, 6115–6120, (2007)
53. A. Nesterov, F. Löffler, K. König, U. Trunk, K. Leibe, T. Felgenhauer, V. Stadler, R. Bischoff, F. Breitling, V. Lindenstruth, M. Hausmann, *Rev. Sci. Instrum.* **78**, (2007)
54. A. Nesterov, F. Löffler, Y. C. Cheng, G. Torralba, K. König, M. Hausmann, V. Lindenstruth, V. Stadler, F. R. Bischoff, F. Breitling, *J. Phys. D: Appl. Phys.* **43**, 2010
55. F. Löffler, J. Wagner, K. König, F. Märkle, S. Fernandez, C. Schirwitz, G. Torralba, M. Hausmann, V. Lindenstruth, F.R. Bischoff, F. Breitling, A. Nesterov, *Aerosol Sci. Tech.* **45**, 65–74 (2011)
56. A. Nesterov, K. König, T. Felgenhauer, V. Lindenstruth, U. Trunk, S. Fernandez, M. Hausmann, F. Ralf Bischoff, F. Breitling, V. Stadler, *Rev. Sci. Instrum.* **79**, (2008)
57. M. Beyer, I. Block, K. König, A. Nesterov, S. Fernandez, T. Felgenhauer, C. Schirwitz, K. Leibe, R. F. Bischoff, F. Breitling, V. Stadler, *Methods in Molecular Biology*, vol. 570, (Clifton, New Jersey, 2009), pp. 309–316
58. C. Schirwitz, I. Block, K. König, A. Nesterov, S. Fernandez, T. Felgenhauer, K. Leibe, G. Torralba, M. Hausmann, V. Lindenstruth, V. Stadler, F. Breitling, F. R. Bischoff, *Curr. Protoc. Protein Sci.* 18.12.11–18.12.13 (2009)
59. K. König, I. Block, A. Nesterov, G. Torralba, S. Fernandez, T. Felgenhauer, K. Leibe, C. Schirwitz, F. Löffler, F. Painke, J. Wagner, U. Trunk, F.R. Bischoff, F. Breitling, V. Stadler, M. Hausmann, V. Lindenstruth, *Sens. Actuators, B: Chem.* **147**, 418–427 (2010)

60. A. Nesterov, E. Dörsam, Y. C. Cheng, C. Schirwitz, F. Märkle, F. Löffler, K. König, V. Stadler, R. Bischoff, F. Breitling, *Methods in Molecular Biology*, vol. 669, (Clifton, New Jersey, 2010), pp. 109–124
61. H. Wenschuh, R. Volkmer-Engert, M. Schmidt, M. Schulz, J. Schneider-Mergener, U. Reineke, *Biopolymer Peptide Sci. Sect.* **55**, 188–206 (2000)
62. F. Molina, D. Laune, C. Gougat, B. Pau, C. Granier, *Pept. Res.* **9**, 151–155 (1996)
63. A. Kramer, U. Reineke, L. Dong, B. Hoffmann, U. Hoffmüller, D. Winkler, R. Volkmer-Engert, J. Schneider-Mergener, *J. Pept. Res.* **54**, 319–327 (1999)
64. M. Takahashi, A. Ueno, H. Mihara, *Chem. A Eur. J.* **6**, 3196–3203 (2000)
65. B. Ay, M. Streitz, P. Boisguerin, A. Schlosser, C.C. Mahrenholz, S.D. Schuck, F. Kern, R. Volkmer, *Biopolymer Pept. Sci. Sect.* **88**, 64–75 (2007)
66. A.M. Bray, N.J. Maeji, A.G. Jhingran, R.M. Valerio, *Tetrahedron Lett.* **32**, 6163–6166 (1991)
67. A.M. Bray, R.M. Valerio, N.J. Maeji, *Tetrahedron Lett.* **34**, 4411–4414 (1993)
68. D.F. Winkler, K. Hilpert, O. Brandt, R. E. Hancock, *Methods in Molecular Biology*, vol. 570, (Clifton, New Jersey, 2009), pp. 157–174

# Chapter 2

## Concept and State-of-the-Art

### 2.1 Purification Concept

Purification of peptide arrays with a density of up to 10,000 different array members per  $\text{cm}^2$  requires a concept compatible with the given array format: Synthesis artefacts must be removed in situ, i.e. without the loss of spatial information provided by the synthesis. In addition, the peptides have to be purified simultaneously because external purification of each array member would diminish the benefits gained from combinatorial synthesis and is not feasible for highly resolved arrays. Hence, a concept consisting of three basic elements has been developed: (1) The peptide arrays are synthesized as usual, but a cleavable linker is inserted between surface coating and peptide; (2) After the synthesis, only the full length peptides are elongated with an additional “key” sequence; (3) The entire peptide array is cleaved and transferred to a second solid support, brought into direct contact with the synthesis support. Only full-length peptides rebind via their “key” sequence which has been designed specifically to bind to the surface of the new solid support. This transfer step must be achieved in the highest possible resolution and, most importantly, without mixing of individual spots, i.e. without lateral diffusion (Fig. 2.1).

In the following paragraph, state-of-the-art technologies for the preparation of synthesis surfaces are described. Furthermore, a brief introduction is given to peptide linker chemistry and surface sensitive analysis techniques applied in this work.

### 2.2 Synthesis Surfaces

Similar to SPPS using modified polymeric beads, peptide array synthesis on a “two-dimensional” surface requires functional groups. These functional groups must be firmly anchored to the support to preserve spatial resolution of the array throughout the entire synthesis process. Furthermore, the surface coating must be inert to a variety of different substances including harsh reagents such as organic

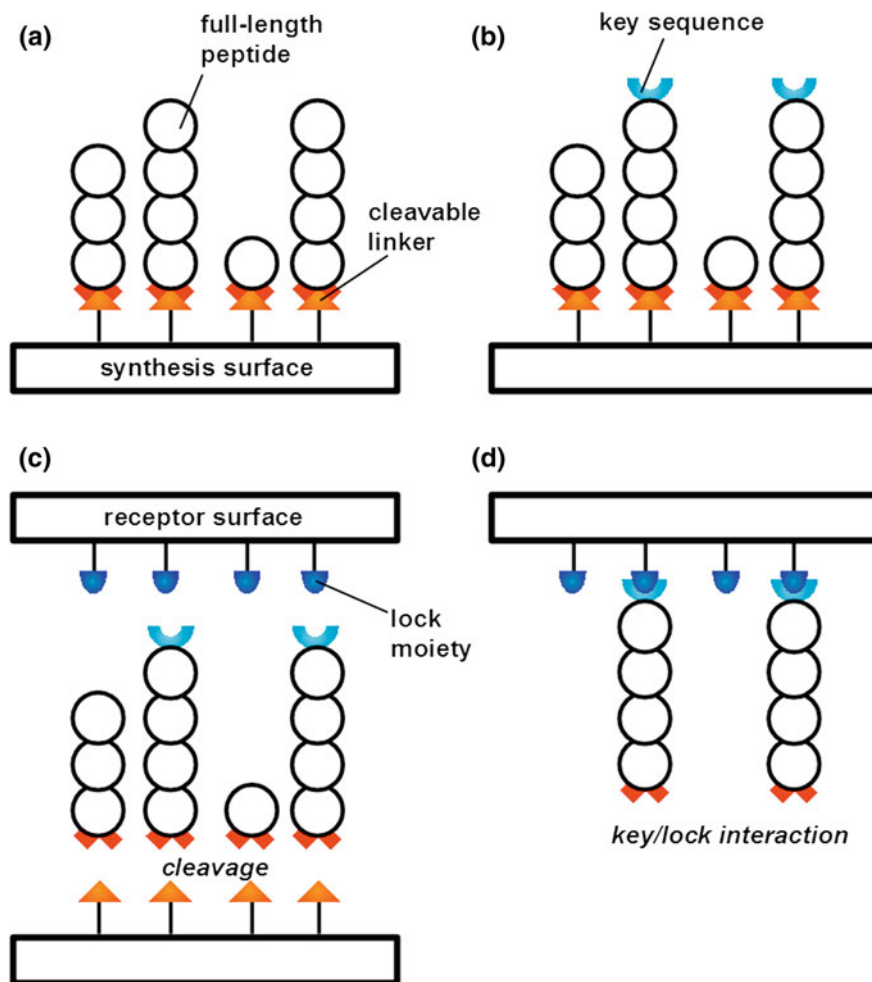


**Fig. 2.1** Concept for peptide array purification: **a** The peptide array is synthesized on a surface which bears a cleavable linker. **b** Only full-length peptides obtain an exclusive key sequence in the last synthesis cycle. **c** The synthesis surface is brought into direct contact with a receptor surface while the cleavage is conducted. Peptides and fragments are released. **d** Only full-length peptides rebound to the receptor surface due to a specific “lock” molecule immobilized on the receptor side. Fragments are removed by washing

acids and bases. Standard microscopy slide glass ( $\text{SiO}_2$ ) is used for the micro particle-based peptide array synthesis in the laser printer approach [1]. In contrast, the CMOS micro chips are equipped with aluminum electrodes ( $\text{Al}/\text{Al}_2\text{O}_3$ , “Peptide Chip 5”) [2, 3]. Both types of surfaces are routinely coated with polymers on the basis of methacrylates whose side-chains can be functionalized with amino groups. For surface sensitive studies, we additionally use silicon wafers which are similarly treated. The following chapter provides an overview of

existing surface preparation techniques that have been applied and, in part, enhanced in this work.

### ***2.2.1 Cleaning and Activation***

Prior to surface functionalization, the surface has to be thoroughly cleaned in order to remove any organic or inorganic contamination. In addition, the upper passivating oxide layers must be “activated” to render them reactive. In this work, glass slides ( $\text{SiO}_2$ ), micro chips ( $\text{Al}/\text{Al}_2\text{O}_3$ ), and silicon wafers, slices of a silicon single crystal (100) with a thin silicon oxide layer, are applied as substrates for peptide synthesis. Driven by the progress in semiconductor research, cleaning techniques for silicon wafers have been investigated and enhanced since the early 1950s [4]. In general, wet chemical cleaning using hydrogen peroxide solutions is wide spread. In our group, the common cleaning and activation process for  $\text{SiO}_2$  surfaces (silicon wafers and glass slides) is based on treatment in hot piranha solution, a mixture of 30 % (v/v)  $\text{H}_2\text{O}_2$  (30 % (v/v) aqueous solution) and 70 % (v/v) concentrated  $\text{H}_2\text{SO}_4$  [5]. However, hot piranha solution is corrosive to metals and, therefore, inadequate to pretreat susceptible micro chips [6]. Instead, the micro chip surfaces are cleaned and activated by UV irradiation in air according to approved protocols [7]. In general, treatment with piranha solution or UV irradiation generates defined oxide layers bearing reactive hydroxy groups on  $\text{SiO}_2$  or  $\text{Al}_2\text{O}_3$  surfaces [6, 8]. Alkylchlorosilanes, alkylalkoxysilanes, and alkylaminosilanes are known to covalently bind to such “activated” surfaces forming self assembled monolayers (SAMs) [9, 10]. Hence, SAMs of organosilanes represent highly stable anchor groups for functional surface coatings as discussed in the following paragraph.

### ***2.2.2 Surface-Initiated ATRP***

The first surface coatings in the micro particle-based peptide array synthesis were films of poly(ethylene glycol) methacrylate (PEGMA) which were prepared by deposition of an olefin silane SAM, subsequent ozonization of the olefin, and radical graft polymerization with PEGMA ( $M_n = 360$  g/mol, *Sigma-Aldrich*, Steinheim/Germany) [5]. PEGMA is a commercial macromonomer with an average side-chain length, in this case, of 4 to 5 ethylene glycol (EG) units. In the course of a polymerization only the methacrylate backbone is polymerized whereas the side-chains remain unaffected. PEGMA films are characterized by a high density of functional groups (up to 40 nmol/cm<sup>2</sup> on a 100 nm thick film), intrinsic protein repelling properties, and good stability to chemical treatments as present in peptide synthesis [5]. The preparation of PEGMA films has been facilitated using the surface-initiated atom transfer radical polymerization (si-ATRP) technique developed by HUANG and WIRTH in 1997 [11]. Since this

development, siATRP has become a standard technique for graft polymer coatings [12, 13]. By means of siATRP even our susceptible micro chip surfaces can be coated with PEGMA films in full control of the resulting film thicknesses [7]. First, the surface is activated with piranha solution or by UV irradiation. Then, it is silanized with a SAM of 2-bromo-*N*-(3-triethoxysilyl propyl) isobutyramide (bromine silane (**1**), Fig. 2.2). The tertiary bromine of the silane is the starting point of a controlled radical polymerization, also referred to as *living polymerization*, which can be conducted with various transition metal catalysts/ligand systems [14, 15]. The advantages of the ATRP technique include fast rates of polymerization, narrow molecular weight distributions, high monomer conversion, and precise control of the polymer composition [16].

In our group, the catalyst is typically a Cu<sup>I</sup> salt with additional organic ligands such as 2,2'-bipyridine (bpy) or 1,1,4,7,7-pentamethyldiethylenetriamine (PMD-ETA) as first described by WANG and MATYJASZEWSKI in 1995 [17]. Further optimization of the brush polymer composition to meet the requirements of biological assays with peptide arrays led to the development of PEGMA-co-PMMA films [18]. These films consist of different mole fractions of PEGMA and polymethylmethacrylate (PMMA) which can be controlled via the monomer concentration in the polymerization solution. PEGMA and methylmethacrylate (MMA) are statistically inserted into the growing polymer chain. The more MMA used the fewer PEG side-chains appear in the film. This reduces the number of functional groups available for peptide synthesis (see Fig. 2.2), but on the other hand, provides better accessibility for proteins such as antibodies or enzymes [18]. If the hydrophilic PEG moieties are reduced, a higher contact angle and, thus, a more hydrophobic character of the surface is observed. However, nonspecific protein adsorption is efficiently suppressed even with a low mole fraction of PEGMA. In this work, a graft copolymer composition of 10 % (n/n) PEGMA and 90 % (n/n) PMMA (10:90-PEGMA-co-PMMA) was the standard surface coating for the peptide array synthesis because it has proven to be the best compromise between intrinsic protein repelling properties and compatibility to standard biological applications (i.e. reference immunostainings, see 5.3.10). Independent of the copolymer composition, the PEG-OH side-chains are further modified with Fmoc- $\beta$ -alanine to yield amino groups necessary for the peptide synthesis (see Fig. 2.2) [5, 7, 18].

### 2.2.3 Cleavable Linkers

Along with solid phase chemistry, numerous cleavable linkers, which facilitate the release of compounds from the solid support after the peptide synthesis, have been developed [19, 20]. During the synthesis, the linker determines the allowable chemistry because it has to fit into the protecting group strategy (see 1.1.3 and 1.1.4) and must not release compounds before the synthesis has been completed. Furthermore, the choice of the linker also depends on the type of compound synthesized: The cleaving conditions may not compromise the integrity of the

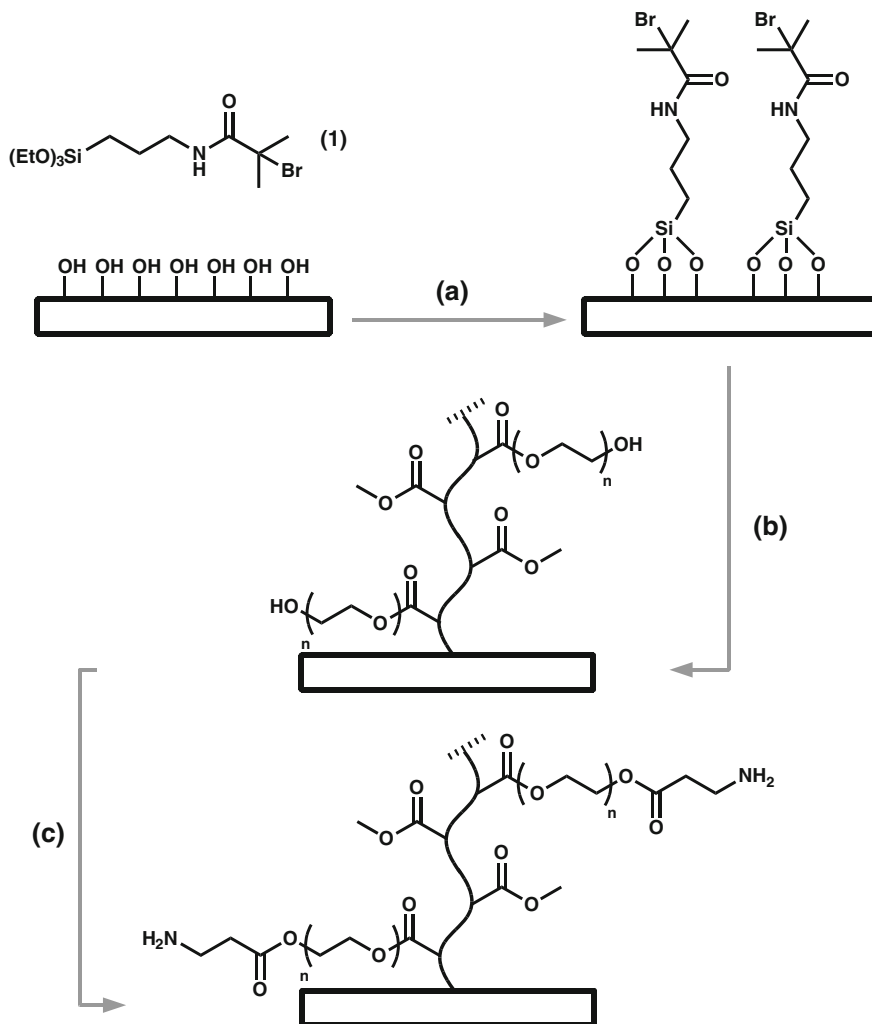


**Fig. 2.2** Silanization and siATRP: **a** An activated surface bearing hydroxyl groups is silanized with bromine silane (1); **b** The resulting silane SAM acts as an anchor group and surface-bound initiator for the siATRP with MMA and PEGMA. The polymethacrylate backbone polymerized in the siATRP is only depicted schematically. **c** Hydroxyl groups in the side-chain of PEGMA can be esterified with  $\beta$ -alanine to yield amino groups

product or the yield. In MERRIFIELD'S first approach peptides were cleaved from the resin by saponification or, in case of halogenated resins, by acid halide treatment [21]. In this initial approach, the linker can be considered part of the solid support, because the peptide is directly anchored to the resin by an ester bond. However, such *integral* linkers are disadvantageous in several respects: Exact control of the loading is difficult, comparatively harsh chemical conditions are needed to cleave

the product (e.g. HF), and steric and electronic properties of the resin can affect the cleavage reaction [19]. Thus, numerous linkers which allow for post-modification of the resin and for “mild” cleavage conditions are the current ideal. Established acid-labile compounds in SPPS are, for example, the WANG linker [22], the SAS-RIN (super acid sensitive resin) linker, [23, 24] the PAL (peptide amide linker) [25, 26], and the RINK type linkers [27] (Fig. 2.3a–d). Besides acid-labile linkers, many other linkers exist which can, for instance, be released by electrophilic, nucleophilic, oxidative, reductive, photo-induced, or metal-assisted cleavage [19, 20]. However, in the  $N^z$ -Fmoc strategy, weak acid-labile linkers are advantageous: They allow for side-chain deprotection and peptide cleavage in a single step and, thus, do not jeopardize peptide integrity. In general, slight modifications of the linker structure can have a strong impact on the cleavage efficiency and stability which is why many variations of the described linkers exist [19].

Besides acid-labile linkers, another important group is the “safety-catch” linkers. In general, safety-catch linkers are sensitive to nucleophiles, but cleavage requires at least two successive steps. First, the linker is destabilized. Then, the peptide can be released by nucleophilic attack under very mild conditions. Examples of safety-catch linkers are the carboxy FRANK linker (2-(1-*tert*butyloxycarbonyl-4-methyl-imidazol-5-yl)-2-hydroxy acetic acid dicyclohexylamine, Fig. 2.3f) which can be destabilized by TFA treatment and cleaved in aqueous buffer, [28, 29] or aryl hydrazine linkers (WIELAND linkers) such as Fmoc-hydrazinobenzoic acid (Fmoc-HBA, Fig. 2.3e), which can be cleaved by mild oxidation of the hydrazine bond and subsequent attack of a nucleophile [30, 31]. The choice of nucleophile determines the functional group formed at the C-terminal end of the peptides. For example, cleavage in (alkaline) aqueous solutions yields carboxylic acids whereas cleavage with amines yields amides. The ability to achieve desired functional groups at the C-terminus through prudent choice of nucleophile, allows for precise control over the functionality of the resulting peptide.

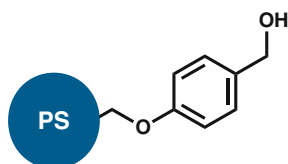
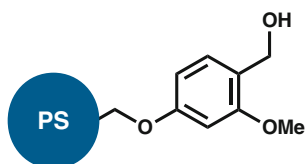
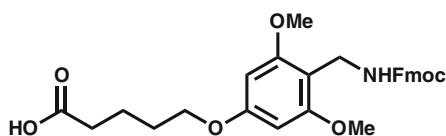
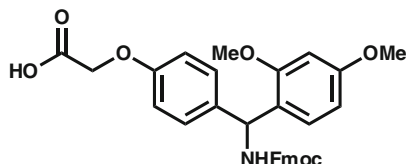
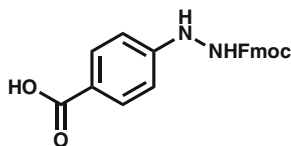
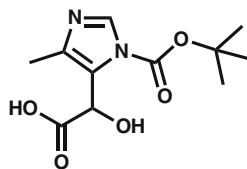
## 2.3 Introduction to Surface Analytical Techniques

### 2.3.1 UV/Vis Photospectrometry

In each coupling cycle of the  $N^z$ -Fmoc strategy of SPPS the N-terminal Fmoc protecting group is cleaved prior to attachment of the next amino acid in the sequence (see 1.1.3). An intermediate in the cleavage step is the piperidine dibenzofulvene adduct (PDFA) which has an absorption maximum at 301 nm (Fig. 2.4).

The concentration of PDFA in the deprotection solution can be measured using UV/Vis photospectrometry by comparing its absorption to that of a blank solution. Hence, the amino group loading on the surface, i.e. the derivatization grade (DG)  $\text{cm}^2$ , can be calculated from the concentration of PDFA in the deblocking solution.



**weak acid-labile linkers (ester type)****(a) WANG resin****(b) SASRIN****weak acid-labile linkers (amide type)****(c) PAL****(d) Fmoc-RAM linker****safety-catch linkers****(e) Fmoc-HBA linker****(f) Carboxy FRANK linker**

**Fig. 2.3** Examples of cleavable linkers in SPSS: **a, b** Standard resin-bound linkers that yield free acids upon cleavage. **c, d** Amide-type linkers yielding peptide amides. **e, f** Safety-catch linkers that can be destabilized and cleaved in aqueous media

According to LAMBERT–BEER's law, the DG of the surface is given by Eq. 2.1 [5, 32]. In our group, a basic calibration of the *SmartSpecs Plus* (Bio-Rad Laboratories, Munich/Germany) photospectrometer yielded a molar extinction coefficient of  $\varepsilon = 5129 \text{ L}\cdot\text{mol}^{-1}\cdot\text{cm}^{-1}$  for the deblocking solution, respectively [5, 33]. However, other groups reported different molar extinction coefficients [34] and fluctuating DG values which can most likely be attributed to the equilibrium of PDFA and dibenzofulvene/piperidine [35]. Therefore, this method is not considered to provide absolute quantities, but values which can be compared to results obtained in previous works in the same manner [33, 36].

$$DG = \frac{n}{A} = \frac{E \cdot V}{\varepsilon \cdot d \cdot A} \quad (2.1)$$

Equation 2.1: Derivatization grade (DG) of surfaces calculated upon Fmoc release.  $n$  = amount of substance in moles,  $A$  = surface area covered with

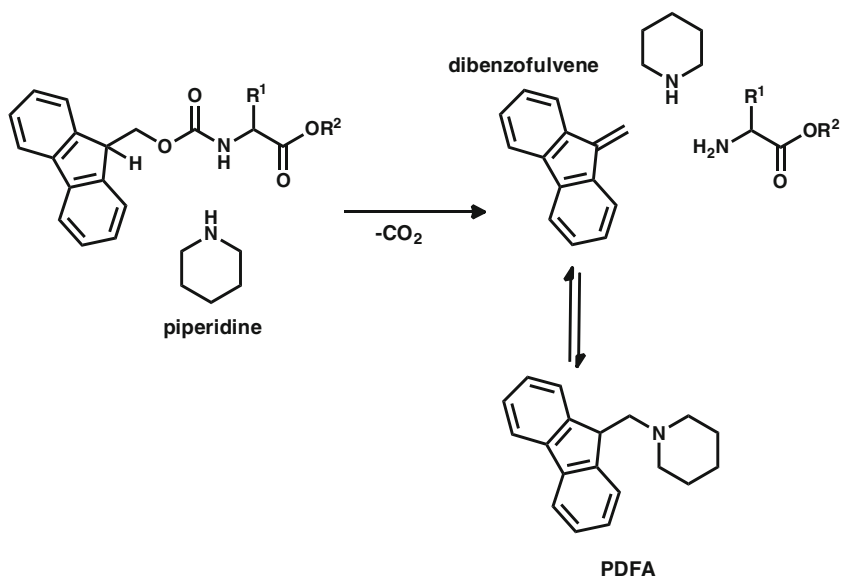


**Fig. 2.4** Fmoc cleavage and PDFFA formation: Deprotection of an Fmoc-protected amino group with 20 % piperidine in DMF yields dibenzofulvene and the free amino group. In presence of piperidine, dibenzofulvene forms the piperidine dibenzofulvene adduct (PDFFA) which has an absorption maximum at 301 nm

deprotection solution,  $E$  = extinction,  $V$  = applied volume of 20 % (v/v) piperidine in DMF,  $\varepsilon$  = extinction coefficient,  $d$  = path length of cuvette.

To determine the DG of irregularly shaped silicon wafer pieces, the surface area  $A$  was calculated from the weight of the wafer piece. For the Si(100) wafers used in this work a conversion factor of  $8.185 \text{ cm}^2 \cdot \text{g}^{-1}$  has been assigned.

### 2.3.2 Spectroscopic Ellipsometry

In spectroscopic ellipsometry information about film thicknesses, optical constants, surface roughness, and material micro structures in multilayered systems is gained by measuring the polarization state of light [37]. A collimated polarized light beam is reflected from (or transmitted through) the sample surface to a detector which analyzes changes in polarization caused by the material. Two major advantages of ellipsometry are the high sensitivity ranging from layers of single atoms to a few  $\mu\text{m}$ -thick films and the nondestructive measuring principle which also works under liquids [37, 38]. For maximum sensitivity, the angle of incidence and the wavelength of the incident beam are controlled. This procedure is referred to as variable angle spectroscopic ellipsometry (VASE).

In general, ellipsometry uses a beam of linearly polarized light whereby the  $s$ - and  $p$ -components of the beam are analyzed.  $s$  refers to the light vector component perpendicular to the plane of incidence and  $p$  refers to the component parallel to the plane of incidence. The beam is directed to a reflecting surface so that the  $s$  and  $p$  components of the electrical field vector  $\vec{E}$  are in phase with each other. Due to interaction with the material, the  $s$ - and  $p$ -components are phase-shifted. The  $s$  component is mostly reflected, whereas the  $p$  component is mostly refracted into the optically denser medium. This causes the projection of the electrical vector to trace out an ellipse in a plane perpendicular to the propagation direction of the beam. The azimuthal angle of the electric field vector along the major axis of the ellipse relative to a plane of reference, the ellipticity, and sometimes the handedness (right- or left-handed) of the electric vector are used to obtain information about the material [37]. Instead of absolute intensities, ellipsometry uses the ratio of reflected and incident light intensity  $R$  which simplifies the instrumentation. The ratio of reflected and incident intensity is described by the square value of the Fresnel reflection coefficient  $r$  as shown in Eq. 2.2.

$$\begin{aligned} R_s &= \frac{I_r^s}{I_0^s} = |r_s|^2 \\ R_p &= \frac{I_r^p}{I_0^p} = |r_p|^2 \end{aligned} \quad (2.2)$$

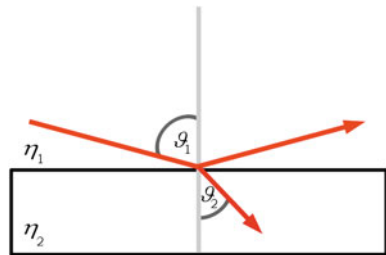
Equation 2.2: Ratio of reflected and incident light intensity  $R$ .  $I$  = intensity,  $r$  = Fresnel reflection coefficient (indices:  $r$  = reflected,  $0$  = incident,  $s$  =  $s$ -polarized,  $p$  =  $p$ -polarized).

Furthermore, the Fresnel reflection coefficient is linked to the components of the electric vector  $E$  and the refractive indices  $\eta$  as shown in Eq. 2.3 (Fig. 2.5).

$$\begin{aligned} r_s &= \frac{E_r^s}{E_0^s} = \frac{\eta_1 \cos(\vartheta_1) - \eta_2 \cos(\vartheta_2)}{\eta_1 \cos(\vartheta_1) + \eta_2 \cos(\vartheta_2)} \\ r_p &= \frac{E_r^p}{E_0^p} = \frac{\eta_2 \cos(\vartheta_1) - \eta_1 \cos(\vartheta_2)}{\eta_2 \cos(\vartheta_1) + \eta_1 \cos(\vartheta_2)} \end{aligned} \quad (2.3)$$

Equation 2.3: Fresnel reflection coefficients.  $r$  = Fresnel reflection coefficient,  $E$  = component of the electric field vector,  $\eta$  = refractive index,  $\vartheta$  = incident

**Fig. 2.5** Reflection and refraction of a beam of light at the interphase between two media



angle (indices:  $r$  = reflected,  $o$  = incident,  $s$  =  $s$ -polarized,  $p$  =  $p$ -polarized,  $l$  = medium A, 2 = medium B).

According to the Snell law the ratio of the sines of the incident angles is equivalent to the opposite ratio of the refractive indices (see Eq. 2.4).

$$\frac{\sin(\vartheta_1)}{\sin(\vartheta_2)} = \frac{\eta_2}{\eta_1} \quad (2.4)$$

Equation 2.4: SNELL law of refraction. The ratio of the sines of the incident angles is equivalent to the opposite ratio of the refractive indices.

In the fundamental equation of ellipsometry, the Fresnel coefficients are related to the amplitude factor,  $\Psi$ , and the phase factor,  $\Delta$  (see Eq. 2.5). Measurements of  $\Psi$  and  $\Delta$  are directly related to the material properties and can also be used to calculate the thickness of individual layers in multilayered systems.

$$\frac{r_p}{r_s} = \tan \Psi \cdot e^{i\Delta} \quad (2.5)$$

Equation 2.5: Fundamental equation of ellipsometry.  $\Psi$  = amplitude factor,  $i$  = imaginary unit,  $\Delta$  = phase factor.

### 2.3.2.1 Ellipsometry in Multilayered Systems

In real systems, multilayers and additional parameters such as surface roughness make an algebraic solution complicated. In multilayered systems, the reflected light is a superposition of all beams reflected from the different interphases (see Fig. 2.6). Therefore, a regression analysis is required to identify unknown parameters such as film thickness or optical constants.

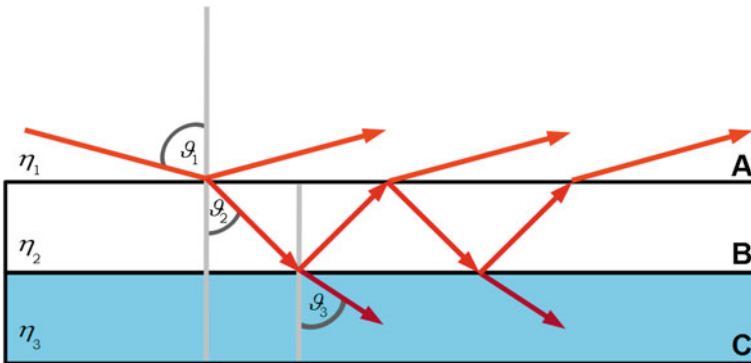


**Fig. 2.6** Reflection and refraction in a three layer system: The incident beam is reflected and refracted at the interphase between medium A and B. The refracted beam in medium B is again reflected and refracted at the interphase between medium B and C

In the present work, ellipsometry has been employed to determine the thickness of organic layers on solid supports. The FRESNEL coefficients for such three layer systems as depicted in Fig. 2.6 (medium A = air, medium B = organic layer, medium C = support) are given by Eq. 2.6.

$$r_s = \frac{r_s^{12} + r_s^{23} \cdot e^{-i2\varphi}}{1 + r_s^{12} + r_s^{23} \cdot e^{-i2\varphi}}$$

$$\text{with } \varphi = 2\pi \left( \frac{d}{\lambda} \right) \eta_2 \cos(\vartheta_2) \quad (2.6)$$

$$r_p = \frac{r_p^{12} + r_p^{23} \cdot e^{-i2\varphi}}{1 + r_p^{12} + r_p^{23} \cdot e^{-i2\varphi}}$$

Equation 2.6: FRESNEL reflection coefficients for a three layer system.  $d$  = thickness of layer B with the refractive index  $\eta_2$ ,  $\lambda$  = wavelength (indices: 1 = medium A, 2 = medium B, 3 = medium C).

According to Eq. 2.6 the thickness of medium B can be obtained by the phase shift of a wave which is reflected at the interphase of medium B and medium C compared to a wave which is reflected at the interphase of medium A and medium B.

To determine the film thicknesses of organic layers on a reflecting substrate, another parameter required is the refractive index of the organic layer. If the refractive indices of these materials are unknown, the CAUCHY model can be applied to parametrize the values (see Eq. 2.7) [39]. According to the CAUCHY model the refractive index of the material decreases with the square of the wavelength which is a good approximation as long as the material does not absorb light at the respective wavelength. To increase the accuracy, measurements are usually performed at multiple wavelengths.

$$\eta(\lambda) = \eta_0 + \frac{Y}{\lambda^2} \quad (2.7)$$

Equation 2.7: CAUCHY parametrization of the refractive index.  $Y$  = CAUCHY parameter.

For further information on the principles of ellipsometry, the setup of an ellipsometer, and applications thereof reference is made to the literature [37, 40].

### 2.3.3 Scanning Electron Microscopy

Scanning Electron Microscopy (SEM) uses a beam of electrons to raster over a surface. Compared to light microscopy, the use of electrons with energies of typically 1–40 keV enhances the maximum achievable resolution. According to the DE BROGLIE relation, the wavelength of such high energy electrons is smaller than the length of atomic bonds, which, in theory, should be sufficient to display

atoms. However, the electron beam has to be focused by a setup of electromagnetic fields which limits the maximum resolution [37]. Hence, the instrument provides the user with a 10x–300,000x magnified image of the target and can display structures and topographies in the nm range which is about 100 fold higher than visible light microscopy [41].

SEM uses interaction of the incoming electrons with surface atoms for imaging: Penetration of the electron beam results in an emission of photons or electrons from the sample which are collected and analyzed in different detectors. SEM works at reasonable costs and is a preferred starting tool for materials characterization.

There are mainly three types of images produced in an SEM: *Primary electron* images, *secondary electron* images, and *elemental X-ray maps*. In general, an electron entering a sample can undergo inelastic scattering with atomic electrons or elastic scattering with atomic nuclei of the material. High-energy electrons reaching the detector are referred to as *primary electrons*. In principle, they have been scattered elastically at the atomic nuclei of the sample without loss of kinetic energy. Therefore, a *primary electron* is also called *backscattered electron* (BSE). However, inelastic scattering with atomic electrons and, thus, a loss of energy can occur before an electron has travelled from source to detector. *Secondary electrons* (SEs) are generated when a *primary electron* hits an electron in the material and transfers enough energy to eject it. Since energy is needed to overcome the binding energy of the electron in the material *secondary electrons* are detected at lower energies than BSEs. In SEM, electrons with energies of less than 50 eV, by convention, are referred to as *secondary electrons* (SE). Most of the SEs are emitted from the first few nm of the surface. Since there are three possible ways of SE emission, the group is further divided: SEIs are generated when the beam enters the sample, SEIIs are emitted when a BSE leaves the sample, and SEIIIs are produced by BSEs interacting with materials in the analysis chamber which are not related to the sample. The SE mode is the standard mode in SEM because it provides the best topographic information. The number of SEs produced changes with the slope of the surface, whereas the change in emission volume is comparatively small.

The third group of interactions is (X-ray) photon emission: When the primary electron collides with a core electron in the solid and ejects it, an electron coming from an outer shell falls back to fill the gap. The resultant excess of energy can either be emitted as a characteristic photon or excite a valence-shell electron to leave the atom. The latter is called an AUGER electron and is detected in the group of SEs. Photons emitted from surface atoms usually have energies in the X-ray region. Since the energy of the photon is characteristic of the element from which it is emitted, sorting the photons by energy provides valuable information on surface composition. X-ray emission in a SEM is not used for direct imaging but for an elemental map of the surface similar to XPS (see 1.3.4). The spatial resolution of such X-ray maps in SEM is, however, limited to approximately 500 nm because the primary electrons can travel through a certain volume of the material and cause interactions at many positions [37].

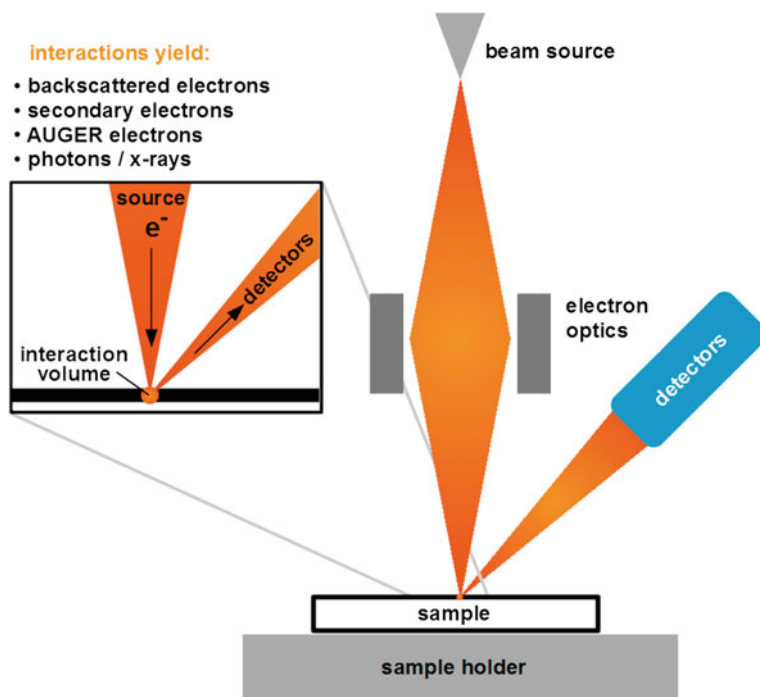


**Fig. 2.7** Schematic of an SEM setup: A beam generated by an electron source is focused with electron optics and rastered over a sample. The incident beam causes different interactions with the surface atoms which are detected and used for imaging (primary and secondary electrons, Auger electrons) or elemental mapping (X-rays)

The setup of an SEM is arranged in a high vacuum chamber and comprises an electron source, electron optics, a movable sample-holder, as well as several detectors (Fig. 2.7). The electron source can either be a thermionic (W or LaB<sub>6</sub>) or a field emission gun. Although the use of the SEM requires vacuum-compatible samples, operation of the microscope is actually very easy. Insulating samples can be studied with low primary beam voltages (<2 keV) or coated with a thin film of carbon, gold, or some other metal to avoid charge build-up [37].

For further information on imaging modes, detectors, electron optics, sample preparation, and applications, reference is made to the literature [37, 41, 42]

### 2.3.4 X-ray Photoelectron Spectroscopy

X-ray photoelectron spectroscopy (XPS) is a surface sensitive analysis technique which provides information on the chemical composition of matter. Based on the discovery and explanation of the photoelectric effect by HERTZ and EINSTEIN, [43, 44]

as well as the pioneering work of SIEGBAHN and co-workers [45, 46] modern spectrometers are widely used in materials analysis. Besides AUGER electron spectroscopy (AES) and secondary ion mass spectrometry (SIMS), XPS is the one of the most dominant surface analysis techniques [37]. In contrast to ultra-violet photoelectron spectroscopy (UPS), which provides information on the character of molecular orbitals, XPS is capable of identifying atoms and their concentration in a defined analysis volume. The technique, which is also referred to as *electron spectroscopy for chemical analysis* (ESCA), uses high energy photons in the form of monochromatic X-rays to ionize surface atoms. The kinetic energy,  $E_{kin}$ , of ejected electrons is measured by a detector. Given the energy of the X-ray photon the binding energy ( $E_b$ ) of the electron can be calculated by Eq. 2.8.

$$E_b = h \cdot \nu - E_{kin} \quad (2.8)$$

Equation 2.8: Binding energy of electrons detected in XPS.  $E_b$  = binding energy,  $\nu$  = frequency,  $h$  = PLANCK'S constant,  $E_{kin}$  = kinetic energy.

The binding energy is characteristic of the orbital and atom the electron it is ejected from and, thus, allows for a detailed analysis of the surface composition. In general,  $E_b$  varies with the effective nuclear charge an electron “experiences” in a multi-electron atom.

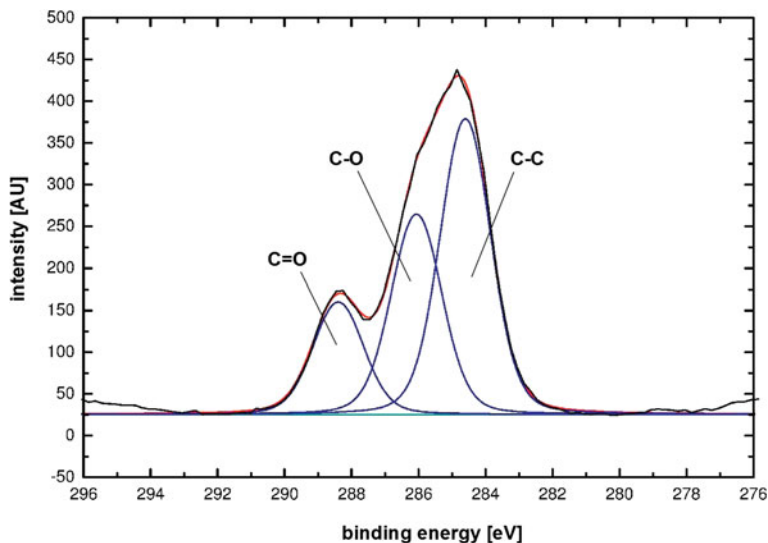


**Fig. 2.8** Chemical shift of the C1s peak in XPS: The carboxy C1s signal of a PEGMA-co-PMMA film on a Si(100) wafer is shifted to higher binding energy (288.39 eV), followed by the ether C1s signal of carbon with a single-bonded oxygen (286.06 eV). The alkylic C1s signal was normalized to 284.60 eV



### 2.3.4.1 Signals and Shifts

In XPS, the energy of the photons is sufficient to eject electrons from core levels, whereas in UPS only electrons from valence levels can be ejected. Hence, XPS provides information which is almost independent of the chemical species the atom is part of. However, due to changes in the effective nuclear charge with different chemical environments electron peaks from the same orbital can show *chemical shifts*: The higher the effective nuclear charge the higher is the binding energy of an electron. Since the effective nuclear charge of an atom depends on the electronegativity of the binding partner, higher binding energies are detected in the presence of a more electronegative binding partner and *vice versa*. Figure 2.8 shows the C1s area of a PEGMA-co-PMMA film (see 1.2.2) polymerized on a Si(100) wafer. The carboxy (C=O) C1s signal is shifted to higher binding energy (288.39 eV), followed by the ether (C–O) C1s signal at 286.06 eV. The alkylic (C–C) C1s signal was normalized to a binding energy of 284.60 eV. Even higher shifts than observed for different chemical environments can be caused by different oxidation states of an atom [37]. Chemical shifts are analytically useful because they provide more detailed information on the chemical state of atoms.

Another analytically useful effect in XPS is spin-orbital splitting. For example, the different energy levels of p-orbitals with  $j = 1/2$  or  $j = 2/3$  ( $j =$  total angular momentum) result in doublet peaks. The spin-orbital splitting is predictable and can help to identify unknown lines in a spectrum. Spin-orbital splitting increases with the nuclear charge ( $\sim Z^4$ ) and is, thus, more prominent for heavy atoms. In addition, spin-orbital splitting also spin-spin splitting can occur when paramagnetic materials are studied.

Furthermore, a spectrum often shows *satellite peaks* which are caused by interaction of electrons. In case an ejected electron hits an electron in a valence level and transfers energy on this second electron, it can either eject the second electron (*shake-off* electron) or excite it to an unoccupied higher level (*shake-up* electron). In both cases the photoelectron loses part of its kinetic energy and appears at higher binding energy. The probability of such interactions is low which causes a low intensity of satellite peaks. However, together with the chemical shift interaction with valence electrons can help to identify chemical states [37]. In addition, AUGER electron peaks (see 2.3.3) can appear in the XP spectrum. In many cases they show larger chemical shifts than core-level peaks and, thus, help to identify unknown spectral lines. An additional benefit of AUGER electrons is that their energy is independent of the photoelectron energy. In AES no monochromatic X-rays are required.

### 2.3.4.2 Spectrometer

An X-ray photoelectron spectrometer typically consist of an ultra-high vacuum chamber ( $p < 10^{-7}$  mbar), an X-ray source (typically an Al- or Mg-coated anode which is bombarded with electrons from a high-voltage cathode), an X-ray

monochromator, a movable sample holder, and a detector setup (e.g. a hemispherical sector). Mg  $K_{\alpha}$  (1256.6 eV) or Al  $K_{\alpha}$  (1486.6 eV) radiation is directed to the sample at a controlled angle of incidence. The informational depth in the case of polymers is typically in the range of 7 nm and reaches a maximum of 10 nm [47]. The spot size of newer instruments can be as small as 3  $\mu\text{m}$  in diameter (or 30 nm if X-rays from a synchrotron are used) [47], but is usually in the mm-range. If a high lateral resolution is required, techniques such as AES and SIMS can alternatively be applied. Furthermore, small-spot analysis for high lateral resolution lowers the count rate of photoelectrons and must be compensated by longer spectrum acquisition times [47]. However, XPS has the advantage of a more developed chemical state analysis and fewer problems in terms of induced sample damage [37].

To avoid charge build-up and related signal shifts, the sample holder in XPS is grounded. The FERMILevels of the sample and the spectrometer are equal. As a consequence, a contact potential exists between the sample and the spectrometer because the work function,  $\Phi_{sp}$ , of the spectrometer is higher than the work function of the sample. Hence, the work function of the spectrometer has to be considered in the calculation of the binding energy, as shown in Eq. 2.9, because the photoelectron needs a small additional amount of energy to transfer to vacuum level [47]. In general, the FERMILevel of the spectrometer serves as an internal reference for the calculation of binding energies.

$$E_b = h \cdot \nu - \Phi_{sp} - E_{kin} \quad (2.9)$$

Equation 2.9: Binding energy in XPS taking into account the work function of the spectrometer  $\Phi_{sp}$ .

### 2.3.4.3 Quantitative Analysis

A major benefit of XPS is that quantitative information on the sample composition, i.e. relative atomic concentrations, can be gained. Integration of the signals in ESCA after appropriate background subtraction provides values which correspond to the fraction of respective atoms in the analysis volume. Background noise arises from X-ray scattering and further interaction of ejected photoelectrons in the material. In principle, the uncertainty of quantitative measurements can vary up to 30 %, but individual calibration of the instrument and relative measurements, e.g. reference measurements of an internal or external standard, greatly improve the accuracy [37].

The intensity of photoelectron peaks depends on several parameters which must be considered in a quantitative comparison of ESCA features. The exact term for the intensity,  $I_A$ , of a core-level electron, A, in XPS is shown in Eq. 2.10 [48].

$$I_A = \sigma_A(h\nu)D(E_b) \int_x^y \int_{\gamma=0}^{\pi} \int_{\phi=0}^{2\pi} L_A(\gamma) \int_x^y \int_{\gamma=-\infty}^{\infty} \int_{x=-\infty}^{\infty} J_0(xy)T(wy\gamma\phi E_b) \int_x^y \int_{z=0}^{\infty} N_A(xyz) e^{\frac{-z}{\lambda_A(E_b)\cos\theta}} dx dy dz d\phi d\gamma \quad (2.10)$$

Equation 2.10: Term for absolute signal intensity of a core-level electron A in XPS.  $\sigma_A(h\nu)$  = photoionization cross-section,  $D(E_b)$  = detection efficiency of photoelectrons,  $L_A(\gamma)$  = angular asymmetry of the photoelectron intensity,  $J_0$  = properties of the X-ray line in the detection plane,  $T$  = transmission function of the energy analyzer,  $N_A$  = atomic density at position xyz,  $\gamma$  = angle between incident beam and analyzer aperture,  $\phi$  = azimuth angle,  $\lambda_A(E_b)$  = attenuation length as a function of binding energy,  $\theta$  = emission angle of the photoelectron.

Since a numerical solution of this term is difficult a less complex equation for the signal intensity is provided in Eq. 2.11. For a good approximation it can be assumed that device specific parameters such as X-ray line properties or detection efficiency are constant for measurements with the same setup. A transmission function,  $T(E_b)$ , which describes the detection probability of photoelectrons at different kinetic energies is determined once experimentally and then routinely used to normalize spectra.

$$I_A = \sigma_A N_A \lambda_A(E_b) T(E_b) \cos \theta \left[1 - e^{\frac{-z}{\lambda_A(E_b)\cos\theta}}\right] \quad (2.11)$$

Equation 2.11: Approximation for the relative signal intensity of a core-level electron A in XPS.  $T(E_b)$  = transmission function of the spectrometer.

Hence, for homogeneous samples atomic concentrations in the analysis volume can be determined by intensity ratios according to Eq. 2.12 given that the signals are measured under identical experimental conditions.

$$\frac{I_A}{I_B} = \frac{\sigma_A N_A \lambda_A(E_b^A)}{\sigma_B N_B \lambda_B(E_b^B)} \text{ and } \frac{N_B}{N_A} = \frac{\sigma_A \lambda_A(E_b^A) I_B}{\sigma_B \lambda_B(E_b^B) I_A} \quad (2.12)$$

Equation 2.12: Intensity ratio and atomic concentration of two elements A and B in XPS.

In this approximation the intensity of a photoelectron peak only depends on ionization cross-section  $\sigma$  and the attenuation length,  $\lambda$ , of an electron exiting the sample. Theoretical cross-sections of electrons in their respective orbitals based on calculations have been published by SCOFIELD [49]. Attenuation lengths depend on the kinetic energy of the X-ray photons, the binding energy of the corresponding photoelectron, and the angle of emission. A common way to calculate attenuation lengths in alkylic monolayers is based on a linear fit introduced by BAIN and co-workers [50]. However, for the spectrometer used in this work an exponential fit according to Eq. 2.13 showed better agreement to experimental data and was, thus, applied instead [51].

$$\lambda_A(E_b) = 0.59 \cdot e^{\left(\frac{594.26 - E_b}{150.43}\right)} + 19.39 \quad (2.13)$$

Equation 2.13: Exponential fit for the attenuation length of photoelectrons in alkylic monolayers based on experimental data by STADLER [51].

Cross-sections and attenuation lengths for atomic orbitals referred to in this work are listed in 5.1.4 (Table 6). For more detailed information on the development, principles, and applications of XPS, reference is made to the literature [37, 47, 48, 52].

## References

1. V. Stadler, T. Felgenhauer, M. Beyer, S. Fernandez, K. Leibe, S. Güttler, M. Gröning, K. König, G. Torralba, M. Hausmann, V. Lindenstruth, A. Nesterov, I. Block, R. Pipkorn, A. Poustka, F.R. Bischoff, F. Breitling, *Angew. Chem. Int. Ed.* **47**, 7132–7135 (2008)
2. M. Beyer, I. Block, K. König, A. Nesterov, S. Fernandez, T. Felgenhauer, C. Schirwitz, K. Leibe, R. F. Bischoff, F. Breitling, V. Stadler, *Methods in Molecular Biology*, vol. 570. (Clifton, New Jersey, 2009), pp. 309–316
3. K. König, I. Block, A. Nesterov, G. Torralba, S. Fernandez, T. Felgenhauer, K. Leibe, C. Schirwitz, F. Löffler, F. Painke, J. Wagner, U. Trunk, F.R. Bischoff, F. Breitling, V. Stadler, M. Hausmann, V. Lindenstruth, *Sens. Actuators, B: Chem.* **147**, 418–427 (2010)
4. W. Kern, *J. Electrochem. Soc.* **137**, 1887–1892 (1990)
5. M. Beyer, T. Felgenhauer, F.R. Bischoff, F. Breitling, V. Stadler, *Biomaterials* **27**, 3505–3514 (2006)
6. O. Senfleben, H. Baumgärtner, I. Eisele, *Mater. Sci. Forum.* 573–574, 77–117 (2008)
7. V. Stadler, M. Beyer, K. König, A. Nesterov, G. Torralba, V. Lindenstruth, M. Hausmann, F.R. Bischoff, F. Breitling, *J. Proteome Res.* **6**, 3197–3202 (2007)
8. M. Grundner, H. Jacob, *Appl. Phys. Solid Surf.* **39**, 73–82 (1986)
9. A. Ulman, *Chem. Rev.* **96**, 1533–1554 (1996)
10. D.K. Schwartz, *Annu. Rev. Phys. Chem.* **52**, 107–137 (2001)
11. X. Huang, M.J. Wirth, *Anal. Chem.* **69**, 4577–4580 (1997)
12. J. Pyun, T. Kowalewski, K. Matyjaszewski, *Macromol. Rapid Commun.* **24**, 1043–1059 (2003)
13. A. Olivier, F. Meyer, J. M. Raquez, P. Damman, P. Dubois, *Progress in Polymer Science*, vol. 37. (Oxford press, Oxford, 2012), pp. 157–181
14. M. Kamigaito, T. Ando, M. Sawamoto, *Chem. Rev.* **101**, 3689–3745 (2001)
15. M. Kamigaito, *Polym. J.* **43**, 105–120 (2011)
16. M. Ouchi, T. Terashima, M. Sawamoto, *Chem. Rev.* **109**, 4963–5050 (2009)
17. J.S. Wang, K. Matyjaszewski, *J. Am. Chem. Soc.* **117**, 5614–5615 (1995)
18. V. Stadler, R. Kirmse, M. Beyer, F. Breitling, T. Ludwig, F.R. Bischoff, *Langmuir* **24**, 8151–8157 (2008)
19. F. Guillier, D. Orain, M. Bradley, *Chem. Rev.* **100**, 2091–2157 (2000)
20. N. Jung, M. Wiehn, S. Bräse, vol. 278, ed. by S. Bräse, V. Balzani, A. Meijere, K. N. Houk, J. M. Lehn, H. Kessler, S. V. Ley, S. L. Schreiber, *Top. Curr. Chem.* **278**, 1–88 (2007)
21. R.B. Merrifield, *J. Am. Chem. Soc.* **85**, 2149–2154 (1963)
22. S.S. Wang, *J. Am. Chem. Soc.* **95**, 1328–1333 (1973)
23. M. Mergler, R. Tanner, J. Gosteli, P. Grogg, *Tetrahedron Lett.* **29**, 4005–4008 (1988)
24. M. Mergler, R. Nyfeler, R. Tanner, J. Gosteli, P. Grogg, *Tetrahedron Lett.* **29**, 4009–4012 (1988)
25. F. Albericio, G. Barany, *Int. J. Pept. Protein Res.* **30**, 206–216 (1987)

26. F. Albericio, N. Kneib-Cordonier, S. Biancalana, L. Gera, R.I. Masada, D. Hudson, G. Barany, *J. Org. Chem.* **55**, 3730–3743 (1990)
27. H. Rink, *Tetrahedron Lett.* **28**, 3787–3790 (1987)
28. S. Hoffmann, R. Frank, *Tetrahedron Lett.* **35**, 7763–7766 (1994)
29. G. Panke, R. Frank, *Tetrahedron Lett.* **39**, 17–18 (1998)
30. Y. Wolman, P.M. Gallop, A. Patchornik, *J. Am. Chem. Soc.* **83**, 1263–1264 (1961)
31. C. Peters, H. Waldmann, *J. Org. Chem.* **68**, 6053–6055 (2003)
32. J. Eichler, M. Bienert, A. Stierandova, M. Lebl, *Pept. Res.* **4**, 296–307 (1991)
33. M. Beyer, *Entwicklung und Anwendung neuartiger Trägeroberflächen zur kombinatorischen Peptidsynthese mit Aminosäure-Tonerpartikeln*, Ph.D. thesis, (University of Heidelberg, 2005)
34. G.B. Fields, R.L. Noble, *Int. J. Pept. Protein Res.* **35**, 161–214 (1990)
35. M. Gude, J. Ryf, P.D. White, *Lett. Pept. Sci.* **9**, 203–206 (2002)
36. I. Block, *Herstellung und Anwendung von hochkomplexen Peptidbibliotheken*, Ph.D. thesis, (University of Heidelberg, 2009)
37. C. R. Brundle, C. A. Evans, S. Wilson, *Encyclopedia of Materials Characterization: Surfaces, Interfaces, Thin Films* (Butterworth-Heinemann, Stoneham, 1992)
38. K. Vedam, *Thin Solid Films* 313–314, 1–9 (1998)
39. A.L. Cauchy, *Bull. des Sci. Mathématiques* **14**, 6–10 (1830)
40. H. Fujiwara, *Spectroscopic Ellipsometry: Principles and Applications* (Wiley, West Sussex, 2007)
41. R.F. Egerton, *Physical Principles of Electron Microscopy: An introduction to TEM, SEM, and AEM* 1st edn. (Springer, New York, 2005)
42. K. Shimizu, T. Mitani, *New Horizons of Applied Scanning Electron Microscopy*, vol. 45 (Springer, Heidelberg, 2009)
43. H. Hertz, *Ann. Phys.* **267**, 983–1000 (1887)
44. A. Einstein, *Ann. Phys.* **322**, 132–148 (1905)
45. C. Nordling, E. Sokolowski, K. Siegbahn, *Phys. Rev.* **105**, 1676–1677 (1957)
46. S. Hagström, C. Nordling, K. Siegbahn, *Phys. Lett.* **9**, 235–236 (1964)
47. M. Stamm, *Polymer Surfaces and Interfaces: Characterization, Modification and Applications*, 1st edn. (Springer, Berlin Heidelberg Germany, 2008)
48. T.L. Barr, *Modern ESCA: The Principles and Practice of X-ray Photoelectron Spectroscopy* (CRC Press, Boca Raton FL USA, 1994)
49. J.H. Scofield, *J. Electron Spectrosc. Relat. Phenom.* **8**, 129–137 (1976)
50. C.D. Bain, G.M. Whitesides, *J. Phys. Chem.* **93**, 1670–1673 (1989)
51. V. Stadler, *Chemische Nanolithographie mit Elektronenstrahlen an Biphenyl-Monoschichten*, Ph.D. thesis, (University of Heidelberg, 2001)
52. K. Siegbahn, *From X-Ray to Electron Spectroscopy*, vol. 746 (Springer, Berlin Heidelberg Germany, 2008)

# Chapter 3

## Results and Discussion

### 3.1 Surface Chemistry A: Synthesis Surfaces

This chapter provides an overview of improvements in the production of synthesis surfaces. The improvements were necessary to obtain reproducible substrates for the development of the peptide array purification method. Since several parameters in the substrate modification are still under investigation, only major considerations and improvements which led to the standard protocols (see [Sect. 5.3.1](#)) are addressed. For the entire chapter it must be considered that the standard synthesis surfaces for the laser printer-based peptide array synthesis have a format of  $22 \times 21 \text{ cm}^2$ . Therefore, only reaction conditions which could easily be up-scaled to this format were of interest. This excludes reactions which only work in small-scale using a permanent inert gas atmosphere (i.e. Schlenk technique). In the second part of this chapter, the focus lies on the coupling of cleavable linkers and their compatibility with mpSPPS in hopes of providing substrates which allow for a controlled cleavage of array members.

#### 3.1.1 Improved Cleaning and Activation

As described in [Sect. 2.2.1](#) the common cleaning and activation process for  $\text{SiO}_2$  surfaces (silicon wafers and glass slides) was based on treatment in hot piranha solution. Although applied in the early stages of this work, the cleaning of glass slides with piranha solution was completely replaced by alkaline etching with 1 M KOH in 2-propanol overnight. KOH/2-propanol is easier and safer to handle than hot piranha solution and appears to achieve a more efficient cleaning of the glass substrates. The use of highly oxidative piranha solution typically produced gases which tended to adsorb to the surface. Hence, gas adsorption sites probably shielded parts of the surface and prevented efficient cleaning. Changing the cleaning protocol had a positive effect on the stability of polymer coatings especially in case of the PEGMA-co-PMMA graft polymers. Thicker films which

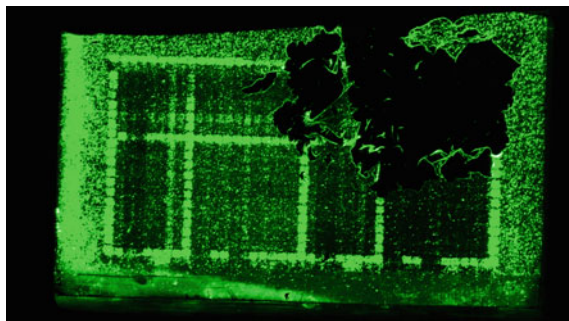


**Fig. 3.1** Insufficient stability of a PEGMA-co-PMMA coating before implementation of KOH/2-propanol cleaning. The copolymer coating was damaged and partially broke away from the microscopy slide surface, probably as a consequence of peptide side-chain deprotection using TFA. The film damage became visible in a subsequent staining of the peptide array with the IRDye 800CW NHS-ester. Readout was performed on the *Odyssey Infrared Imager*

occasionally tended to be torn off the surface in the past (see Fig. 3.1) were stable throughout the peptide synthesis if KOH/2-propanol cleaning was applied.

KOH/2-propanol etching was not applied to CMOS chips and Si(100) wafers because these smaller surfaces could be efficiently cleaned and activated by UV irradiation as discussed in Sect. 2.2.1 and described in Sect. 5.3.1.1. However, if no UV equipment is available, homogenous etching of Si(100) wafers should be possible with 3 M KOH + 2 M 2-propanol or 5 M KOH + 1 M 2-propanol in water as reported by ZUBEL et al. [1, 2]. Throughout this work, all polymeric films synthesized on CMOS chips or Si(100) wafers were stable independent of their subsequent use. The polymer coatings typically reached a thickness of 50 nm and did not exceed a thickness of 80 nm. Besides thorough cleaning of the surfaces, this comparatively low polymer thickness is thought to be an additional reason for increased film stability.

### 3.1.2 Silanization for siATRP

As described in Sect. 2.2.2, a SAM bearing a tertiary bromine is required to coat a substrate by siATRP. In this work, 2-bromo-*N*-(3-triethoxysilyl)propyl isobutyramide [bromine silane, Fig. 3.2, (1)] was routinely used. The silane is not commercially available and was synthesized prior to surface functionalization (see Sect. 5.3.1.2) [3]. The established protocol for the silanization with the bromine silane was conceived for a 10 mM solution in anhydrous dichloromethane [3–5]. Compared to earlier protocols, the silane concentration had already been reduced by three quarters [6]. However, the synthesis of the bromine silane is labor-intensive and comparatively high amounts were needed to silanize the  $22 \times 21 \text{ cm}^2$  laser printer substrates. Thus, the standard protocol had been

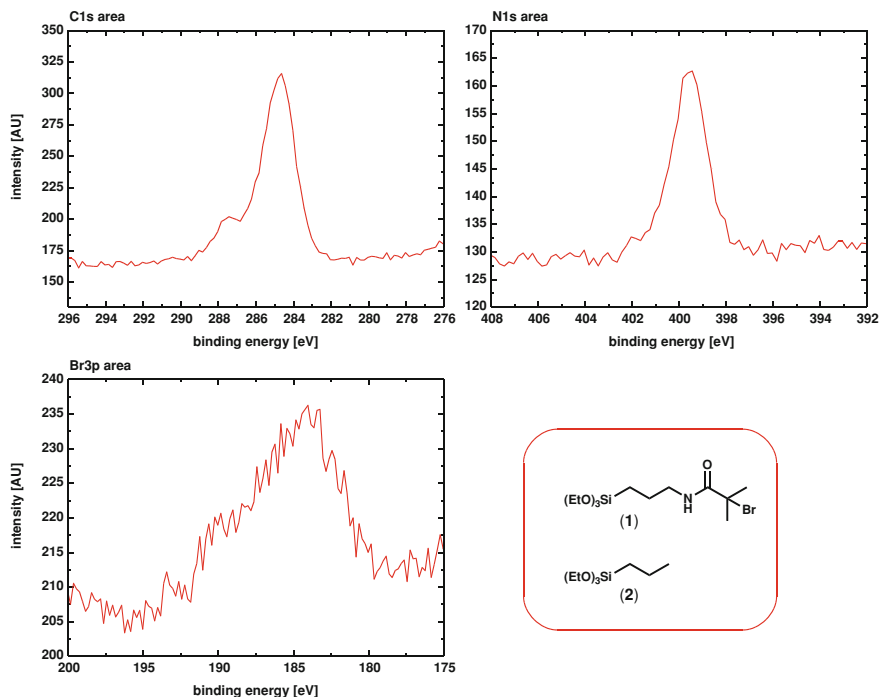


**Fig. 3.2** C1s, N1s and Br3p areas in the XP spectrum of a SAM formed by co-adsorption of bromine silane (1) with PTES (2). The signal in the Br3p area indicates the presence of the tertiary bromine silane (1) required for siATRP

amended to a 2 mM solution of bromine silane and 8 mM of additional *N*-propyl triethoxysilane [PTES, Fig. 3.2, (2)]. PTES was co-adsorbed from the bromine silane solution which, as communicated, had no impact on the film thickness and composition of the polymer [7]. The amended protocol produced PEGMA-co-PMMA films of equal quality and was, thus, routinely applied in the present work. However, the surface initiator density is known to affect the rate of chain growth and, as a consequence, the resulting polymer thickness [8, 9]. Hence, the 2 mM solution probably still rendered sufficient bromine silane density to obtain the desired film thicknesses. To check the presence of bromine atoms on the target substrates before polymerization, a piece of Si(100) was routinely added to the silanization reaction as an XPS reference. Moreover, a silanized wafer piece was also routinely processed in the siATRP to measure film thicknesses via ellipsometry if the target substrates were glass slides or micro chips. After silanization, all samples were routinely tempered for 2 h at 110 °C in air to achieve full condensation of the silanes with hydroxy groups on the surface [5]. Compared to the previous protocol, the “baking” step was extended by 1 h which probably also added to the observed increase in film stability (see Sect. 3.1.1). Figure 3.2 exemplarily shows the C1s, N1s, and Br3p areas of a bromine silane/PTES SAM on



Si(100). Although low in intensity, the signal in the Br3p area clearly indicates the presence of bromine atoms on the surface.

For an exact analysis of the co-adsorption process, angle-resolved XPS measurements would be required. By varying the take-off angle  $\theta$  (see Eq. 2.11), information on the conformation of the molecules in the SAM could be gained because the contribution of near-surface groups to the signal intensity is always higher. However, the exact characterization of the bromine silane SAMs was not in the focus of the present work. Moreover, small contaminations in the C1s and N1s areas due to baking and air exposure (adsorption of nitrogen and carbon compounds from the atmosphere) probably distorted the quantitative information. Thus, the presence of a Br3p signal, a good stability of the SAM, and reproducible polymer thicknesses (see Sect. 3.1.3) were important for an application in siATRP.

### 3.1.3 Improved siATRP for Synthesis Coatings

In the preparation of PEGMA-co-PMMA coatings a frequent problem was gelation of the entire solution. Especially, in the synthesis of graft polymer coatings consisting of 10 % (n/n) PEGMA and 90 % (n/n) MMA, which were the standard surface coatings for the peptide array synthesis, gelation often occurred in the first hours of incubation (see Fig. 3.3).

However, according to the underlying protocol by STADLER et al., who polymerized these copolymer films on Si(100) wafers by siATRP, no gelation was expected [10]. In the literature protocol, the polymerization was conducted with  $\text{Cu}^I$  as a catalyst and PMDETA as a ligand, whereby additional tri(ethylene glycol) monomethyl ether (TEGMME) was added as a solvent if the PEGMA content was

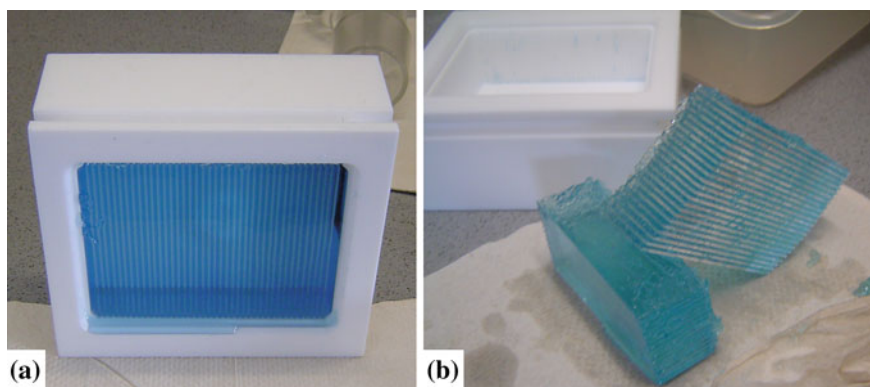


**Fig. 3.3** Gelation of the siATRP solution. A frequent problem was gelation of the ATRP solution in the production of PEGMA-co-PMMA coatings. **a** An entire batch of 40 microscopy slides coated inside a Teflon container is enclosed in the polymer gel. **b** The slides cannot be removed separately and purification is futile

below 50 % (n/n). Above a molar fraction of 50 % (n/n) PEGMA the polymerization was conducted in the pure monomer mixture.

### 3.1.3.1 Influence of the $\text{Cu}^{\text{I}}:\text{Cu}^{\text{II}}$ System

The protocol by STADLER et al. had been developed based on a publication by KIMANI and MORATTI who, instead, used a  $\text{Cu}^{\text{I}}/\text{Cu}^{\text{II}}$  initiator system to efficiently control the polymerization rates of their ATRP [11].  $\text{Cu}^{\text{II}}$  was applied as an inhibitor to slow down the reaction rates which had already been considered beneficial for the control of the polymerization by WANG and MATYJASZEWSKI in 1995 [12]. Since then, the addition of  $\text{Cu}^{\text{II}}$  as a deactivating species has been extensively studied, but precise strategies to completely control the polymerization rates in siATRP are still under investigation [13]. For example, KIMANI and MORATTI described a three times reduced reaction rate over 24 h of polymerization for their  $\text{CuBr}/\text{CuCl}_2/\text{PMDETA}$  (0.5:0.5:1 eq) catalyst system in TEGMME [14].

### 3.1.3.2 Influence of Ligand, Monomer, Solvent, and Initiator

Besides the catalyst system, the ligand (PMDETA) and the solvent (TEGMME) also have an impact on the polymerization rate. The influence of PMDETA as a ligand has been intensively studied by Nanda and Matyjaszewski, whereby a ratio of  $\text{PMDETA}/\text{Cu}^{\text{I}}$  of 1:1 or higher was reported to result in the highest number of active catalyst species [15]. Hence, a  $\text{PMDETA}/\text{Cu}^{\text{I}}$  ratio of 2:1 as applied in the protocol by STADLER et al. could also be a critical parameter causing high polymerization rates and the observed gelation. Furthermore, TEGMME is considered to accelerate the polymerization due to a coordinating effect on the inhibiting  $\text{Cu}^{\text{II}}$  species which shifts the equilibrium to a higher number of active  $\text{Cu}^{\text{I}}$  species [14]. A similar effect has been reported for the polymerization of oligo(ethylene glycol) methacrylates which obviously tend to coordinate  $\text{Cu}^{\text{I}}$  with their side-chains [16]. This suggests that higher PEGMA concentrations can also accelerate the polymerization rate. Finally, as described above, the initiator density on the surface also has an effect on the polymerization rate (see Sect. 3.1.2). JONES et al. found a linear relationship between initiator density and brush polymer thickness [8]. Taking all the above into account, the siATRP system intended for the production of synthesis surfaces in this work was very complex because every compound had to be considered to have an impact on the polymerization rate. Accordingly, all attempts to control the polymerization via  $\text{Cu}^{\text{II}}$  addition and variations in the TEGMME concentration failed. The polymerization either produced layer thicknesses below 10 nm (too strong inhibition) as determined by ellipsometry or failed due to gelation (too low inhibition).

### 3.1.3.3 Inhibitor and Catalyst in Large-Scale siATRP

Attempts to control the siATRP were additionally complicated because CuCl, MMA, and PEGMA had to be used as received. Typically, Cu<sup>I</sup> salts are purified from Cu<sup>II</sup> residues prior to polymerization, e.g. by stirring in glacial acetic acid, filtration, washing, and storage under nitrogen [15]. MMA and PEGMA are stabilized with small amounts of an inhibitor (approximately 100 ppm in MMA and 500–800 ppm in PEGMA) such as monomethyl ether hydroquinone (MEHQ) which can be removed by distillation over CaH<sub>2</sub> under reduced pressure [15]. However, the setup required for siATRP on 22 × 21 cm<sup>2</sup> glass substrates made thorough purification of the compounds difficult. Instead of a SCHLENK flask, larger containers were used in the surface modification (see Fig. 3.4). Thus, large monomer quantities were needed which were difficult to distill with a standard laboratory setup prior to use without the risk of direct polymerization. Furthermore, the siATRP reaction could not be conducted in an absolutely inert atmosphere. The container was routinely evacuated in a desiccator and kept under an inert gas atmosphere, but the solution had to be poured in in the presence of air which inevitably caused partial oxidation of the Cu<sup>I</sup> catalyst. The presence of oxygen generates the inhibiting Cu<sup>II</sup> species in situ as is visible by slight color changes and, thus, renders Cu<sup>I</sup> salt purification useless. Hence, exact control of the Cu<sup>I</sup>/Cu<sup>II</sup> ratio was difficult and rather a “robust” protocol was needed to circumvent catalyst/inhibitor problems.

**Fig. 3.4** Desiccator equipped with a custom-built container for surface chemistry on 22 × 21 cm<sup>2</sup> glass slides. The container holds 14 large glass slides and has a volume of 2.5 L (unequipped)



### 3.1.3.4 Optimization of the siATRP Process

In fact, optimization of the siATRP is still an on-going process. However, experimental results which were obtained in the context of a diploma thesis [17] and throughout this work improved the reliability of the siATRP system. In the following paragraph important modifications which led to the current protocol for synthesis surface preparation by siATRP (see Sect. 5.3.1.4) are summarized.

A replacement of the solvent used in siATRP was considered to be the most effective parameter to avoid gelation. siATRP can be conducted in both polar and nonpolar solvents, whereby, in general, higher polymerization rate constants were reported for polar solvents [15, 18]. Nevertheless, control over the reaction was always highly dependent on the entire system. A series of polymerizations with 10 % (n/n) PEGMA and 90 % (n/n) MMA was performed to investigate the effect of different solvents whereby the ratio of PMDETA:Cu<sup>I</sup> was kept constant. All reactions were conducted in an air conditioned laboratory at room temperature (RT, 23 °C). In accordance with the protocol by STADLER et al. the ratio was initially set to 2:1 (PMDETA:Cu<sup>I</sup>) and the monomer fraction was adjusted to 6.7 mL (63 mmol) of MMA and 2.3 mL (7 mmol) of PEGMA [10]. Instead of using TEGMME as a solvent and reducing the overall monomer fraction, 11 mL of a solvent were added to give a total volume of 20 mL. Furthermore, the original amounts of 35 mg (0.35 mmol) CuCl and 146 μL (0.70 mmol) PMDETA were doubled with respect to the change in volume. It must be mentioned that for a polymerization of PEGMA and MMA, only solvents which equally dissolve both monomers could be used. In this experiment, dimethyl sulfoxide (DMSO), acetonitrile (MeCN), DMF and tetrahydrofuran (THF) were used. DMSO was found to be superior to MeCN, DMF, and THF in terms of resulting film thickness, although the maximum achieved polymer thickness was only around 15 nm which is too low for an application as a synthesis surface.

However, based on these findings the polymer thickness could be improved by using 10 mL of DMSO as a solvent and an additional 1 mL (6.3 mmol) of TEGMME as a co-ligand which is in good agreement with the increase of polymerization rates upon use of TEGMME observed by KIMANI and MORATTI [14]. With a respective ratio PMDETA:Cu<sup>I</sup>:TEGMME of 1:1:4.5 the polymer thickness reproducibly reached about 50 nm which was in the required range for the peptide array synthesis. Variations of the PMDETA/Cu<sup>I</sup> ratio from 2:1 to 0.5:1 showed no impact on the obtained film thickness which agrees with the findings of NANDA and MATYJASZEWSKI [15]. Hence, the PMDETA/Cu<sup>I</sup> ratio was amended to 1:1 to efficiently solve Cu<sup>I</sup> in the polymerization solutions. Furthermore, a reduction of the Cu<sup>I</sup> amount to 35 mg, as initially used by STADLER et al. (see above, the amount was first doubled), further increased the film thicknesses to about 70 nm.

Even higher thicknesses of about 80 nm were achieved upon doubling the TEGMME amount to a ratio PMDETA:Cu<sup>I</sup>:TEGMME of 1:1:9. This, in turn, allowed for a bisection of the monomer fraction adding additional DMSO which still gave film thicknesses in the desired range of 50 ± 5 nm. The diluted reaction mixture proved to be even less prone to gelation. In fact, the problem of gelation

was solved with the described amendments. However, it must be mentioned that recent results still hint at dependency of film thicknesses on the monomer batch. Probably due to a slightly varying amount of inhibitor added by the manufacturer dilution may result in insufficient polymer thicknesses. Therefore, test polymerizations on Si(100) wafers are routinely conducted for every new monomer batch to find the optimum monomer concentration reproducibly yielding >50 nm polymer thickness before coating the laser printer slides or the micro chips. The protocol applied in the preparation of synthesis surfaces in this work can be found in the Materials and Methods section (see [Sect. 5.3.1.4](#))

### 3.1.3.5 Verification of the Copolymer Composition

The composition of the PEGMA-co-PMMA coating obtained by the amended protocol was verified via XPS. Figure 3.5 exemplarily depicts a quantitative analysis of the C1s area of a 10:90-PEGMA-co-PMMA film on Si(100). In theory, the peak areas  $C_{C=O}:C_{C-O}:C_{C-C}$  should constitute a ratio of 1:1.8:3. The experimentally determined ratio of 1:1.78:2.63 is, thus, in good agreement with this. Hence, the film composition is not compromised by the amended synthesis protocol.

### 3.1.3.6 Summary

In summary, the use of DMSO as a solvent generally helps to avoid gelation. With the optimized protocol the polymerization is probably conducted in a range in which an excess of DMSO dominates the polymerization rates. This apparently makes the system more stable even if the concentration of some compounds slightly varies. However, the use of a defined  $Cu^I:Cu^{II}$  ratio, the use of monomers purified of inhibitors, and an apparatus to coat the laser printer substrates without the introduction of oxygen would greatly help to reduce the need of test runs for each new monomer batch in the future.

## 3.1.4 SAMs for the Peptide Array Synthesis

State-of-the-art in the particle-based peptide array synthesis is a nm-scale polymeric film (10:90-PEGMA-co-PMMA film, see [Sect. 2.2.2](#)). This coating is compatible with most biological applications and bears the advantage of intrinsic protein repelling properties [10]. However, the surface composition, i.e. the right balance of protein repelling EG units and less sterically hindering groups, remained a crucial parameter throughout this work and had to be considered separately for each assay. In addition to the well-established copolymer coatings, SAMs were considered to be a potential starting point for a peptide array synthesis.

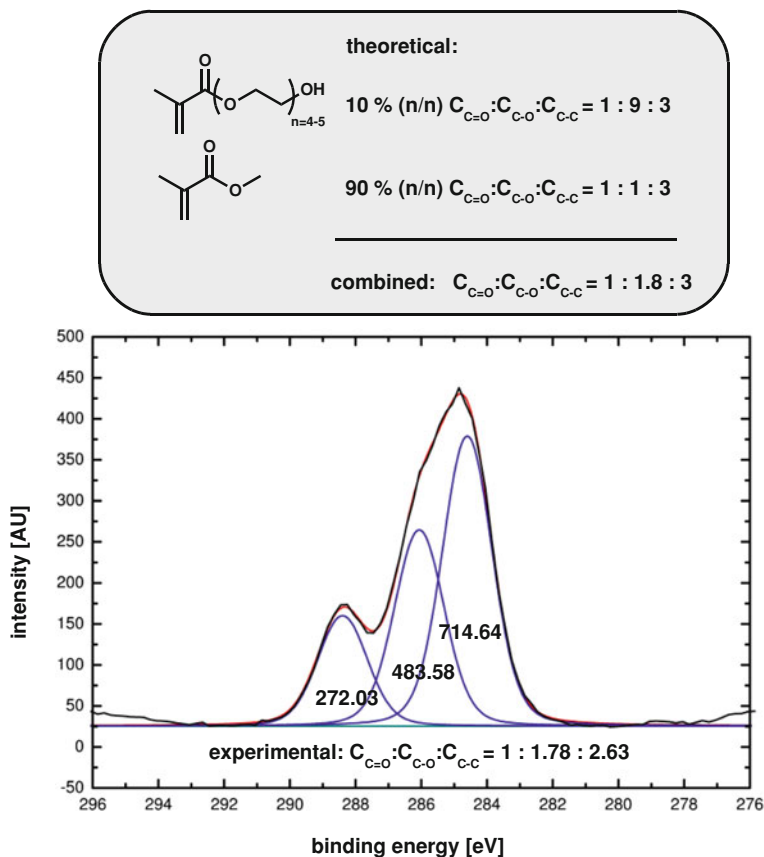


**Fig. 3.5** Quantitative analysis of the C1s area of a 10:90-PEGMA-co-PMMA film on Si(100). The wafer was polymerized with a solution containing 10 % (n/n) PEGMA and 90 % (n/n) MMA which, in a statistical polymerization, should result in a  $C_{C=O}:C_{C-O}:C_{C-C}$  peak ratio of 1:1.8:3. The experimental ratio of 1:1.78:2.63 is, thus, in good agreement with respect to the uncertainty in quantification in XPS. Moreover, small variations in the composition can be caused by variations in the PEGMA side-chain length which typically consists of 4 or 5 EG units as estimated on the basis of the number average of the molecular weight ( $M_n$ )

However, the initial density of amino groups in a “two-dimensional” SAM is assumedly lower than in a “three-dimensional” graft polymer coating. This, in turn, directly affects the total amount of peptide that can be synthesized on a SAM. On the other hand, SAMs are extremely versatile and their properties can be changed with minimum effort [19–21]. Furthermore, a peptide standing out from a two dimensional surface is expected to be more easily accessible to a reaction partner than a peptide embedded in the three-dimensional network of a polymeric film. Therefore, in this work SAMs were applied as a surface coating for the mpSPSS for the first time.

### 3.1.4.1 Initial Considerations

To coat glass slides with a SAM similar to the PEG-NH<sub>2</sub> side-chains of the graft polymer, a combination of two literature-based approaches was considered. In a SPOT synthesis approach, AST et al. pre-modified a cellulose sheet with epibromohydrin and opened the resulting epoxy group with 1,13-diamino-4,7,10-trioxatridecane (DATT) to obtain a homogenous amino coating [22]. Using a bifunctional compound to open the epoxy rings of a 3-(glycidyl)oxypropyl trimethoxysilane (3-GPS) SAM was extensively studied by PIEHLER et al. and SALES et al. [23, 24]. The technique has been further developed by MEHNE et al. to obtain PEG-NH<sub>2</sub> SAMs of mixed chain length for reflectometric interference spectroscopy (RIFS) in the label-free detection of biomolecules [25]. Hence, the synthesis supports for the peptide array synthesis should be silanized with 3-GPS (Fig. 2.13 a) and, then, reacted with DATT to give an amino terminated SAM (Fig. 2.13b). Compared to the PEG diamines used by MEHNE et al. DATT would only provide three EG units. However, SAMs with several EG units were reported to efficiently suppress nonspecific protein adsorption [26], whereby a length of two to three EG units was sufficient [27–29]. In addition, considering a good accessibility for proteins to specifically interact with peptides in the array, a high protein resistance as present in case of PEG chains can probably also be counterproductive: If the protein resistance is too high the antibody could be hindered in reaching the binding site. Hence, starting with a short intermolecular EG<sub>3</sub> spacer was considered logical for biological applications, particularly if standard blocking agents could additionally be applied. With respect to the terminal amino group and the intramolecular EG<sub>3</sub> group the coatings were named AEG<sub>3</sub> SAMs.

### 3.1.4.2 First AEG<sub>3</sub> SAMs on Si(100) and Glass

In the first trial, microscopy slides and pieces of a Si(100) wafer were coated. After standard cleaning and activation by KOH/2-propanol treatment and UV irradiation, respectively, the surfaces were incubated in a 30 mM solution of 3-GPS in anhydrous DCM overnight. After subsequent washing, the supports were reacted with a 20 % (v/v) solution of DATT in anhydrous DMF over 48 h (see Fig. 3.6). Ellipsometry measurements on Si(100) constituted a layer thickness of  $10.0 \pm 1.2 \text{ \AA}$  after 3-GPS self-assembly and a further increase to  $20.2 \pm 3.1 \text{ \AA}$  after DATT coupling. The thickness of the 3-GPS SAM is in good agreement with the results by LUZINOV et al., who reported a thickness ranging from 7 to 10 Å, whereby 10 Å was thought to be closer to a complete monolayer [30]. A more recent publication by WONG et al. determined thicknesses of  $11 \pm 3.5 \text{ \AA}$  by ellipsometry [31]. The composition of the SAM was checked by XPS both on microscopy slide glass and on Si(100). Figure 3.7 shows the C1s and N1s areas of the AEG<sub>3</sub> coatings in comparison with a 10:90-PEGMA-co-PMMA film on Si(100) which was functionalized with a single β-alanine as a reference (10:90-PEGMA-co-PMMA-NH<sub>2</sub>).

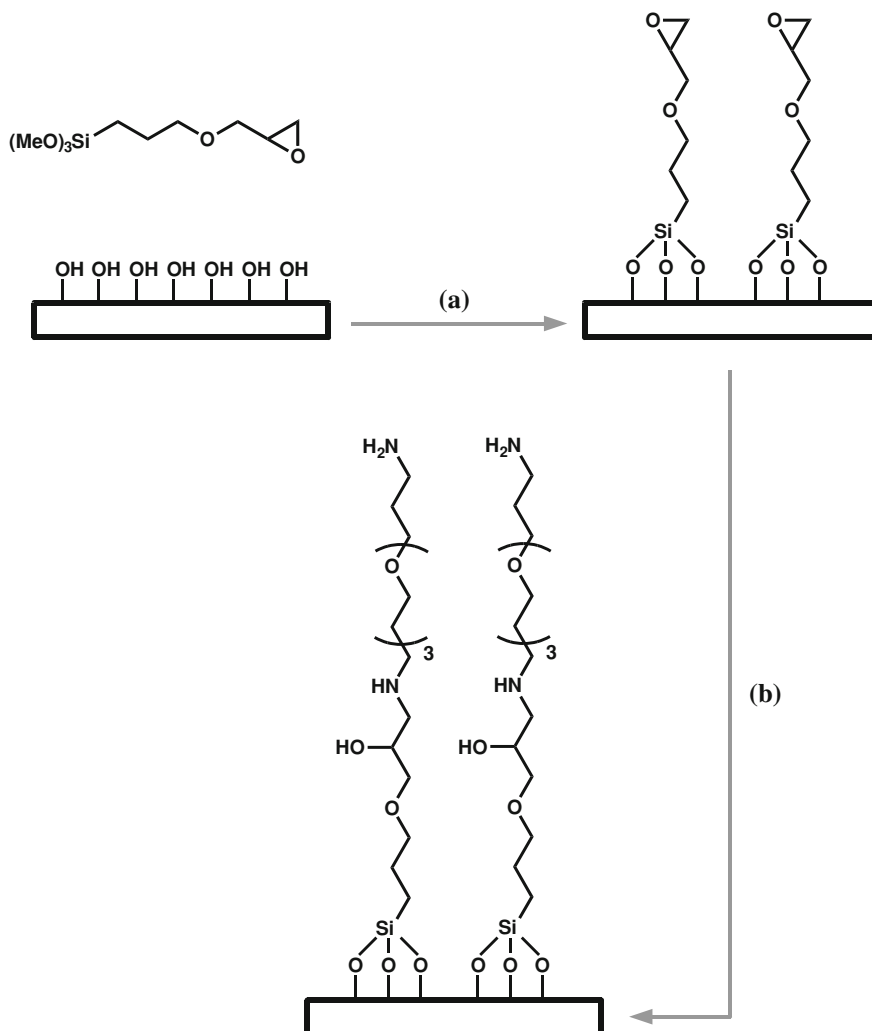


**Fig. 3.6** Coating of substrates with an amino-terminated SAM. **a** The activated substrate is silanized with 3-glycidyloxypropyltrimethoxysilane (3-GPS) which yields an epoxide-terminated SAM. **b** Subsequent epoxide opening with 1,13-diamino-4,7,10-trioxatridecane yields an amino-terminated surface with intramolecular  $\text{EG}_3$  moieties. The coatings were, thus, named  $\text{AEG}_3$  SAMs

As expected, the C1s signal of the two dimensional  $\text{AEG}_3$  SAMs is less intense than the signal for the three dimensional polymeric film. However, a comparison of the N1s areas reveals that, surprisingly, the N1s signal intensity of  $\text{AEG}_3$  SAMs is similar to the N1s signal intensity of a 10:90-PEGMA-co-PMMA film functionalized with a single  $\beta$ -alanine (see Fig. 3.7). This would mean that the amount of amino groups in the SAM is equal to the amount of amino groups available in



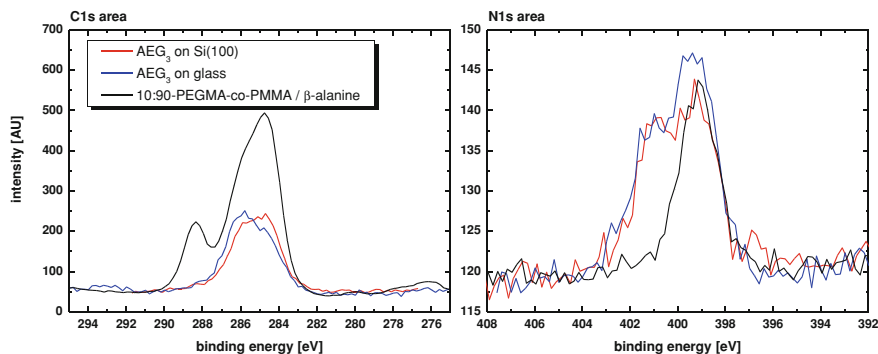


**Fig. 3.7** The C1s and N1s areas of AEG<sub>3</sub> SAMs assembled on Si(100) and microscopy slides in comparison with a 10:90-PEGMA-co-PMMA film on Si(100). The 10:90-PEGMA-co-PMMA film was functionalized with a single  $\beta$ -alanine. As expected, the C1s signal of the two dimensional AEG<sub>3</sub> SAMs is less intense than the signal for the three dimensional polymeric film. Surprisingly the N1s signal intensities of the AEG<sub>3</sub> SAMs are similar to the N1s signal intensity of a 10:90-PEGMA-co-PMMA equipped with a single  $\beta$ -alanine

the 10:90-PEGMA-co-PMMA polymer in which around 2 nmol/cm<sup>2</sup> were determined by the PDBFA method (see Sect. 2.3.1). However, the analytical depth of XPS is typically 7–10 nm (see Sect. 2.3.4) meaning that in a 50 nm polymeric film, at maximum only the upper 20 % of the layer is analyzed. With the analytical techniques available in this work, it could not be determined to which extent PEG-side chains are functionalized with amino groups in the depth of the film, and how accessible such amino groups are in the course of a peptide synthesis.

### 3.1.4.3 Quantitative Analysis and Comparison of AEG<sub>3</sub> SAMs

Comparing the N1s areas of AEG<sub>3</sub> SAMs and polymer in Fig. 3.7, an important difference became apparent. The N1s signals of the AEG<sub>3</sub> SAMs are generally broader than those of the 10:90-PEGMA-co-PMMA-NH<sub>2</sub> film. The AEG<sub>3</sub> N1s signals consist of at least two peaks, probably caused by two different chemical binding states. A quantification of the C1s and N1s areas of the three surfaces is depicted in Fig. 3.8. The N1s area of the AEG<sub>3</sub> SAMs consists of two peaks around 399 and 401 eV respectively. The peak at lower binding energy obviously appears at a similar binding energy as the signal of the amino group in the 10:90-PEGMA-co-PMMA-NH<sub>2</sub> film (399.13 eV on Si(100)). A quantitative comparison of both N1s peaks on Si(100) constitutes a N<sub>401</sub>:N<sub>399</sub> ratio of 0.86:1. Since no other nitrogen species should be present in the AEG<sub>3</sub> SAMs, the second signal at 401 eV is thought to be caused by the secondary amine in the chain. The slightly smaller N1s intensity from the in-chain amine could be explained by higher intensities for near-surface atoms which in the AEG<sub>3</sub> SAMs presumably come from free NH<sub>2</sub> groups (see Fig. 3.8). However, further angle-resolved XPS measurements would

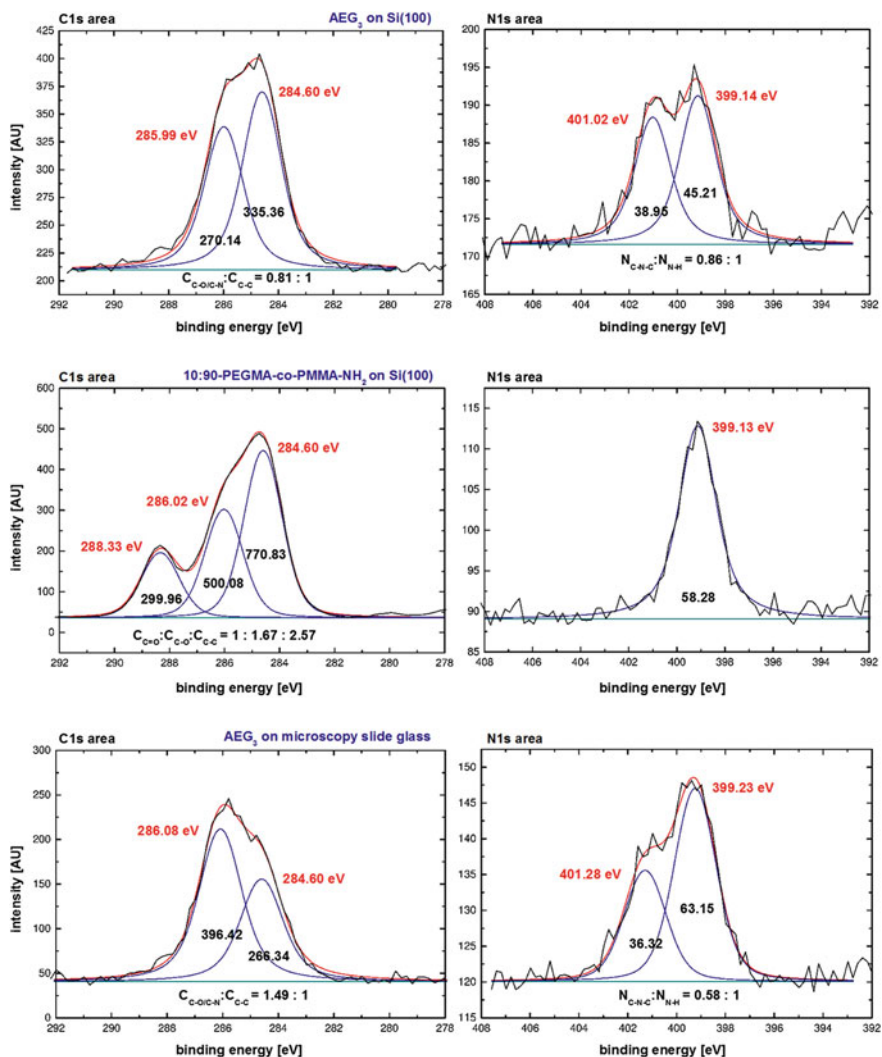


**Fig. 3.8** Quantitative comparison of AEG<sub>3</sub> SAMs on Si(100) and microscopy slide glass with a 10:90-PEGMA-co-PMMA-NH<sub>2</sub> film on Si(100) in XPS. For each surface type the C1s and N1s areas are depicted. Peak centers are depicted in red figures and peak areas in black figures. Peak ratios are stated below the baseline

be needed to determine the exact SAM conformation which was not within the focus of this work.

Comparing the N1s and C1s areas of the AEG<sub>3</sub> SAM on Si(100) with that on microscopy slide glass, a higher intensity of amino peak (N<sub>N-H</sub> peak) in the N1s area as well as a higher C<sub>C-O</sub>:C<sub>C-C</sub> ratio of 1.49:1 is observed on the microscopy

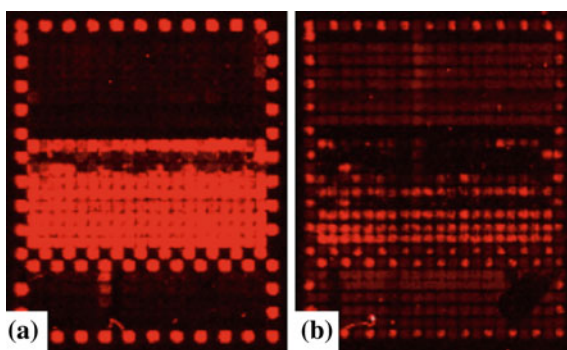
slides. This finding could hint at a higher degree of functionalization with DATT on the microscopy slide glass.

In the second step of the SAM preparation (see Fig. 3.6b), DATT is used to open the epoxides of the 3-GPS SAMs which is evidently a time and temperature dependent process [22]. From the molecular structure (see Fig. 3.6), a theoretical  $C_{C-O}:C_{C-C}$  ratio of 2:1 would be expected for 3-GPS SAMs, whereas for the AEG<sub>3</sub> SAMs the same ratio should increase to 3:1. Although the experimental  $C_{C-O}:C_{C-C}$  ratios are generally lower, which in addition to the discussed angle-dependence in XPS probably indicates incomplete reaction with DATT, a higher intensity of the  $N_{N-H}$  peak at 399 eV corresponding to a higher  $C_{C-O}:C_{C-C}$  ratio was frequently observed in the preparation of these SAMs. On the microscopy slide in Fig. 3.7 the  $N_{N-H}$  peak area was even greater than the corresponding area of the 10:90-PEGMA-co-PMMA-NH<sub>2</sub> reference providing sufficient evidence to indicate that a peptide array synthesis on AEG<sub>3</sub> SAMs was considered technically feasible.

#### 3.1.4.4 Peptide Array Synthesis on AEG<sub>3</sub> SAMs

The first laser printer (see Sect. 1.2.2) was capable of printing directly on microscopy glass slides if a mask was used to fix the slides in a  $22 \times 21 \text{ cm}^2$  arrangement. Hence, microscopy slides with the new AEG<sub>3</sub> SAM and 10:90-PEGMA-co-PMMA-NH<sub>2</sub> films could be simultaneously applied in a peptide array synthesis to compare the surface quality. A reference array printed on each surface type containing permutations of the HA epitope (YPYDVPDYA) as well as the wild-type epitope was immunostained with the IRDye 700DX–anti–HA conjugate (see Sect. 5.3.10). Thereby, synthesis, staining, and readout with the *Odyssey Infrared Imager* were simultaneously performed under the same conditions. The fluorescence image revealed good signals on the AEG<sub>3</sub> SAM (Fig. 3.9a), whereas on the 10:90-PEGMA-co-PMMA–NH<sub>2</sub> film the fluorescence intensity was lower (Fig. 3.9b). It must be mentioned that at the time these images were obtained the quality of the 10:90-PEGMA-co-PMMA was below the current standard (for improvements in the synthesis see Sect. 3.1.3).

**Fig. 3.9** Comparison of a peptide array synthesized on an AEG<sub>3</sub> SAM (a), with the same array synthesized on 10:90-PEGMA-co-PMMA–NH<sub>2</sub> (b). Both arrays were immunostained with the IRDye 700DX- antiHA conjugate



Nevertheless, the AEG<sub>3</sub> SAMs seemed to be an especially promising alternative for the peptide array synthesis, because they are fairly easy to prepare. In fact, further XPS measurements suggest that the  $N_{N-C-N}:N_{N-H}$  and  $C_{C-O}:C_{C-C}$  ratios are a quality criterion for the AEG<sub>3</sub> SAMs in regards to a peptide array synthesis. A rather small  $N_{N-C-N}:N_{N-H}$  ratio and a high  $C_{C-O}:C_{C-C}$  ratio come along with a high intensity of the  $N_{N-H}$  peak. This, in turn, means higher functional group loading which is assumed to increase the overall peptide yield. A fresh AEG<sub>3</sub>-coated microscopy slide and a slide bearing a peptide array were analyzed by XPS. Both slides were from the same batch as the slide the array depicted in Fig. 3.9 was synthesized on. On the unreacted AEG<sub>3</sub> SAM, the measurements showed a comparatively small  $N_{N-C-N}:N_{N-H}$  ratio of 0.34:1 and a high  $C_{C-O}:C_{C-C}$  ratio of 1.62:1 as depicted in Fig. 3.10. On the array slide, the presence of peptides became visible in the C1s and N1s areas of the spectrum. In the C1s area, an additional carboxyl  $C_{C=O}$  signal appeared at 288.19 eV and the ratio of  $C_{C-O}:C_{C-C}$  significantly changed to a higher  $C_{C-C}$  fraction (see Fig. 3.10). In the N1s area, the  $N_{N-H}$  peak gained intensity, whereas the  $N_{C-N-C}$  peak of the AEG<sub>3</sub> SAM lost intensity.

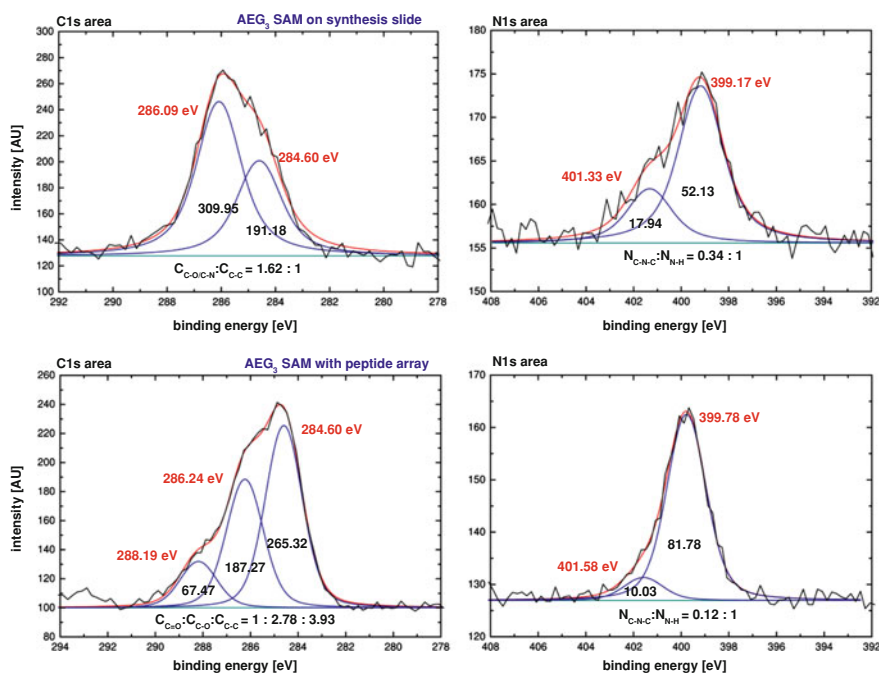


**Fig. 3.10** Quantitative analysis of the C1s and N1s areas of an AEG<sub>3</sub> SAM on glass before and after a peptide array synthesis. The peptide array synthesis caused a change in signal shape. In the C1s area, an additional carboxyl ( $C_{C=O}$ ) peak appeared. In the N1s area, an increased intensity of the amino-signal ( $N_{N-H}$ ) was detected. The amide signal of the peptide bond apparently occurs at similar binding energy (399.78 eV) and dominates the signal intensity. Peak centers are depicted in red figures, peak areas in black figures. Peak ratios are stated below the baseline

Apparently, the binding energies of amino and amide N1s electrons in peptides are very similar. Only one peak is usually detected in peptide SAMs [32]. The device specific X-ray spot size is around  $4 \times 8 \text{ mm}^2$ , which ensured that both peptide spots and untreated AEG<sub>3</sub> SAM (“background”) were always analyzed.

### 3.1.4.5 Parameters Determining the Quality of AEG<sub>3</sub> SAMs

In the preparation of the “high-quality” AEG<sub>3</sub> SAMs which were successfully applied in the peptide array synthesis (see Fig. 3.10) an amendment had been made to the preparation protocol. Instead of assembling the 3-GPS SAM from solution, two microscopy slides were coated with 50  $\mu\text{L}$  of the pure substance. This was done by placing the clean and dry slides on top of each other with 3-GPS in between as suggested by MEHNE et al. (“sandwich technique”) [25]. The resulting “good” AEG<sub>3</sub> SAM quality (see Fig. 3.10, reference slide) is in good agreement with LUZINOV et al. who reported a decreasing 3-GPS SAM quality as less 3-GPS was used in their solution approach [30]. Formation of multilayers for low 3-GPS concentrations was explained by a high loss of 3-GPS due to hydrolyzation. Therefore, it can be assumed that the less water is present in the solvents and the more careful the surfaces are dried the better is the resulting 3-GPS film quality even if assembled from solution. Hence, a silanization with a thoroughly dried Si(100) substrate and anhydrous DCM was conducted. The substrate was immediately immersed in the DMF/DATT solution after washing with dry DCM. The resulting AEG<sub>3</sub> SAM showed a C<sub>C-O</sub>:C<sub>C-C</sub> ratio of 2.21:1 and a corresponding high N<sub>N-H</sub> peak (see Fig. 3.11) which was better than previously achieved.

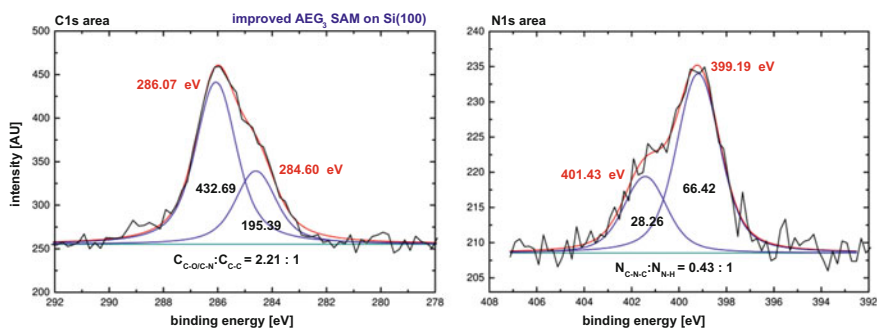


**Fig. 3.11** Quantitative comparison of the C1s and N1s peak areas of an improved AEG<sub>3</sub> SAM on Si(100). The 3-GPS SAM was assembled after thorough drying of the substrate and adsorbed from anhydrous DCM. The reaction conditions with DATT were unchanged. Peak centers are depicted in red figures, peak areas in black figures. Peak ratios are stated below the baseline

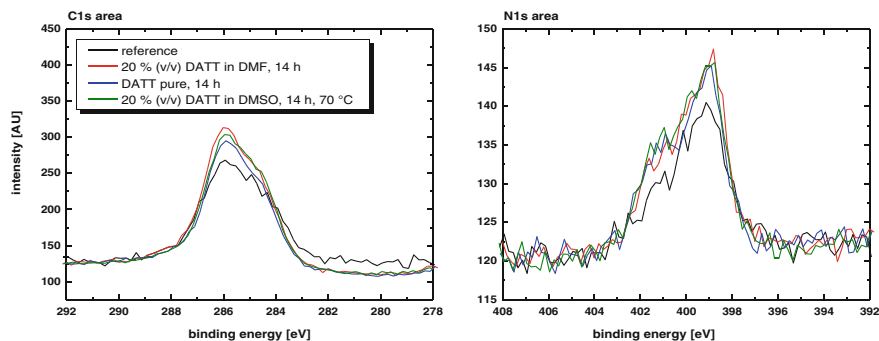


**Fig. 3.12** The C1s and N1s areas of AEG<sub>3</sub> SAMs on microscopy slides. In the two step synthesis, the 3-GPS SAM of the three slides (*red*, *blue*, and *green* signals) was assembled from solution after thorough drying of the substrates. The slides were then reacted with DATT according to the stated conditions. The *black* line is the reference surface prepared by the “sandwich” technique on which a peptide array synthesis had been successful (see Fig. 3.10). In summary, the reaction with DATT seems to be less critical than the 3-GPS assembly

In the two step reaction yielding AEG<sub>3</sub> SAMs, the assembly of the 3-GPS SAM is probably crucial for the overall quality of the monolayer. To investigate the role of DATT in the reaction, microscopy slides which were simultaneously coated with 3-GPS were reacted with DATT under different conditions. In general, the reaction time was shortened to 14 h. Figure 3.12 shows a comparison of the corresponding C1s and N1s areas with the spectrum of the “reference” SAM which was prepared by the “sandwich” technique and on which a peptide array synthesis was apparently feasible (see Fig. 3.10). As visible in Fig. 3.12, the different reaction conditions do not influence the AEG<sub>3</sub> SAM quality. In contrast, the improved 3-GPS assembly probably leads to higher signal intensities for all newly prepared surfaces. The reaction time can obviously be limited to overnight reactions (also see Sect. 5.3.1.6).

### 3.1.4.6 Summary

In summary, the implementation of AEG<sub>3</sub> SAMs as an alternative surface coating for the peptide synthesis looks promising. The stability of the AEG<sub>3</sub> SAMs was apparently good which is in good agreement with WANG et al. who reported increasing stability of amino-terminated SAMs the longer the intramolecular spacer between head and tail group [33]. A high stability of the coating is crucial for the peptide array synthesis and subsequent biological applications. Furthermore, a high C<sub>C=O</sub>:C<sub>C-C</sub> ratio and a high N<sub>N-H</sub> peak in XPS are critical parameters which seem to hint at a high loading of functional groups. Here, the silanization of the substrate with 3-GPS probably determines the quality of the AEG<sub>3</sub> SAMs. The silanization has been extensively studied in literature, and was therefore not further investigated [23, 30, 31]. However, up-scaling of the reaction to coat the

22 × 21 cm<sup>2</sup> laser printer slides is still an on-going process. So far, only “lower quality” coatings could be achieved even if higher concentrations of 3-GPS in the silanization step were applied. This was presumably caused by a high rest-humidity in the large synthesis containers (see Sect. 3.1.3, Fig. 3.4). In solving these problems, carefully dried substrates, solvents, and reaction containers as well as a further increase in 3-GPS concentration could help. Moreover, according to SALES et al., a synthesis of the AEG<sub>3</sub> silane from 3-GPS and DATT before self-assembly could also lead to an increased density of functional groups [24].

In this work, AEG<sub>3</sub> SAMs were applied solely in the microscopy slide format. Here, high-quality SAMs could be routinely achieved as described above. However, regarding AEG<sub>3</sub> SAMs as a standard coating for peptide array supports, further results will have to show if they can outperform the PEGMA-co-PMMA films. Most likely, a choice of the surface coating dependent on the application of the peptide array would be reasonable. In most cases, the right balance of intrinsic protein repelling properties to block nonspecific background and specific access of analyte molecules will be crucial.

## 3.2 Cleavable Linkers

### 3.2.1 Choice of Cleavable Linkers

In this work, an acid-labile linker and a safety-catch linker were chosen in regard to facilitate peptide cleavage from the array support.

#### 3.2.1.1 RAM Linker

The RINK amide (RAM) linker (Fig. 2.14d) [34, 35] was selected because amide-type linkers are, in general, easy to cleave, show good cleaving efficiencies, and are routinely applied in SPPS [36, 37]. Furthermore, the Fmoc-RAM linker is commercially available as a free carboxylic acid, whereas ester-type linkers are typically available as resin-bound compounds. Thus, the RAM linker could be directly coupled to an amino-terminated synthesis surface using standard DIC/*N*-methylimidazole (NMI) activation (see Fig. 1.3). Moreover, the RAM linker had been successfully used on amino-terminated PEGMA (PEGMA-NH<sub>2</sub>) graft coatings in previous works to release and characterize peptide epitopes via mass spectrometry and HPLC [38–40]. Therefore, the RAM linker was considered to be directly applicable in the peptide array purification.

### 3.2.1.2 HBA Linker

A versatile linker from the group of safety-catch linkers is Fmoc-HBA (Fig. 2.14 e). The major advantage of this linker over standard acid-labile linkers is the mild cleaving conditions which would allow for various key/lock systems (including biological systems such as biotin/streptavidin) in the peptide transfer (see Fig. 2.12 ). After oxidation of the hydrazine bond to the reactive diazene intermediate using *N*-bromosuccinimide (NBS)/pyridine (py),  $\text{Cu}(\text{OAc})_2/N$ -propylamine or  $\text{Cu}(\text{OAc})_2/\text{py}$ , the diazene bond is susceptible to cleavage by nucleophiles (Nu) such as  $\text{OH}^-$  in water (see Fig. 3.15) [41]. Furthermore, Fmoc-HBA is also commercially available as a free carboxylic acid that could be directly reacted with the amino-terminated synthesis surfaces. Due to the sterically challenging benzoic acid, PyBOP/HOBt activation with *N,N*-diisopropylethylamine (DIPEA), as suggested by BERST et al. [42], should be used to obtain an efficient loading of the support. The carboxy FRANK linker (see Fig. 2.14f) which had also been designed for a peptide release in aqueous buffers [43], was communicated to show varying cleavage efficiencies, probably dependent on the first amino acid added to the chain. Therefore, this linker was not considered to be a candidate for the development of the peptide array purification method.

### 3.2.1.3 Implementation in the Peptide Array Synthesis

Figure 3.13 shows, how the cleavable linkers should be implemented in the synthesis strategy. After functionalization of the synthesis surface with amino groups either the Fmoc-RAM or the Fmoc-HBA linker should be coupled to the support. The linkers would then have to withstand the entire mpSPPS including heating steps, acylation, and Fmoc deprotection, until the peptides were fully assembled.

According to the purification concept (see Fig. 2.12), the array members should be released after attaching a key sequence to the full-length array members. Both the target surface and the key/lock system would have to be selected on the basis of the cleavage conditions. Hence, the cleavable linker would define the overall conditions for the purification method. In addition, the key/lock system would have to be compatible with the target surface. Regarding versatile key/lock chemistry, the HBA linker was the favored candidate because it should allow for cleavage in aqueous solution, whereas the RAM linker requires the presence of acids.

## 3.2.2 Coupling of Cleavable Linkers

To investigate the conditions of RAM or HBA linker coupling, the standard 10:90-PEGMA-co-PMMA-NH<sub>2</sub> coatings were chosen. Although these surfaces provide a lower amino group density per cm<sup>2</sup> than the pure PEGMA-NH<sub>2</sub> coatings [10, 44],



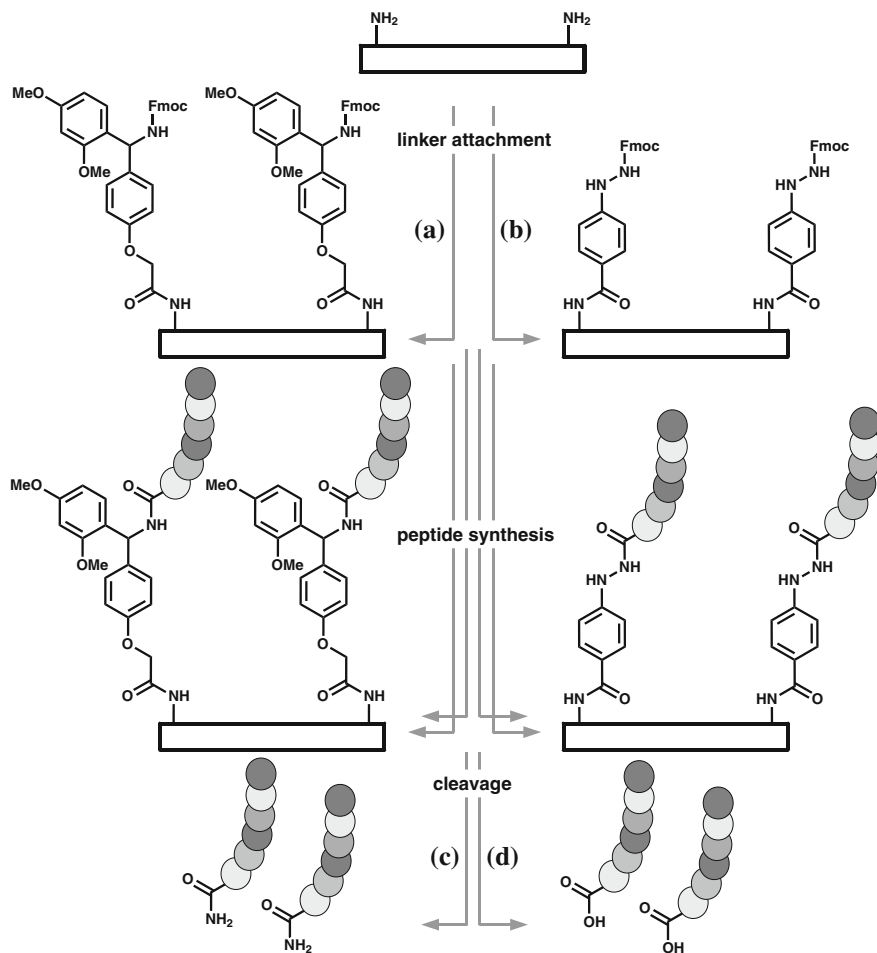


**Fig. 3.13** Implementation of cleavable linkers in the peptide array synthesis. Starting from amino-terminated supports, either the Fmoc-RAM or the Fmoc-HBA linker is coupled to the surface prior to peptide synthesis. **a** The Fmoc-RAM linker is coupled with DIC/NMI. **b** The Fmoc-HBA linker is coupled using PyBOP/HOBt/DIPEA. **c** The RAM linker is cleaved with TFA yielding peptide amides. **d** The Fmoc-HBA linker is oxidized with NBS/py and then cleaved in aqueous buffer yielding free carboxylic acids

they are reference synthesis surfaces on which the peptide array synthesis is routinely performed. Since the purification method should be mainly adapted to arrays synthesized with the laser printer, a variation of the synthesis surface was not considered reasonable. Moreover, the synthesis of the 10:90-PEGMA-co-PMMA films had been optimized to yield a reproducible film quality (Sect. 3.1.3).

After functionalization of the 10:90-PEGMA-co-PMMA films with Fmoc- $\beta$ -alanine the density of amino groups was typically determined by the PDFA

method (see Sect. 2.3.1). Typical values for the DG on a microscopy slide ( $19.76 \text{ cm}^2$ ), calculated with Equation 1, were varying between 1.5 and  $2.5 \text{ nmol/cm}^2$ . To couple the Fmoc-RAM linker, a 0.1 M solution activated with 1.2 eq DIC and 2.0 eq NMI was used. For the Fmoc-HBA-linker, a 0.1 M solution activated with 1.0 eq PyBOP, 1.0 eq HOBt, and 2.0 eq DIPEA was applied. In the subsequent capping step (see Fig. 1.11), slides with the Fmoc-RAM linker were regularly acylated, but slides with the Fmoc-HBA linker were capped with the sterically hindered pivalic anhydride (PVA) to prevent acylation of the HBA linker [45]. After attachment of the respective linker, the DG was again calculated in the course of the Fmoc cleavage. According to this data, the RAM linker could be coupled to synthesis slides in up to 90 % yield, whereas the HBA-linker gave up to 70 % yield. However the PDFA method was not considered to give exact quantities because a variation in extinctions for different samples of the same batch was frequently observed (also see Sect. 2.3.1). Presumably, various parameters such as ambient conditions, handling of the samples, cuvettes, and pipette tips have an impact on the measured extinction. In general, the extinctions measured on 10:90-PEGMA-co-PMMA films were close to the detection limit of the photometer. Furthermore, the equilibrium between PDFA and dibenzofulvene/piperidine is assumed to affect the experimental results [46]. Hence, all coupling efficiencies calculated on the basis of the PDFA method for the 10:90-PEGMA-co-PMMA-NH<sub>2</sub> coatings were considered as approximate figures which help to decide whether the coupling was successful or not. In the present work, only surfaces were applied on which a DG of  $>0.5 \text{ nmol/cm}^2$  after linker coupling was determined.

In summary, both linkers could be coupled to the standard synthesis surface in acceptable yield. A DG of  $>0.5 \text{ nmol/cm}^2$  was considered to be sufficient for the synthesis and detection of at least 10 meric peptides. However, the Fmoc-HBA linker typically coupled with lower efficiency than the Fmoc-RAM linker. In principle, the DG could have been calculated more precisely by using PEGMA-NH<sub>2</sub> synthesis supports with higher starting densities of amino groups (up to  $40 \text{ nmol/cm}^2$ ). These surfaces were applied in previous works to determine coupling efficiencies in the synthesis of peptides [38–40]. However, the PEGMA-NH<sub>2</sub> surfaces have completely different surface properties, e.g. swelling behaviour, which were not comparable to the standard synthesis surfaces. For example, pre-swelling of the PEGMA-NH<sub>2</sub> films in DMF vapour was reported to produce higher coupling efficiencies which is thought to be an effect of higher film thicknesses and a higher amino group loading [39]. In contrast, no noticeable difference in coupling efficiencies upon pre-swelling of the approximately 50 nm-thick 10:90-PEGMA-co-PMMA was observed in the present work. In addition, pre-swelling of the polymeric films to obtain higher coupling efficiencies [39] was technically not feasible in the laser printer approach. Irrespective of this, uncertainties in the PDFA method were also reported for the PEGMA-NH<sub>2</sub> surfaces [40].

### 3.2.3 Cleavage Efficiency of the HBA Linker

As described above, HBA was the favored linker candidate because it would ideally allow for release of peptides under physiological conditions. Moreover, the cleavage with NBS/py was preferred over a cleavage with  $\text{Cu}(\text{OAc})_2$  because the former was considered to allow for a separation of diazene formation and peptide cleavage (“safety-catch” route, Fig. 3.15a, b). This would mean that the receptor surface in the peptide transfer is not exposed to the NBS/py solution. However, it was communicated that the cleavage efficiency of the HBA linker was lacking compared to the cleavage efficiency of the RAM linker [47]. Cleaving efficiencies below 40 % were determined by the PDFFA method (see Sect. 2.3.1) in the cleavage of Fmoc-GG dipeptides from cellulose sheets (see Fig. 3.14). The cleavage experiments had been conducted by a co-worker prior to the present work, whereby the cellulose had been modified according to the protocol in his Ph.D. thesis [39, 47]. Compared to the 10:90-PEGMA-co-PMMA coatings cellulose can be modified with much higher amino group densities which is why cellulose is, for instance, applied in the SPOT synthesis [48, 49].

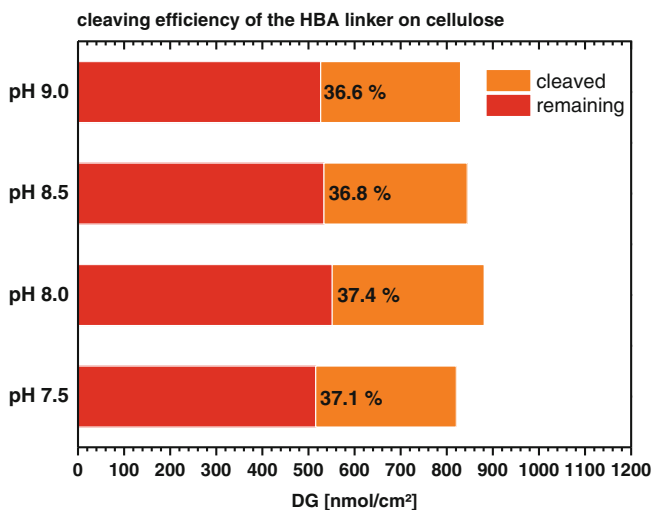


**Fig. 3.14** Cleavage efficiency of the HBA linker on cellulose sheets dependent on the pH of the buffer solution. The depicted cleavage efficiencies were determined prior to the present work [47]. Cellulose modification was administered according to established protocols [39]. Cellulose sheets were first functionalized with the HBA linker. Subsequently, Fmoc-GG was coupled to the cellulose. The HBA linker was oxidized with NBS/py and the peptides were cleaved in phosphate buffer (pH 8.0, 0.07 M) overnight. The DG was calculated before and after the cleavage based on the PDFFA method

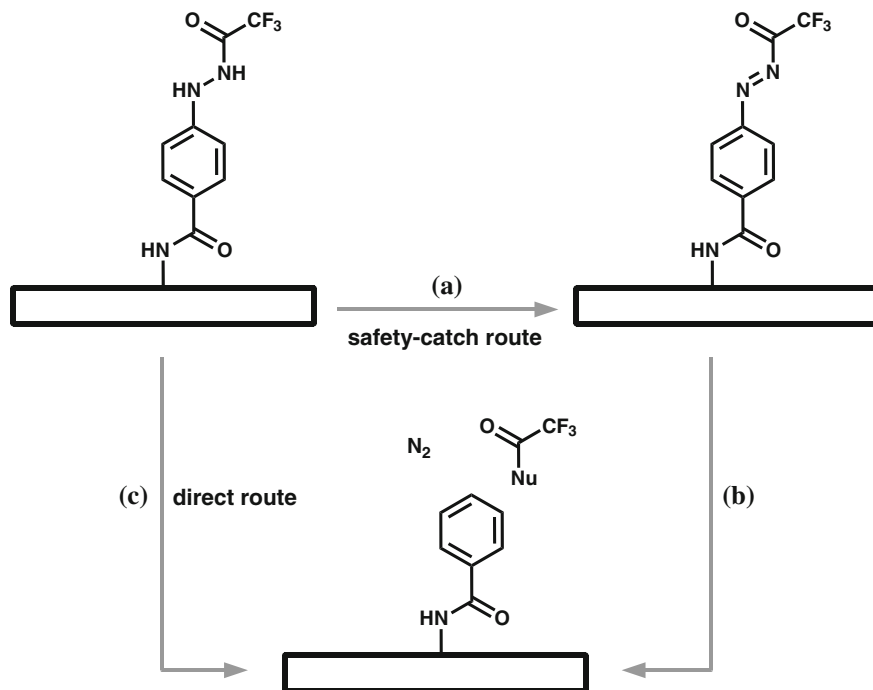


**Fig. 3.15** Schematic of the HBA cleavage with a fluorine marker attached to the linker. Two routes are possible: The safety-catch route with an oxidation step and subsequent cleavage with aqueous buffer (Nu = OH<sup>-</sup>) or the direct route where oxidation and cleavage are performed in one step. **a** NBS/py/DCM, **b** aqueous buffer, pH 8.0, **c** Cu(OAc)<sub>2</sub>/*N*-propylamine or Cu(OAc)<sub>2</sub>/py/MeOH. In both routes, TFA and nitrogen are finally released from the surface

### 3.2.3.1 Determination of the HBA Cleavage Efficiency by XPS

Since the PDFA method was not considered to give reliable results on 10:90-PEGMA-co-PMMA-NH<sub>2</sub> films due to much lower DGs, the cleavage efficiency of the HBA linker was pre-examined by XPS measurements. Si(100) wafers were coated with a standard 10:90-PEGMA-co-PMMA-NH<sub>2</sub> film. The polymer film was subsequently modified with the HBA linker. To monitor the cleavage efficiency in XPS, a trifluoroacetyl (TFAC) moiety was directly coupled to the hydrazine moiety after Fmoc cleavage using trifluoroacetic acid anhydride (TFAA) in absolute THF. The TFAC moiety should be released upon linker cleavage, whereby a loss of F1s signal intensity would indicate the cleavage (see Fig. 3.15).

Before each experiment, the modified wafer was cut into two pieces. One piece was kept under Ar atmosphere as a reference, while the second piece was oxidized. To follow the safety-catch route, the oxidation was conducted with a 10 mM solution of NBS and 16 mM py (in absolute DCM for 10 min at RT) providing an excess of oxidizing agents over the substrate. However, with respect to the marker

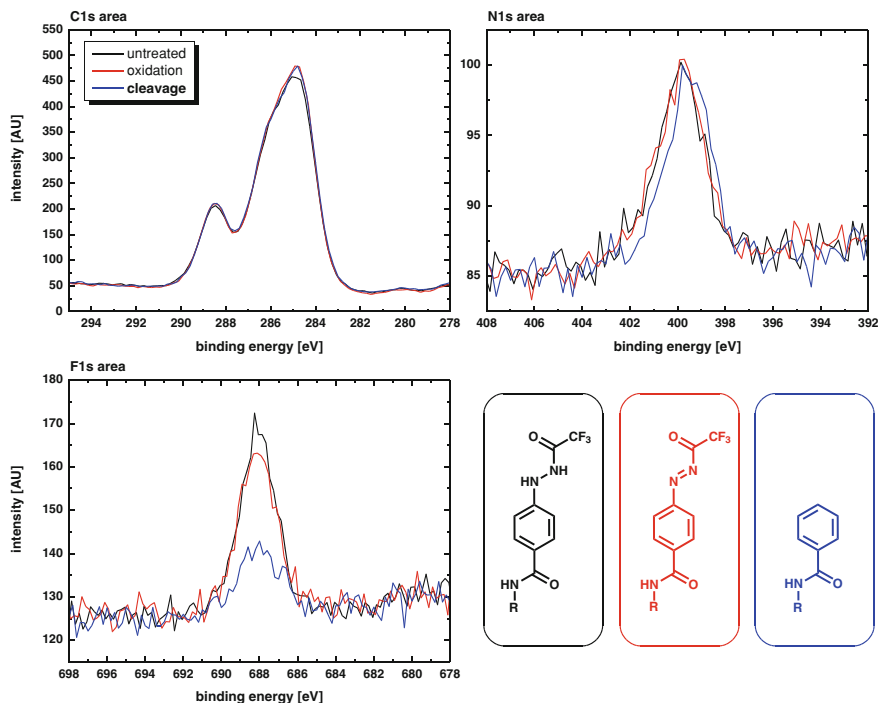


**Fig. 3.16** C1s, N1s, and F1s areas at different stages of the HBA linker cleavage. TFAc was attached to the hydrazine moiety as a marker. The F1s signal intensity only slightly decreased upon oxidation, but a significant loss was detected after overnight cleavage in aqueous buffer. This probably indicates a release of TFA

side-reactions were considered unlikely. The oxidized piece of wafer was again cut into two pieces. One was stored under Ar atmosphere the other was gently rocked in phosphate buffer (pH 8.0, 0.07 M, 0.05 % (v/v) TWEEN 20) overnight for marker cleavage. Subsequently, XP spectra of all three wafer pieces were measured. Fig. 3.16 shows the C1s, N1s, and F1s areas in the course of a cleavage experiment. Only a small decrease in F1s signal intensity was observed upon oxidation, whereas after overnight cleavage the signal was significantly less intense. In contrast, the signal intensity in the N1s and C1s areas remained almost unchanged. This could be explained by a high “background” from the surface coating which, most likely, obscures any changes in the relatively small signals which would indicate loss of carbon/nitrogen upon cleavage. However, a marginal shift of the N1s signal to lower binding energies was observed after cleavage which could be due to nitrogen release (see Fig. 3.15).

To determine the cleavage efficiency, the F1s and N1s signals were quantitatively analyzed. Determined peak areas and binding energies are depicted in Fig. 3.17. Merely based on the F1s signal intensities, the effective release of TFAc amounted to 62 %, whereby a loss of around 7 % already occurred in the oxidation

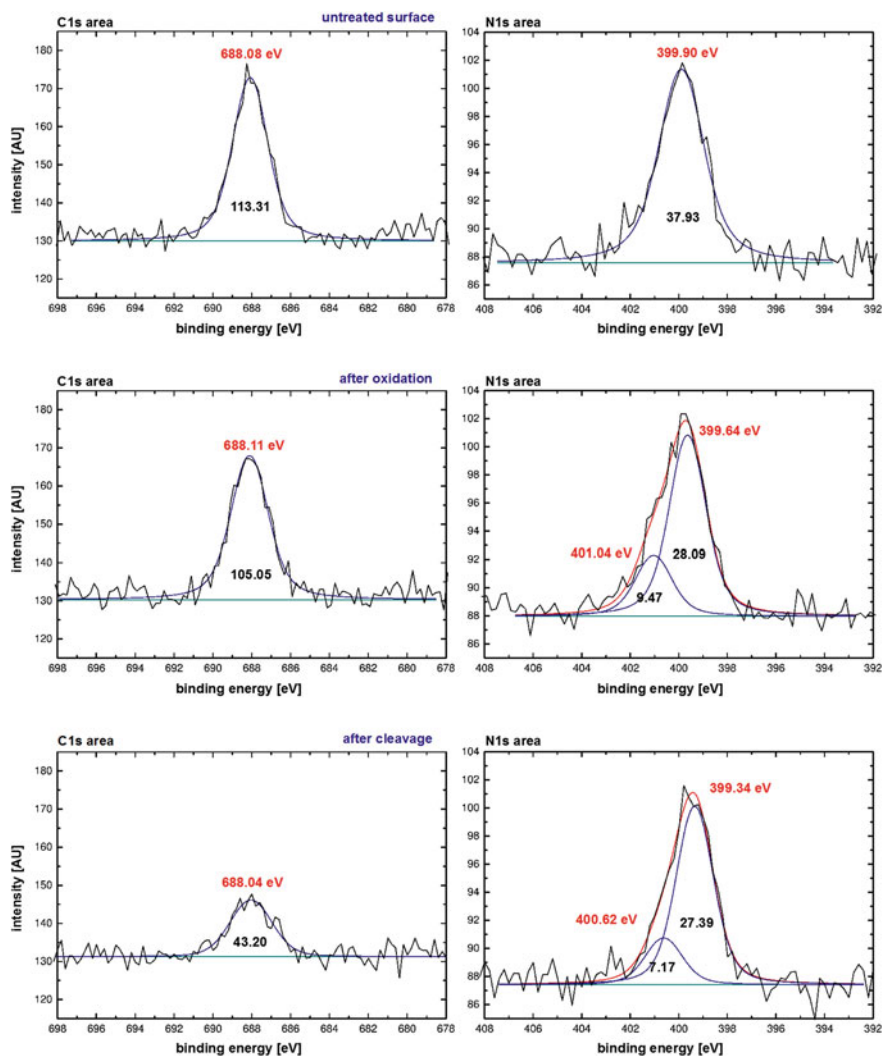


**Fig. 3.17** Quantitative analysis of the F1s and N1s areas at different stages of the HBA linker cleavage. Merely based on the F1s signal intensities, a cleavage efficiency of about 62 % was determined. However, a loss of about 7 % was already observed upon oxidation of the sample which means a controlled compound release of 55 %. In the N1s area, no noticeable loss in signal intensity was observed. However, the N1s signal intensity was comparatively low and, thus, difficult to analyze. Most of the N1s signal intensity probably arose from the  $\beta$ -alanine modification of the surface. Peak centers are depicted in red figures, peak areas in black figures

step. Taking the slightly different C1s signal intensity into account, the cleavage efficiency was also calculated from the F:C ratio (see Eq. 2.12). Therefore, the overall intensity of a respective signal (AUC of the C1s and F1s area, respectively)

**Table 3.1** Cleavage efficiency of the HBA linker calculated from the F:C ratio determined in XPS. The corresponding F1s areas are depicted in Fig. 3.17. The quantification of the C1s signals is not shown

Sample	AUC C1s	AUC F1s	F:C ratio	Amount of TFAC cleaved
Reference	1472.57178	113.30789	0.02116	–
Oxidized	1525.39660	105.05450	0.01894	10.5 %
Cleaved	1503.32625	43.19780	0.00790	62.7 %

was divided by the product of ionization cross-section and attenuation length (see Table 5.6) to obtain relative intensities.

However, the cleavage efficiency obtained from this calculation only slightly varied from the previous value: 63 % of TFAC were cleaved, 11 % were already lost in the oxidation step (see Table 3.1). With respect to the measuring accuracy in XPS, the controlled release of TFAC amounts to about 50 % which is somewhat higher than the cleavage efficiency determined by the PDFFA method (see Fig. 3.14). Most likely, the loss of TFAC in the oxidation step is caused by rest-humidity which could not completely be avoided. However, a reproducible cleavage efficiency of above 50 % would make the linker a potential candidate for the peptide purification. The advantage of a mild cleavage would have to be traded off against a loss of peptide because of incomplete cleavage.

In contrast to peptides, the cleavage of a TFAC moiety is probably easier. Since the  $\text{CF}_3$  moiety in TFAC has a strong electron-withdrawing effect, nucleophilic attack on the carboxy carbon is favored.

To determine if the cleavage efficiencies were lower when amino acids were coupled to the HBA linker, the XPS experiment was repeated with different amino acids coupled between linker and TFAC marker. Lys, Phe, and Asp were coupled using a 0.1 M solution of the O<sub>2</sub>Pfp-activated amino acid in anhydrous DMF. The O<sub>2</sub>Pfp-esters were chosen to apply the same carboxyl-activation as used in the mpSPPS. To allow for a direct comparison, all reactions were conducted in the same container except for the amino acid coupling. Moreover, pieces of the same modified Si(100) wafer were used. Oxidation and cleavage were conducted as before. Fig. 3.18 shows a comparison of the F1s areas measured in this experiment with the F1s areas obtained in the previous experiment where TFAC was directly linked to the HBA linker. Obviously, the amount of TFAC was noticeably reduced if an amino acid was coupled to the HBA linker prior to TFAC. Although the cleavage apparently worked in the presence of all three amino acids, the F1s signal intensities were too low for a meaningful quantification of the cleavage efficiency.

In contrast, no remarkable difference in the signal intensities was observed in the N1s areas (see Fig. 3.19). The density of amino groups in the polymeric film appeared to be nearly constant. Thus, the decreased F1s signal intensity was assumed to arise from coupling an amino acid to the HBA linker. The attachment of the fluorine marker using TFAA was not thought to be crucial because the anhydride readily reacts with amino groups. Difficulties in the coupling amino acids to the HBA linker would stand against an application of this linker in the

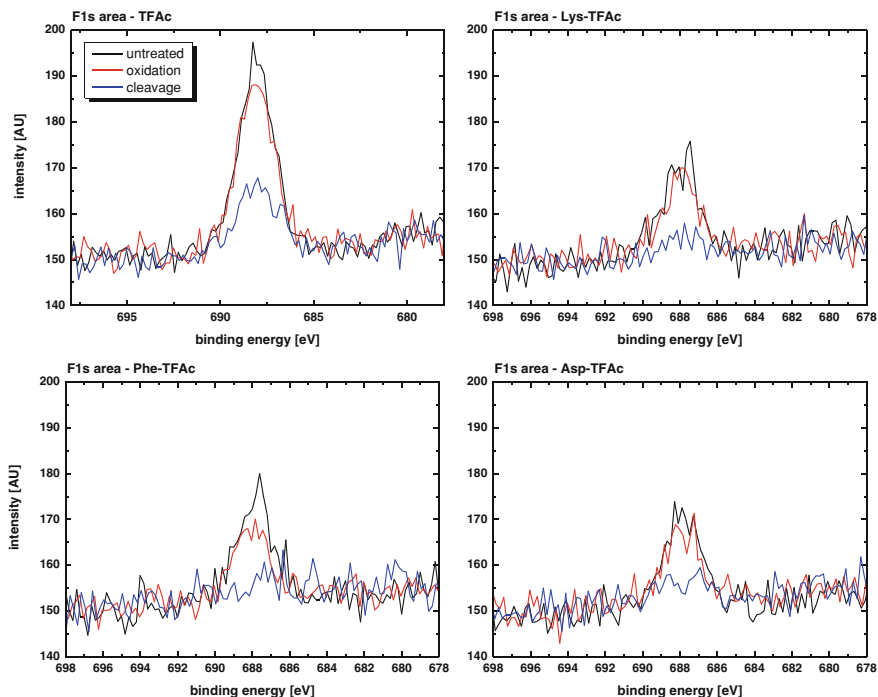


**Fig. 3.18** Comparison of the F1s areas at different stages of the HBA linker cleavage. A higher F1s signal was observed if TFAc was directly attached to the hydrazine moiety. Coupling of Lys, Phe, or Asp as Oppf-activated compounds and subsequent TFAc attachment reduced the signal intensity which made a quantification of the cleavage efficiency difficult. However, cleavage seemed to take place independently of the amino acid

purification of peptide arrays. Considering a cleavage efficiency of around 60 % as determined in the previous experiment, a loss of starting groups for the peptide synthesis due to difficult couplings would not be acceptable. Less starting groups would mean less overall peptide yield which was especially critical regarding the comparatively low DGs on 10:90-PEGMA-co-PMMA-NH<sub>2</sub> films (standard synthesis supports in mpSPPS,  $\sim 2.5$  nmol/cm<sup>2</sup>).

### 3.2.3.2 Cleavage of Spotted Peptides Using the HBA Linker

In parallel to the XPS approach, experiments with spotted peptides were conducted to further investigate the HBA linker. Both 10:90-PEGMA-co-PMMA-NH<sub>2</sub> and AEG<sub>3</sub> SAM surfaces bearing the HBA-linker were reacted with succinimidyl-*trans*-4-(*N*-maleimidylmethyl)cyclohexane-1-carboxylate (SMCC).

SMCC introduces a maleimide function which allows for the covalent immobilization of peptides across a cysteine according to the well known principle of



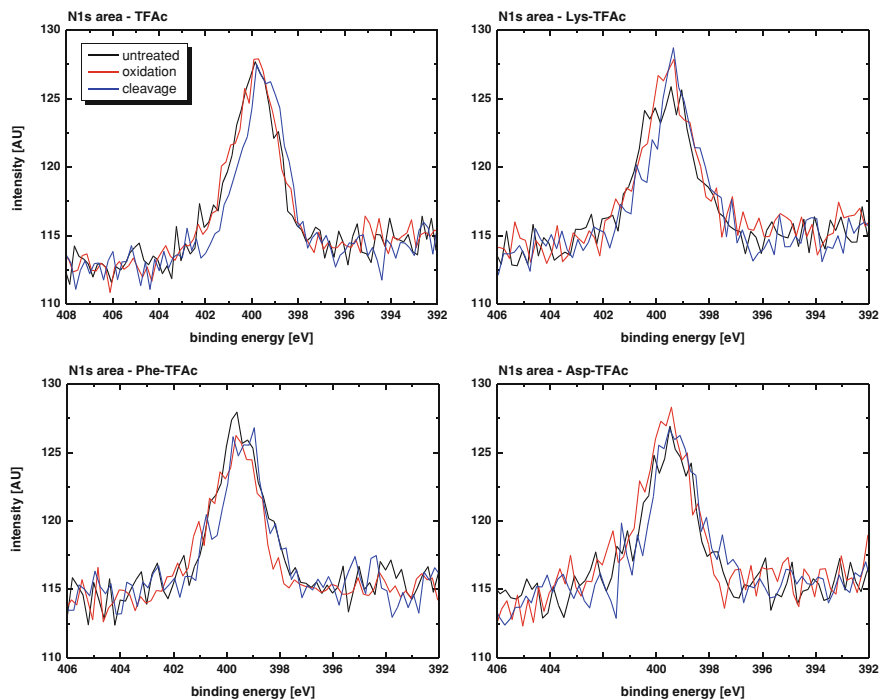


**Fig. 3.19** Comparison of the N1s areas at different stages of the HBA linker cleavage. No remarkable difference in N1s signal intensity was determined for surfaces with and without an additional amino acid between the HBA linker and the TFAc marker. Obviously, the density of amino groups in the analysis volume was nearly constant

“click chemistry” (see Fig. 3.20) [50, 51]. Thus, pre-synthesized peptides could be coupled to the surfaces under ambient conditions. Spotting of carboxyl-activated peptides from anhydrous solutions would have required different equipment which was not available in the present work.

Subsequently, two pre-synthesized peptides with a C-terminal cysteine were spotted onto the surfaces from a phosphate buffer (pH 7.0, 7 mM). Both peptides were labelled with an *N*-terminal 5(6)-carboxytetramethyl rhodamine (TAMRA) fluorescent dye. Hence, the spot pattern could be checked directly with the *GenePix 4000B* scanner (TAMRA:  $\lambda_{\text{ex}} = 555$  nm,  $\lambda_{\text{em}} = 580$  nm). In addition, both peptides bore a biotin attached to a lysine side-chain (see Fig. 3.21). Streptavidin, a protein from *Streptomyces* bacteria, binds to biotin forming one of the strongest known non-covalent bonds [52]. The DyLight 680-streptavidin conjugate (DyLight 680:  $\lambda_{\text{ex}} = 682$  nm,  $\lambda_{\text{em}} = 712$  nm) could, thus, be used to additionally stain the array after spotting (Fig. 3.20c). Arrays stained with DyLight 680-streptavidin were scanned using the *Odyssey Infrared Imager*.

The two peptides were spotted onto the modified glass slides in a checkerboard pattern in three different concentrations. A total of eight array replicas fitted on a

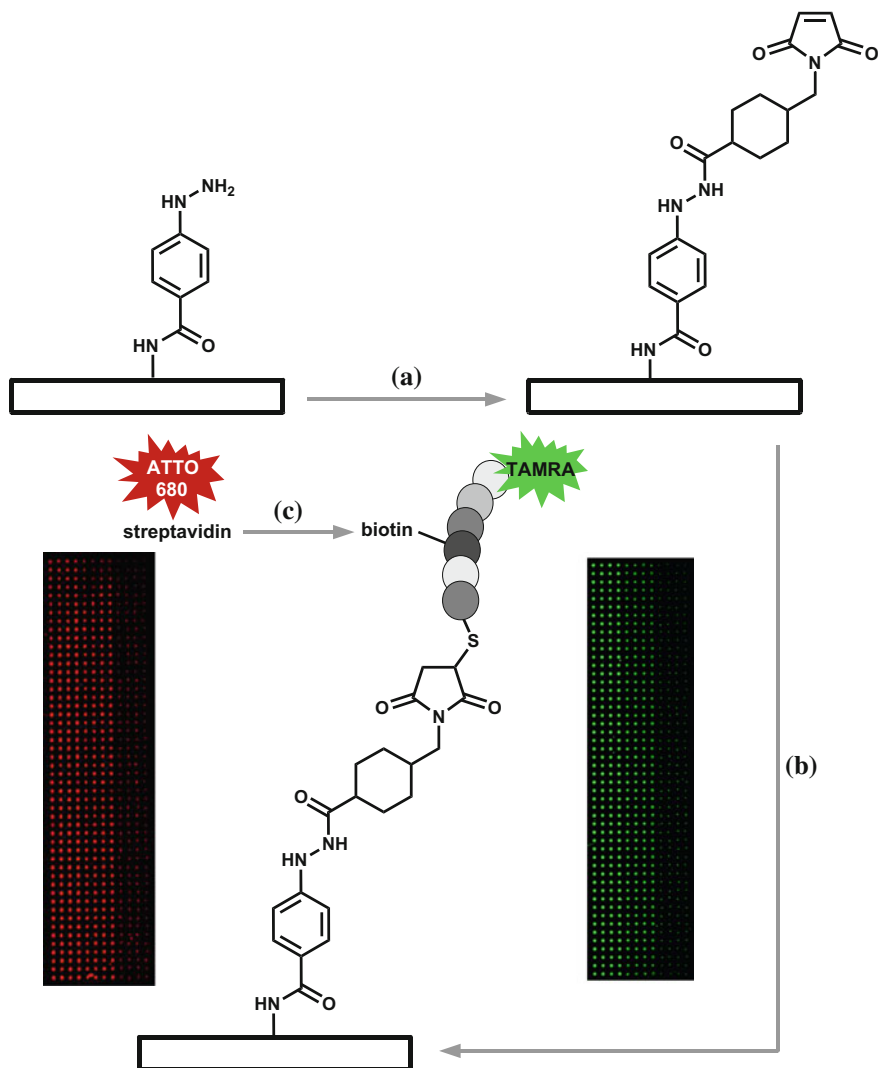


**Fig. 3.20** Schematic: Spotting of peptide arrays onto surfaces equipped with the HBA and SMCC linkers. **a** A 4-(*N*-maleimidomethyl)cyclohexanecarboxyl moiety was coupled by reacting a surface-bound HBA linker with SMCC. **b** A pre-synthesized peptide with a C-terminal cysteine was spotted onto the surface from phosphate buffer (pH 7.0, 7 mM), whereby the thiol in the cysteine side-chain added to the maleimide. The spot pattern could be directly checked by a 5(6)-carboxytetramethyl rhodamine (TAMRA, *green*) dye attached to the *N*-terminal end of the peptide. **c** The peptide could be additionally stained with the DyLight 680-streptavidin conjugate. Here, streptavidin bound to a biotin moiety attached to a lysine. The fluorescence images were obtained with the *GenePix 4000B* scanner (TAMRA, displayed *green*) and the *Odyssey Infrared Imager* (DyLight 680, displayed *red*). The array layout is explained in Fig. 3.40

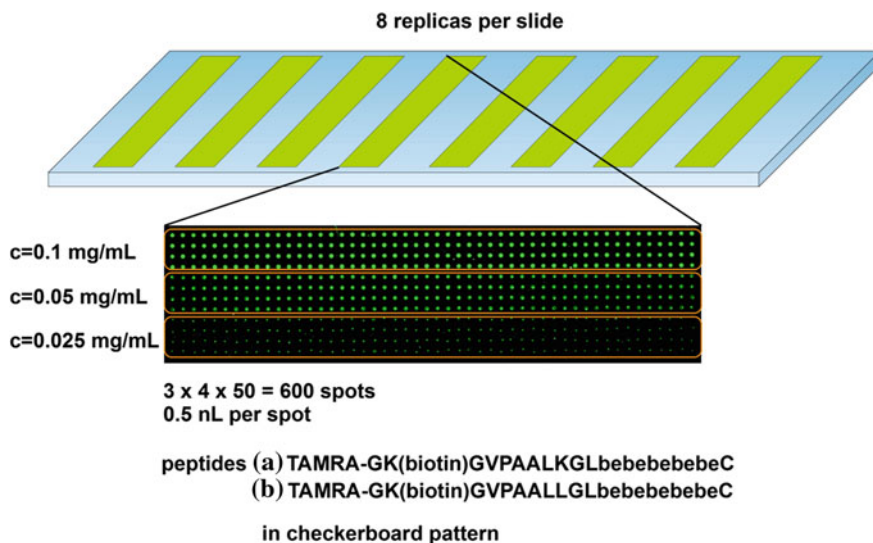


**Fig. 3.21** Slide and array layout of spotted peptide arrays. Each slide contained eight array replicas. A total of 600 ( $12 \times 15$ ) spots were combined in each array, whereby four rows with 50 spots each were spotted in one of three concentrations. Furthermore, the peptide array consisted of two different peptides spotted in a checkerboard pattern. The peptides differed in a K/L exchange and were equipped with a spacer of  $\beta$ -alanine (“b”) and  $\epsilon$ -amino caproic acid (“e”) which was required in the context of a different project

single microscopy slide. The layout of an array consisted of  $12 \times 50$  spots, whereby four rows of 50 spots were each spotted in the same concentration (see Fig. 3.21). Both peptides were elongated with a spacer sequence alternately containing  $\beta$ -alanine (“b”) and  $\epsilon$ -amino caproic acid (“e”). The spacer and checkerboard pattern of two slightly different peptides (exchange of exactly one amino acid) were required in the context of another project which is not further addressed here. In the present work, the peptides were chosen because of the two different labelling sites. TAMRA could be used to directly view the array after spotting. In addition, biotin would allow for a secondary staining if the TAMRA dye was damaged by the cleavage procedure. This was especially important in order to distinguish between dye loss (damage) and peptide loss.

After peptide coupling the slides were scanned to determine the quality of the spot pattern. At times, an irregular checkerboard pattern was observed (see Fig. 3.22, 10:90-PEGMA-co-PMMA-NH<sub>2</sub> slide, concentration 0.1 mg/mL). For instance, if a small contamination adhered to the needle of the spotting robot the droplet was not perfectly addressed to the slide. Moreover, a slightly different concentration of both peptides must have been applied which becomes visible by different fluorescence intensities in the checkerboard pattern. Since the SPPS-synthesized peptides were not extra HPLC purified, different amounts of contained TFA salts were likely to affect the weighted samples. However, an unsteady

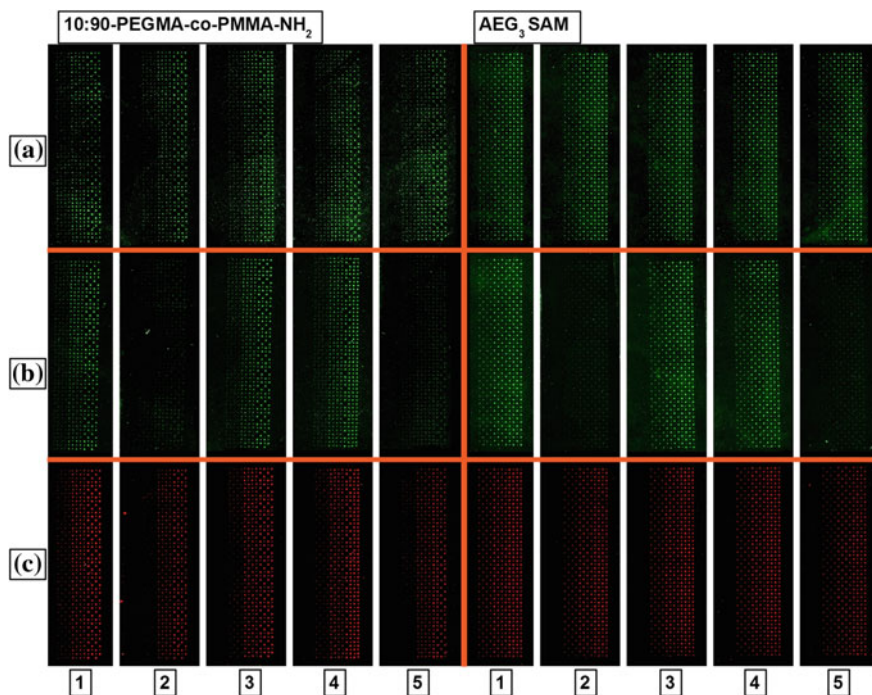


**Fig. 3.22** Fluorescence images (a) before and (b, c) after attempted cleavage of the HBA linker. Images from the *GenePix 4000B* scanner (a, b), Images acquired with the *Odyssey Infrared Imager* (c). Cleavage agents: (1) none (reference washed for 2 h in DCM); (2) 0.5 eq  $\text{Cu}(\text{OAc})_2$ , *N*-propylamine, 2 h; [41] (3) 2 eq NBS, 2 eq py, DCM, 45 min; then MeOH overnight; [41] (4) 2.5 eq NBS, 10 eq py, 10 min; then phosphate buffer (pH 8.0, 0.07 M, 0.05 % (v/v) TWEEN 20) overnight; [53] (5) 500 eq  $\text{Cu}(\text{OAc})_2$ , *N*-propylamine. All amounts noted in eq are based on an estimated DG of 5 nmol HBA per array. Each array was incubated in 1 mL of the corresponding solution

pattern and slightly different concentrations were not problematic as long as the same features appeared on an entire slide, i.e. on all replicas which should be compared. On the contrary, the slightly different pattern was often helpful to identify peptides and slide orientation in the fluorescence scans.

To test different literature-known cleavage agents for the HBA linker [41, 53], arrays were cut from the microscopy slides according to the layout (see Fig. 3.21). Subsequently, one array of each surface type was treated according to the cleavage protocol and then directly stained with the DyLight 680-streptavidin conjugate. After scanning all arrays with the *Odyssey Infrared Imager* in one run, the pieces of one slide had to be glued to another microscopy slide in order to scan them in the *GenePix 4000B* scanner. In doing so, all arrays of a slide could again be scanned in one run. Figure 3.22 shows a comparison of fluorescence images obtained before and after exposure to the cleavage agents.

In literature, the amount of cleavage agents is typically calculated from the amount of substrate and noted in equivalents (eq). Regarding the peptide arrays, an exact calculation was difficult. Therefore, an excess of NBS and py had been used in the XPS approach (10 and 16 mM respectively) because the TFAc marker was not at risk of oxidation. With respect to unprotected peptides attached to the HBA linker, the amount of cleavage agent was, however, reduced to avoid unwanted side-reactions. Based on the highest possible DG of approximately 2 nmol HBA per  $\text{cm}^2$  ( $\approx 40$  nmol per microscopy slide) it was estimated that around 5 nmol HBA could be cleaved per array. Thus, the cleavage solutions were prepared accordingly.

The fluorescence images in Fig. 3.22 show, that the experiment with spotted peptides was too imprecise to display low cleavage efficiencies. From the *GenePix 4000B* scan (Fig. 3.22, row b) a cleavage upon  $\text{Cu}(\text{OAc})_2/N$ -propylamine treatment could be concluded, especially when a 1000fold excess of this mix was applied (Fig. 3.22, columns 5). However, the secondary staining with DyLight 680-streptavidin revealed that the TAMRA dye is apparently damaged by the  $\text{Cu}(\text{OAc})_2/N$ -propylamine treatment and less peptide than expected was cleaved (Fig. 3.22, row c). Hence, the secondary staining was important to distinguish between damage of the dye and cleavage of the peptide. Furthermore, the potential decrease in fluorescence was obscured by high variations in the fluorescence intensity within different replicas and within a slide. An internal reference, e.g. a peptide which is not cleavable, would be helpful to normalize fluorescence intensities, but was technically not realizable. In the present work, the linker always had to be attached to the entire support. Although  $\text{Cu}(\text{OAc})_2/N$ -propylamine treatment seemed to be slightly more effective than NBS/py treatment, the HBA linker should ideally be cleaved under physiological conditions which is not given by  $\text{Cu}(\text{OAc})_2/N$ -propylamine treatment. The secondary staining with the biotin/streptavidin system also bore a conceptual disadvantage: If the bulky DyLight 680-streptavidin conjugate binds less densely i.e. requires less peptide per area than available after marginal cleavage the resulting fluorescence staining will lack in sensitivity with respect to cleavage-induced differences in peptide density. In summary, the approach with spotted peptides would have only provided reliable information if a near-quantitative cleavage occurred which was not the case in the above experiments.

In spite of the difficulties, some important information was gained in this experiment: Peptide arrays could be spotted on the “new” AEG<sub>3</sub> supports, whereby the quality of the resulting pattern seemed to be superior to 10:90-PEGMA-co-PMMA surfaces in terms of homogeneity (see Fig. 3.22). Although the AEG<sub>3</sub> SAMs did not show better cleavage, they could be a promising support for other applications.

### 3.2.3.3 Side-Reactions in the Destabilization Step

Regarding an application of the HBA linker in the purification of peptide arrays, a similar experiment with spotted peptides revealed a serious disadvantage: In the destabilization step, side-reactions can occur. Instead of a randomly chosen sequence as in the experiment before, this time the pre-synthesized peptides contained the HA sequence (YPYDVDPYA, see Fig. 3.23). The array was again spotted onto a surface functionalized with HBA linker and SMCC. In the array, three identical peptides with different *N*-terminal labels were arranged. Each row contained 30 spots, whereby four rows per peptide were spotted in different concentrations. One of the epitopes was equipped with a biotin which allowed for interaction with DyLight 680-streptavidin (see Fig. 3.23). Cleavage of the spotted peptides was attempted using the protocol which worked in the XPS experiment (10 mM NBS, 16 mM py, anhydrous DCM, 10 min, RT, then phosphate buffer (pH 8.0, 0.07 M, 0.05 % (v/v) TWEEN 20), overnight). The oxidized array and a reference array were subsequently stained with the ATTO 680-anti-HA antibody (ATTO 680:  $\lambda_{\text{ex}} = 680 \text{ nm}$ ,  $\lambda_{\text{em}} = 700 \text{ nm}$ ) according to the standard protocol (see Fig. 3.23a). No fluorescence was detected on the oxidized array which was first thought to be a quantitative cleavage. However, in a secondary staining with DyLight 680-streptavidin the peptide bearing a biotin was again detected (see Fig. 3.23b). Thus, the oxidation medium probably caused a side-reaction at a site which is important for the antibody recognition, whereas the HBA linker was not destabilized.

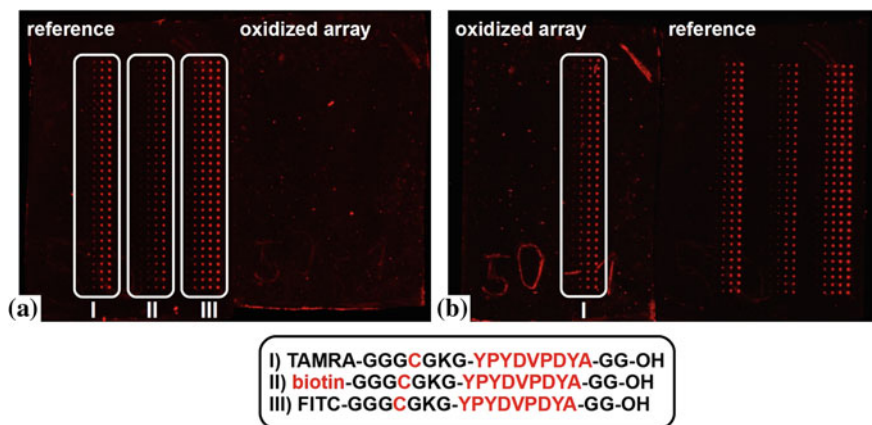


**Fig. 3.23** Side-reactions in the HBA linker oxidation. **a** Two peptide arrays after immunostaining with ATTO 680-anti-HA antibody. One array was treated with NBS/py to cleave the linker, the other array served as a reference. The antibody did not recognize the peptide epitope in the oxidized array. **b** After the secondary staining with the DyLight 680-streptavidin conjugate the pattern of biotinylated peptides became visible. Presumably, the NBS/py treatment caused a side-reaction jeopardizing epitope/antibody interaction. The linker showed no remarkable cleavage

### 3.2.3.4 Summary

In summary, the HBA linker was first considered to be a promising alternative to standard acid-labile linkers for a “mild” peptide array cleavage. However, several disadvantages were determined which exclude an application of this linker: (A) XPS measurements revealed that coupling of the linker or coupling of the first amino acid to the hydrazine group is difficult and takes place with low efficiency. This would reduce the overall yield of peptide in the array synthesis. Moreover, the maximum determined cleavage efficiency of about 60 % is low and significantly adds to the peptide loss. Furthermore, cleavage can already take place in the destabilization step. (B) The surface-bound linker is apparently not easy to cleave when peptides are coupled to it. Variation of the cleavage agent to  $\text{Cu}(\text{OAc})_2$  meant no remarkable improvement. (C) In the destabilization step, side-reactions can occur. A pre-synthesized HA epitope was not recognized by the specific antibody after treatment with NBS/py. Regarding in situ synthesized peptide arrays, the amount of cleavage agent cannot easily be adapted to the actual amount of linker on the support. Therefore, such side-reactions would be difficult to prevent.

Due to the problems in an effective and mild cleavage, the HBA linker was not further applied. Instead, the RAM linker was used for the peptide array purification. Consequences resulting for the target surfaces and the key/lock system will be discussed in the following chapters. The RAM linker is a standard linker in SPPS. As mentioned before, it had already been applied in the characterization of peptides synthesized by mpSPPS [38–40] and was therefore considered to effectively release peptides. Furthermore, it could be coupled to the synthesis surfaces in good yield (up to 90 %, see above) which was also important to sustain the amount of functional groups required for a peptide array synthesis.

## 3.3 Surface Chemistry B: Receptor Surfaces

### 3.3.1 Membranes as Receptor Surface

#### 3.3.1.1 Initial Considerations

In the following chapter, the design of receptor surfaces for the peptide array transfer is discussed. As a result of the problems in applying the HBA linker (see Sect. 3.2), the method should be further developed using the RAM linker. Regarding the receptor surfaces and the key/lock system this led to several limitations. To cleave the RAM linker, TFA in organic solvents must be applied. This a priori excluded biological key/lock systems such as biotin/streptavidin. Another major concern was the format of the receptor surface: In principle, the optimum target surface should be similar to the synthesis surface in the laser printer

approach: The peptide arrays are synthesized on a  $22 \times 21 \text{ cm}^2$  glass slide which is afterwards cut into smaller units (e.g. microscopy slides size:  $7.6 \times 2.6 \text{ cm}^2$ ). The amino-terminated coating of the standard synthesis slides would be compatible with the attachment of various key/lock molecules and stability to TFA was approved (see Sect. 3.1). However, a problem arising from the use of two rigid slides with regard to the array purification concept (see Sect. 2.1) would be lateral diffusion. Two slides brought together with a fluid film in between would give rise to lateral diffusion due to capillary forces. Moreover, the slides would be hard to separate again due to capillary forces. Therefore, an application of flexible polymer membranes as the receptor surface was favored. In this context, polyvinylidene fluoride (PVDF) membranes have outstanding properties regarding their mechanical robustness, thermal stability, and chemical resistance. PVDF is dissolved or degraded in the presence of esters, ketones, or strong bases, but shows a high stability to aliphatic, aromatic, and chlorinated solvents [54]. Most importantly, preliminary experiments showed high stability to TFA. Due to their flexibility, the membranes could easily be soaked with the required cleavage medium, brought into close contact with the rigid synthesis support, and finally removed from the support again.

### 3.3.1.2 Membrane Types and Stability

In this work, two different PVDF membrane types were applied. Table 3.2 summarizes information provided by the manufacturer (*Millipore GmbH*, Schwalbach/Germany).

Besides the different pore size of 450 and 100 nm respectively, the membranes differed in their wettability. In general, unmodified PVDF has a strong hydrophobic nature, but considerable effort is devoted to a hydrophilic modification, e.g. for filtration and water purification applications [54]. Correspondingly, the small pore size membrane is dedicated to filtration assays, whereas the larger pore size membrane is used in protein blotting. Preliminary XPS measurements showed that the hydrophilic functionalization of the small pore size membrane results in an additional O1 s signal, a less intense F1s signal and a different structure of the C1s signal (see Fig. 3.24). This was probably due to surface modification with compounds containing additional C–C, C–O, and C = O species. Untreated PVDF typically shows only two C1s peaks at 290.8 eV (C–F) and 286.3 eV (C–H) [55]. Although no detailed information was provided by the manufacturer, it was communicated that the surface coating was covalently bound [56]. In the peptide

**Table 3.2** Manufacturer information on the membrane properties

Membrane	Material	Pore size [nm]	Thickness [ $\mu\text{m}$ ]
<i>Immobilon-P</i> [74]	Hydrophobic PVDF	450	<i>Not available</i>
<i>Durapore</i> [75]	Hydrophilic PVDF	100	125



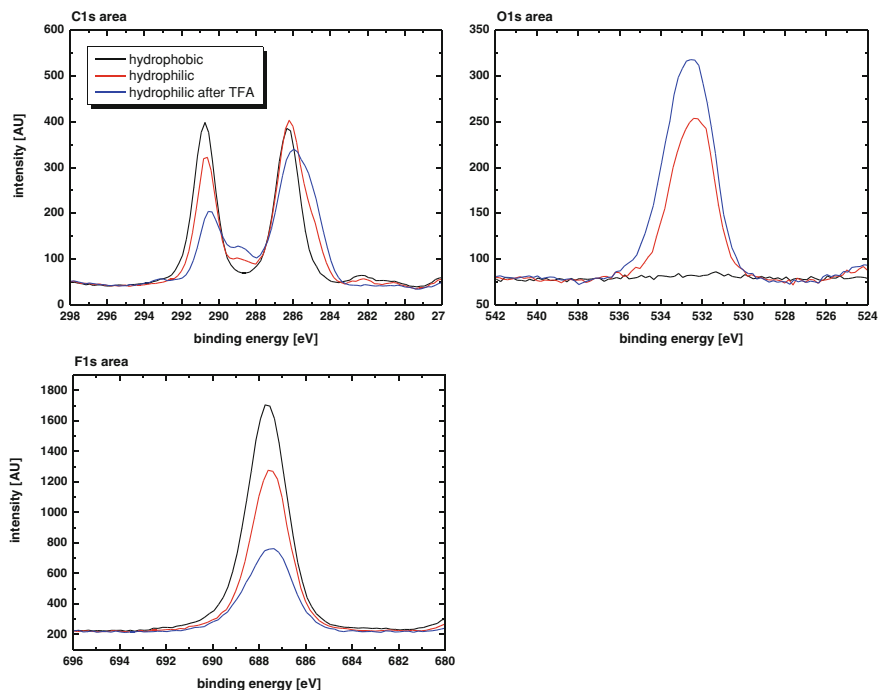


**Fig. 3.24** C1s, O1s, and F1s areas of different PVDF membranes. The hydrophobic *Immobilon-P* membrane showed the typical signal structure of untreated PVDF (black lines) [55]. The hydrophilic modification of the *Durapore* membrane became visible in an additional O1s signal, a less intense F1s signal, and a different signal structure in the C1s area (red lines). Upon TFA treatment of the hydrophilic membrane the C1s signal structure changed, the F1s signal intensity further decreased, and the O1s signal became more pronounced. Presumably, this displayed oxidation of the hydrophilic modification

array purification, a hydrophilic surface was favored to avoid nonspecific adsorption of peptide fragments in the purification step or proteins in subsequent immunostainings. However, the hydrophilic coating had to withstand TFA treatment. Incubation of a sample in 100 % TFA for 90 min caused a decrease in F1s signal intensity, an increase in O1s signal intensity, and a different signal structure in the C1s area. These changes showed that the hydrophilic modification is altered upon TFA treatment, probably due to oxidation. However, no noticeable decrease in mechanical stability, wettability, or membrane color was observed.

In addition to the stable membrane support, a TFA-compatible key/lock system was required. In keeping with the purification concept (see Sect. 2.1) the peptide/lock bond must be formed while the linker/peptide bond is being cleaved. Furthermore, the lock molecules have to be thoroughly attached to the membrane during the whole process. In fact, there are numerous ways to functionalize PVDF membranes with other polymers, inorganic particles, and functional coatings [54]. For example, plasma or ozone activation and subsequent graft polymerization is a

common way to obtain membranes with the desired functional groups [54, 57–59]. However, combining a functional coating with a key/lock system in which all components are stable to TFA and, furthermore, can even form a bond under these conditions, was a considerable challenge.

### 3.3.2 Sputter Coating

Instead of grafting a functional polymeric film onto the PVDF membranes, a comparatively simple approach to enable a specific transfer of peptide arrays to PVDF membranes was based on the introduction of a thin gold layer. Gold coatings allow for the immobilization of peptides bearing an *N*-terminal cysteine, whereby the thiol in the cysteine side-chain forms a covalent bond to the gold surface [60]. In fact, the self-assembly of thiols on metal, metal oxide, and semiconductor surfaces is an intensively studied field and has diverse applications [19, 21]. Most importantly in this context, the self-assembly of thiols on gold-surfaces was reported to take place under TFA-acidic conditions [61].

However, to use cysteine as a specific key, the side-chain protecting group had to be simultaneously cleaved with the RAM linker. According to the literature, Trt in cysteine requires a comparatively high TFA concentration of 95 % (v/v) (see Table 1.1) [62]. In contrast, the RAM linker was expected to quantitatively release amides in only 5 % (v/v) TFA in DCM [36, 63].

For the peptide array purification, samples of both hydrophilic and hydrophobic PVDF membranes (see Table 3.2) were sputter-coated in a standard device without pre-treatment. Sputter coating was conducted at  $5 \cdot 10^{-2}$  mbar and 60 mA for 15, 20, 30, and 35 s. According to a device calibration curve the sputter time was linearly linked to gold thickness [64]. However, this calibration was only applicable to flat substrates, whereas for the porous membranes slightly different thicknesses were expected. Moreover, the gold thickness was assumed to be lower inside the pores. Therefore, the gold thicknesses listed in Table 3.3 should be considered as approximate values.

Preliminary experiments showed that the gold coating on both membrane types was highly stable to 100 % TFA. No degradation or ablation was observed. 15 s sputtering gave a gray color on the membranes. After 20 s the membrane looked brown. Around 30 s sputter time the color turned gold brown. To check how

**Table 3.3** Expected gold thicknesses in dependence of sputter time. The values were calculated on the basis of a device calibration on flat substrates

Sputter time [s]	Gold thickness [nm]
15	22
20	30
30	47
35	54

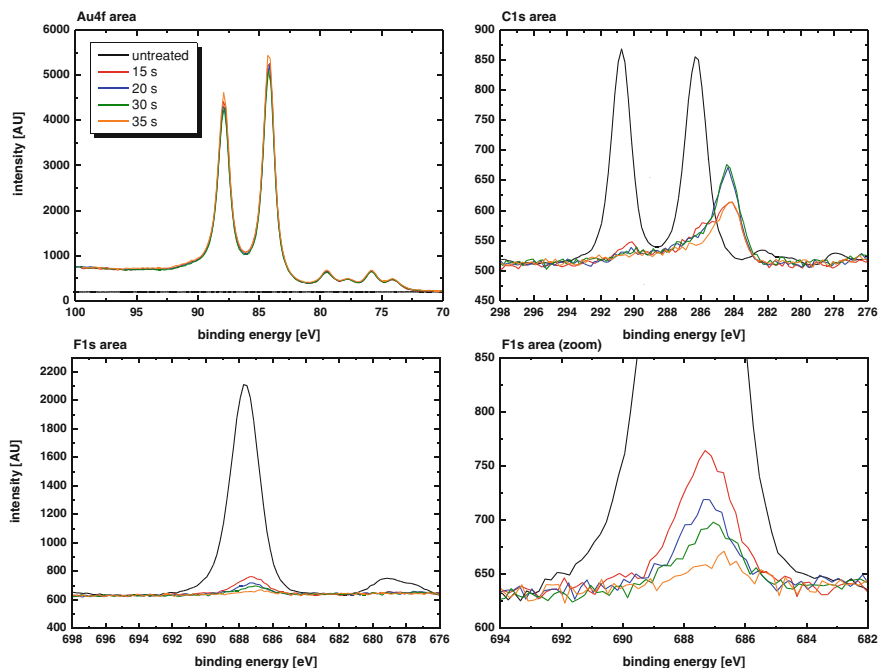


**Fig. 3.25** Au4f, C1s, and F1s areas of gold-coated PVDF membranes in comparison with an untreated membrane. The membranes were sputter-coated for 15, 20, 30, and 35 s. In the Au4f area, the Au4f<sub>5/2</sub> peak at 87.88 eV and the Au4f<sub>7/2</sub> peak at 84.21 eV were detected. A decrease in the remaining F1s signal intensity with longer sputter times indicated a thicker gold film with increased sputter time. The signal in the C1s area around 284.6 eV is probably caused by aliphatic carbon from the atmosphere which adsorbed to the membrane

densely the membranes were coated, XPS measurements were conducted. Figure 3.25 exemplarily shows the Au4f, C1s, and F1s areas of membrane samples coated for 15, 20, 30, and 35 s in comparison with a pristine membrane. On all four sputter-coated membranes a strong Au4f signal consisting of the Au4f<sub>5/2</sub> peak at 87.88 eV and the Au4f<sub>7/2</sub> peak at 84.21 eV was detected. Furthermore, the typical C1s and F1s signals from the underlying membrane were noticeably attenuated. In the C1s area, the remaining signal was completely covered by a peak around 284.6 eV which was probably caused by aliphatic carbon adsorbed from the atmosphere and the carbon tape which was used to fix the membranes on the sample holder. Although a weak signal was still detectable in the F1s area, the signal intensity decreased with longer sputter times, indicating an increase in gold thickness. With regard to the analytical depth in XPS of maximum 10 nm (see Sect. 2.3.4) the F1s signal was probably caused by gold thicknesses below 10 nm inside the pores of the membrane. Since the F1s signal had almost completely disappeared after 35 s of sputtering a dense gold coating was assumed. However, the reverse side of the membranes remained uncoated.

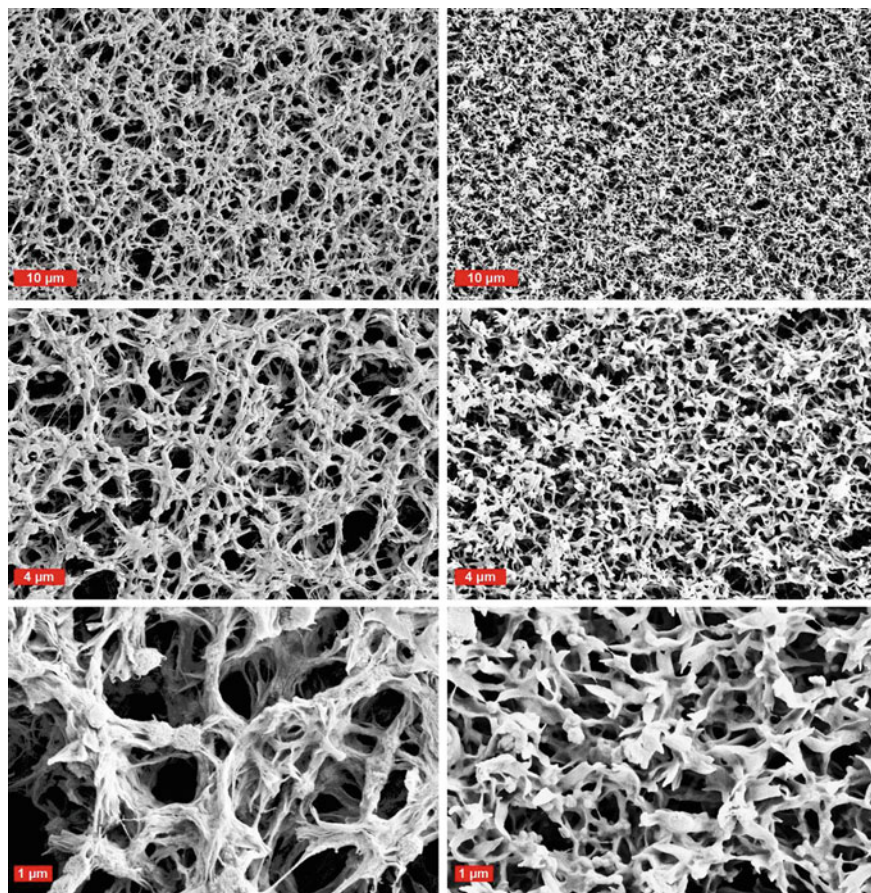


**Fig. 3.26** SEM images of gold-coated PVDF membranes with 450 nm (*left*) and 100 nm (*right*) pore size. **a, b** 5 K magnification; **c, d** 10 K magnification; **e, f** 30 K magnification

Furthermore, the Au coated membranes were examined by SEM. Figure 3.26 shows a comparison of a gold-coated membrane with 450 and 100 nm pore size respectively. Due to the diffuse movement of gold atoms in sputtering, the reverse side of the fiber-like PVDF network was also expected to be partly coated, especially in the upper regions.

In summary, depositing a thin gold coating on PVDF was a rather simple way to obtain a functional coating. In principle, the coating should be capable of selectively binding peptides across a cysteine under TFA-acidic conditions. Furthermore, the gold coating was deposited with minimum effort. Due to their obviously good stability the membranes were directly applied in the purification experiments described in the following chapter.

## 3.4 Peptide Transfer and Purification

### 3.4.1 *Synthesis of Model Peptide Arrays with the Laser Printer*

The first peptide arrays for the transfer and purification experiments were synthesized with the prototype of the peptide laser printer (see Sect. 1.2.2). As mentioned before, this device was capable of directly printing on microscopy slides if a mask was used to fix the slides in a  $22 \times 21 \text{ cm}^2$  arrangement. Hence, PEGMA-co-PMMA surfaces were consecutively modified with three  $\beta$ -alanine residues as routinely performed for an in situ peptide array synthesis [44]. Subsequently, the RAM linker was coupled from solution, here yielding a DG of  $1\text{--}2 \text{ nmol/cm}^2$  of amino groups for the actual peptide synthesis (see Sect. 3.2.2). Afterwards, the microscopy slides were pre-structured with a glycine pattern (see Fig. 3.27a). Five glycine array replicas were printed per microscopy slide, whereby each array contained a total of 180 spots. Each spot was approximately  $512 \text{ }\mu\text{m}$  in diameter with  $1024 \text{ }\mu\text{m}$  center-to-center spacing (see Fig. 3.27). After routine coupling, washing, capping, and Fmoc cleavage (see Sect. 1.2.4), a pre-synthesized HA epitope (Fmoc-GGGYPYDVPDYAGGG-OH) was coupled to all glycine spots from solution using HOBt/HBTU/DIPEA. The side-chains of the peptide epitope were still protected with the standard acid-labile protecting groups (see Table 1.1). After Fmoc cleavage, cysteine was selectively coupled to 95 out of the 180 HA epitope spots in a second micro particle-based synthesis step. Thereby, a slightly modified checkerboard pattern was produced (see Fig. 3.27b).

Only the peptides in the 95 selected spots were thus equipped with a thiol group for specific binding to gold surfaces. In case of a specific transfer, only full-length peptides from the 95 cysteine spots should couple to the gold-coated membrane (see Fig. 3.27b). Peptides from the remaining 85 spots without an N-terminal cysteine should also be cleaved but are not equipped to react with the receptor membrane.

### 3.4.2 *Setup in the Peptide Array Purification*

In the experimental transfer setup, emphasis was placed on ensuring good contact between the receptor membrane and the synthesis support. Laying the synthesis support face-down onto the receptor membrane was essential to limit lateral diffusion and to preserve spatial information (see Fig. 3.28). Thus, close contact was achieved by weighting the synthesis support. Moreover, the receptor membrane was placed on top of a filter paper soaked with the transfer medium which acted as an effective reservoir of the fluid. In the cleavage of side-chain protecting groups solutions of TFA in DCM are commonly applied. Due to the fact that DCM rapidly evaporates, toluene was instead used as a solvent in this peptide array purification.

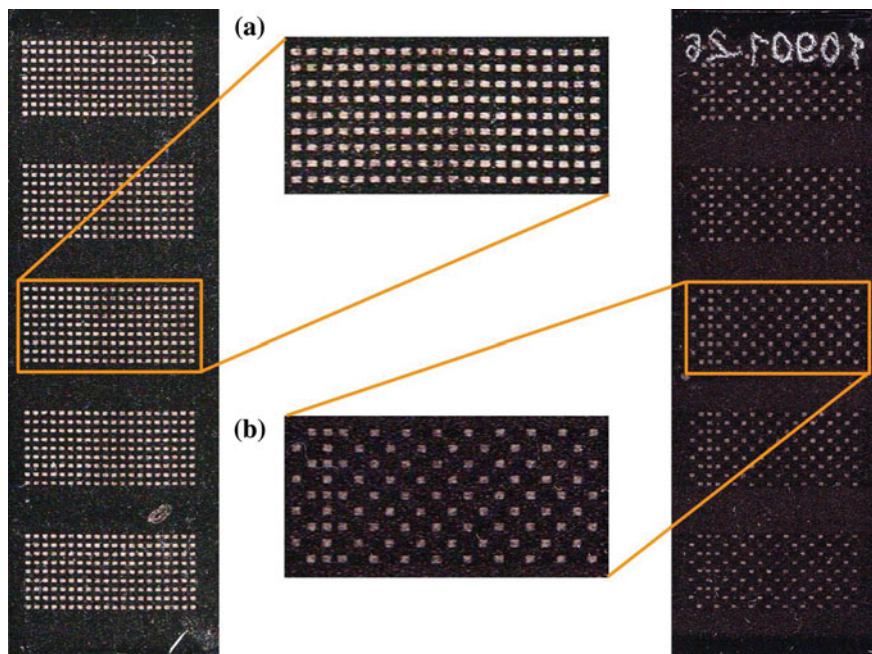


**Fig. 3.27** Particle deposition pattern on microscopy slides. Microscopy slides with a 10:90-PEGMA-co-PMMA-NH<sub>2</sub> coating were equipped with the RAM linker. **a** The slides were pre-structured with glycine particles addressed with the laser printer. Five array replicas were arranged per slide. Each array was formed of 180 glycine spots. The particle spots were subsequently melted at 90 °C in an oven to initiate the coupling reaction. After subsequent acylation, Fmoc cleavage, and washing steps to remove residues of the particle matrix, a pre-synthesized HA epitope Fmoc-GGGYPYDVPDYAGGG-OH was coupled to the glycine spots from solution (not shown). The epitope was left side-chain protected and only the Fmoc protecting group was cleaved. **b** In a second laser printer cycle, only 95 of the 180 spots were loaded with cysteine particles. Thus, a specific pattern of cysteine-terminated peptides was generated

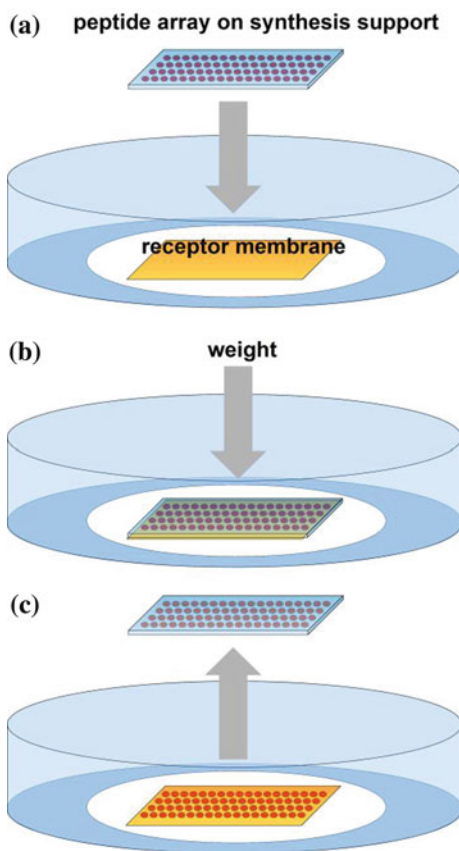
After each transfer experiment, the synthesis support had to be carefully lifted from the receptor membrane. From time to time, the membrane stuck to the support and was removed with tweezers.

### 3.4.3 Specific Transfer of Model Peptides

#### 3.4.3.1 First Transfer Experiments

As mentioned above, the Trt protecting group of cysteine was reported to require 95 % (v/v) TFA as well as additional scavengers for an effective release [62]. However, in the routine peptide array synthesis in our group, 51 % (v/v) TFA,

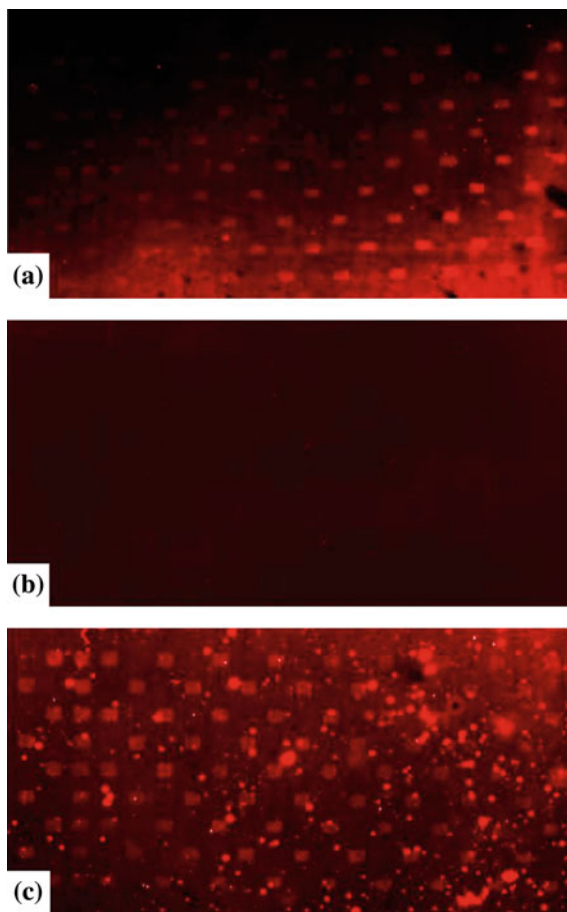
**Fig. 3.28** Experimental setup. **a** The receptor membrane is placed on a filter paper soaked with the transfer medium. **b** The synthesis slide is positioned face-down onto the membrane and then weighted. **c** After the transfer the synthesis slide is lifted from the membrane



44 % (v/v) DCM, 3 % (v/v) TIBS, and 2 % (v/v) H<sub>2</sub>O are applied to remove the side-chain protecting group and have proven to be sufficient [3, 4, 65]. Therefore, the first transfer experiments were attempted with a simple mixture of 50 % (v/v) TFA and 50 % (v/v) toluene. Samples of the 450 nm pore-size membrane, sputter-coated for 35 s, were chosen because this membrane was assumed to have a very dense gold-coating and a high-stability to TFA (see Sects. 3.3.1 and 3.3.2).

Figure 3.29 shows an immunostaining with the ATTO 700-anti-HA antibody on a membrane (a) and synthesis slide (b) after 45 min transfer time. The transfer was conducted according to the setup in Fig. 3.28. Specific transfer of only the cysteine-terminated peptides was clearly indicated by a specific fluorescence pattern on the membrane (see Figs. 3.29a and 3.27b). Hence, the feasibility of peptide array purification by specific transfer to a gold-coated membrane has been proved. Surprisingly, the first series of peptide transfers also revealed that a concentration of 10 % (v/v) TFA in toluene was sufficient to achieve a specific transfer. The specific pattern of cysteine-terminated peptides was visible, although the background was higher (see Fig. 3.29c). Thus, 10 % (v/v) TFA obviously

**Fig. 3.29** First transfer experiments. Peptides from the model arrays (see Fig. 3.27) were transferred to a gold-coated membrane. The membrane was sputter coated for 35 s which corresponds to a gold thickness of about 47 nm on flat substrates. In the case of membrane **a** and synthesis slide **b** 50 % (v/v) TFA solutions were used in the transfer. The transfer time was 45 min. In the case of membrane **c** only 10 % (v/v) TFA was applied in the transfer, but the transfer time was increased to 1 h. The membranes and arrays were stained with ATTO 700-antiHA according to the standard protocol. Readout and tonal value correction were performed with the *Odyssey Infrared Imager*



suffices to simultaneously cleave the linker and the Trt protecting group of cysteine. As mentioned above, removal of the Trt protecting group on cysteine was expected to require higher concentrations of TFA. The low concentration required here could hint at a catalyzed Trt cleavage in the presence of the gold surface. However, the fluorescence signals in the transfer using 50 % (v/v) TFA showed lower background which is why a concentration of 50 % (v/v) TFA was routinely applied in the following experiments.

Furthermore, no remaining peptides were detected on the synthesis slide indicating absolute cleavage. As a precautionary measure, the synthesis slides and membranes were immersed in 50 % (v/v) TFA after the transfer to ensure complete deblocking of the side-chains which most likely completed the cleavage. Most importantly, the transferred peptide array was not removed from the receptor membrane by the additional TFA treatment which demonstrates the stability of the newly formed thiol/gold bonds.



### 3.4.3.2 Improvement of the Transfer

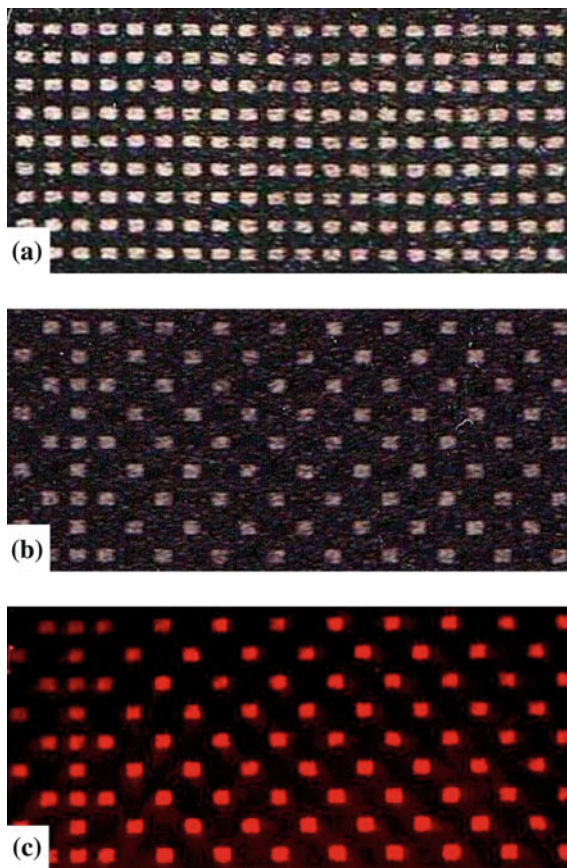
In general, the peptide spots did not seem to suffer from lateral diffusion. The slightly different spot shapes are in good agreement with typical variations in feature size in the particle deposition pattern (see Fig. 3.27b). However, a gradient in fluorescence intensity was obvious (see Fig. 3.29a). The gradient seemed to relate to the local color variations of the gold-coated membrane. In the first transfer, a piece was cut from the edge of the sputtered membrane where, apparently, a gradient in gold density was present. The less intense spots in the fluorescence pattern were situated on the more densely coated part of the surface. Therefore it was assumed that quenching of the fluorescent dyes occurred, which is a known phenomenon in close proximity to gold surfaces [66].

More homogeneous transfers and better immunostainings could be achieved by the following improvements: (A) Gold membranes with a minimum of 15 s and a maximum of 30 s sputter time were used (also see Sect. 3.5.2). According to the calibration of the sputter coater (see Sect. 3.3.2, Table 3.3) this corresponds to a gold thickness between 22 and 47 nm. (B) Homogeneously colored pieces from the middle of the sputter coated membranes were exclusively used. (C) In addition to the routine blocking (see Sect. 5.3.9), the membranes were incubated in a 2 mM solution of *O*-(2-mercaptoethyl)-*O'*-methylhexaethyleneglycol (EG<sub>7</sub>-SH) for 24 h before the immunostaining. This would serve to assemble a thiol with protein repelling properties at free binding-sites on the membrane and, thus, improve the specificity of the immunostaining [27, 28]. The EG<sub>7</sub>-SH assembly is further discussed in Sect. 3.5.1. (D) The membranes were pressed to the scanner support (*Odyssey Infrared Imager*) using a low fluorescence glass plate to avoid corrugation.

Figure 3.30 exemplarily shows the fluorescence pattern after a transfer following the improved parameters listed above. The fluorescence image revealed strong fluorescence signals and low background. The immunostaining was most likely enhanced by the EG<sub>7</sub>-SH self-assembly which obviously did not interfere with the peptides on the membranes and which presumably equipped the gold-membrane with intrinsic protein repelling properties. Furthermore, the membrane used in this approach was only sputter-coated for 15 s which corresponds to 22 nm gold thickness on a flat surface (see Sect. 3.3.2, Table 3.3). The transfer time was reduced to 30 min which seemed to suffice transferring a considerable amount of peptides.

In fact, cleavage kinetics constitute an important parameter in the transfer purification, but measuring the cleavage kinetics of small peptide spots in complex array is challenging. A fivefold successive transfer from one synthesis array to pieces of the same gold-coated membrane was conducted to find out how fast the peptides were cleaved and if duplication was possible.

**Fig. 3.30** Improved specific transfer of a model peptide array to a gold-coated membrane. In this transfer, a more homogeneously metal-coated membrane was applied. The sputter time was 15 s which corresponds to 22 nm gold on a flat substrate. Furthermore, immunostaining was enhanced by additionally blocking the membrane with EG<sub>7</sub>-SH. **a** Glycine particle deposition pattern: The HA-epitope was coupled to each of these spots. **b** Cysteine particle deposition pattern: Only HA peptides at these spots obtained an *N*-terminal cysteine. **c** Fluorescence pattern after 30 min transfer, blocking with EG<sub>7</sub>-SH and immunostaining with the ATTO 680-antiHA conjugate



### 3.4.3.3 Multiple Transfers

Each of the five successive transfers was conducted for 10 min. Subsequently, the membranes were immunostained and scanned in one run. The readout revealed decaying fluorescence intensity from the 1st to the 5th transfer (see Fig. 3.31a). To evaluate the percentage of transferred peptides per run the mean fluorescence intensity of all 95 spots was quantified with the *GenePix Pro Acquisition and Analysis Software* with automated irregular feature recognition. Subsequently, the relative intensity per transfer was calculated on the basis of the intensity sum of all five transfers (see Fig. 3.31b).

The quantification shows that  $45 \pm 9\%$  of the peptides were transferred in the first 10 min, followed by additional  $22 \pm 4\%$  in the next 10 min (see Fig. 3.31b). In the 5th transfer still  $8 \pm 2\%$  of the peptides were transferred, but the intensity of the fluorescence signals was noticeably lower compared to the background. In summary, the production of array replicas in the course of the array purification

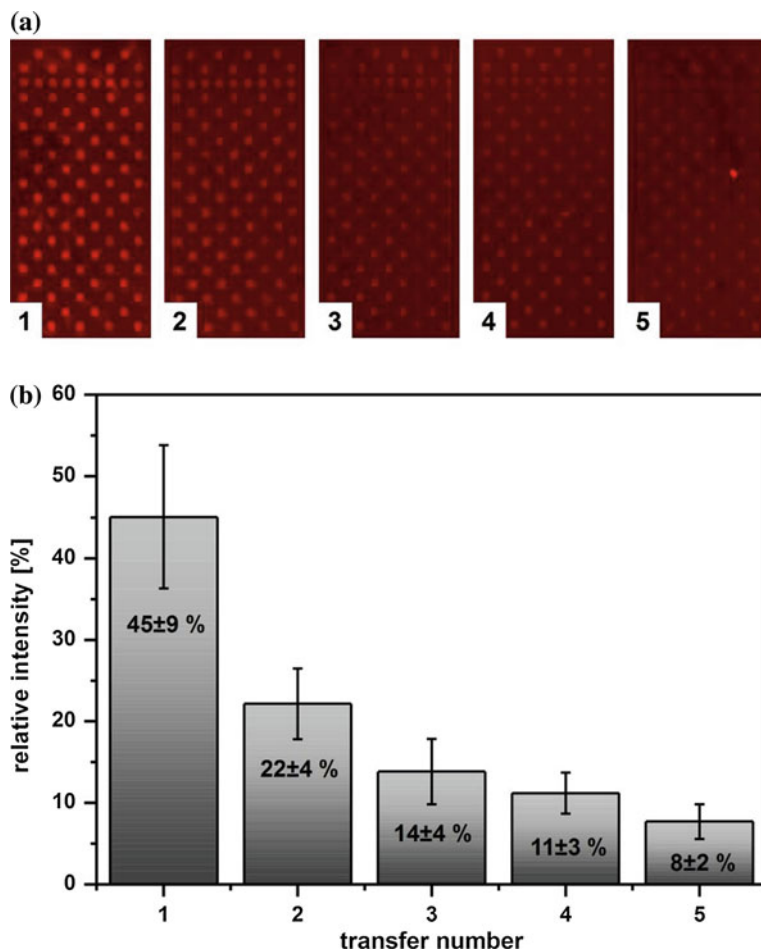


**Fig. 3.31** Fivefold transfer of peptides from a model peptide array to pieces of gold-coated PVDF. Each transfer was conducted for 10 min. **a** The subsequent immunostaining revealed a specific transfer of peptides in each run, whereby the fluorescence intensity decreased with the replica number. **b** A quantification of the mean fluorescence intensity of all 95 spots was performed with the *GenePix Pro 6.0 Acquisition and Analysis Software* using the automated irregular feature recognition. The analysis showed that after the first two transfers about two-thirds of the peptides were already transferred

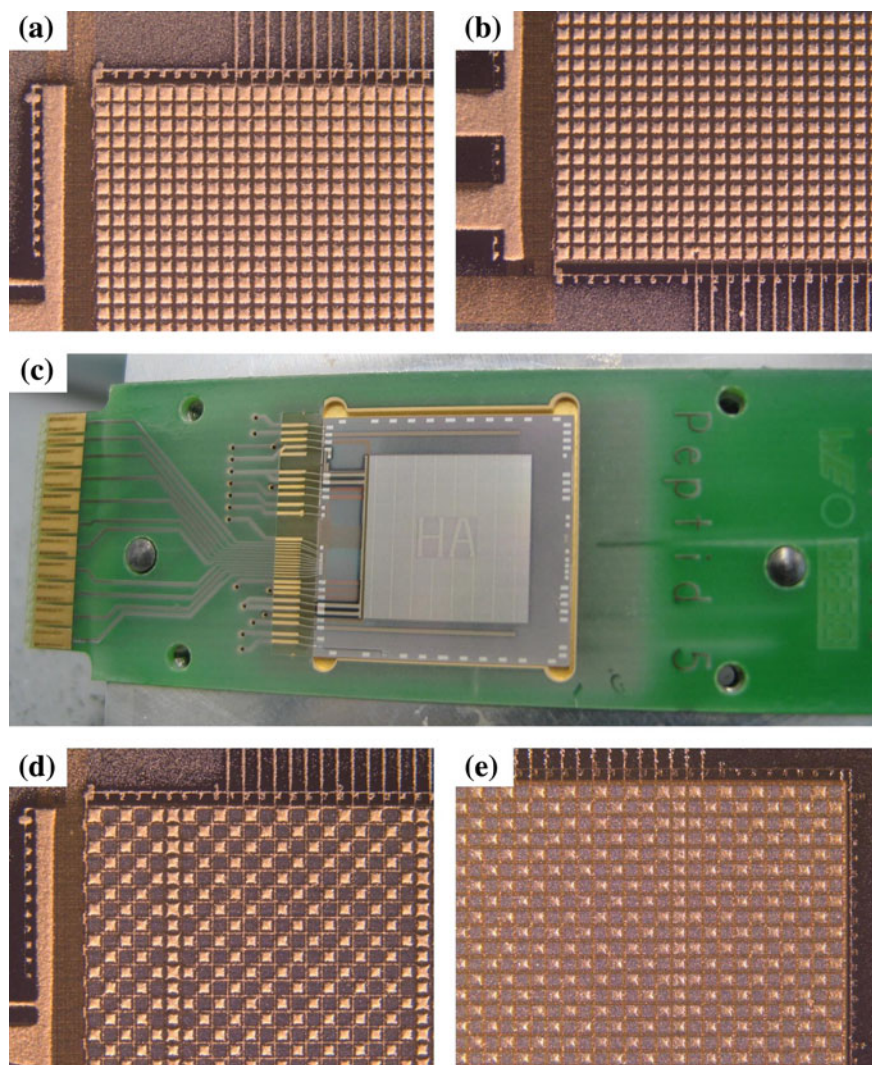
seems possible. Especially in the first two runs, most of the peptides are transferred. However, the amount of peptides in the model arrays was probably higher than in in situ synthesized arrays. Therefore, the feasibility of replica production should be further investigated.

### 3.4.4 Specific Transfer of Model Peptides in High-Resolution

In the specific transfer of model peptide arrays containing 180 spots with approximately 512  $\mu\text{m}$  in diameter and with 1024  $\mu\text{m}$  center-to-center spacing were used (see Sect. 3.4.1, Fig. 3.27). To study the peptide array purification method with highly-resolved arrays, the same model peptides were synthesized in a chip-based approach. As described in Sect. 1.2, the chip-based array synthesis is capable of producing arrays with up to 40,000 peptides per  $\text{cm}^2$  [67]. However, the current CMOS chip “Peptide Chip 5” was improved in terms of particle deposition and, as a consequence, “only” features 16,384 synthesis pixels and an areal density of 10,000 peptides per  $\text{cm}^2$  [68]. Alanine particles were first deposited on every pixel of the chip using the improved particle deposition method (see Fig. 3.32a, b) [69]. After the complete coupling and washing cycle, Fmoc-GGGYPYDVPDYAGGG-OH was coupled to each of the alanine-containing pixels as before. Subsequently, cysteine particles were deposited and coupled to the HA peptides in a selected pattern (Fig. 3.32c–e). The micro chips were thus equipped with a defined pattern of cysteine-containing and cysteine-free peptides which all had the HA epitope in common.

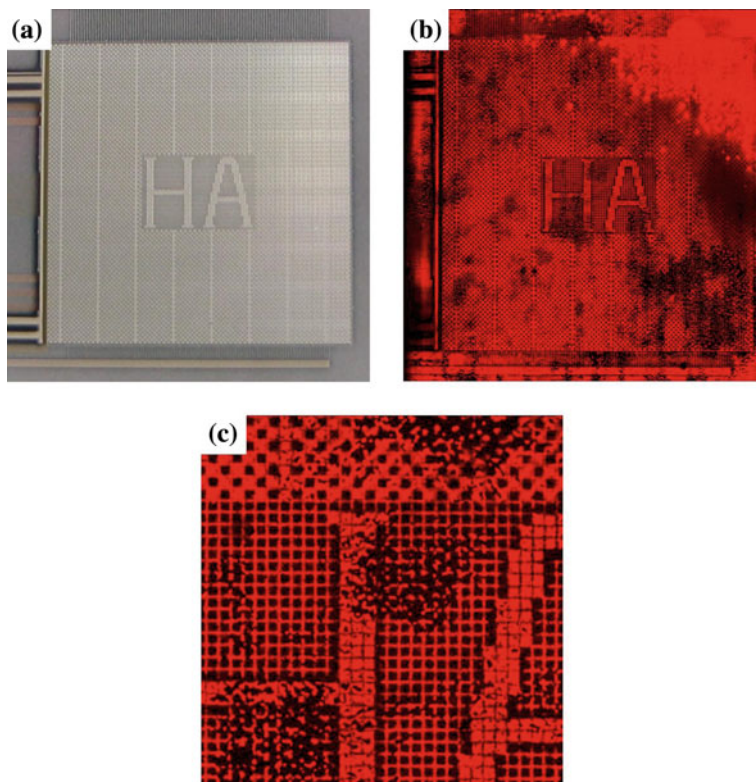
The first transfer from a micro chip was conducted following the same approach used with the laser-printed arrays. A gold-coated membrane (20 s sputter time) with 450 nm pore-size was used. However, to detect the peptides a different scanner was required because the pixel electrodes on the microchip have a dimension of  $84 \times 84 \mu\text{m}^2$  with 100  $\mu\text{m}$  pitch. In contrast, the *Odyssey Infrared Scanner* has a maximum resolution of 21  $\mu\text{m}$  per pixel which would mean only 4–5 pixels per feature on the micro chip. Hence, the *GenePix 4000B* scanner with 5  $\mu\text{m}$  maximum resolution per pixel was used. However, the *GenePix 4000B* scanner is only capable of scanning slides and uses different wavelengths. Therefore, the membranes in the micro chip transfer had to be (A) immunostained with the Cy5-anti-HA conjugate and (B) glued to a microscopy slide surface with spray adhesive (see Sect. 5.1.6).

Figure 3.33 shows a fluorescence image obtained after peptide transfer to the membrane with 450 nm pores. In principle, the specific transfer, i.e. the peptide array purification, was successful but in certain areas the fluorescence pattern was blurred (Fig. 3.33b, c). From the appearance of the blurred areas, it was concluded that either the pore size of the membrane or the contact between membrane and micro chip had caused problems in the highly-resolved transfer. Therefore, the 100 nm pore size membranes (see Sect. 3.3.1) and a smaller quantity of transfer medium were applied in the next transfer. In the previous transfers, 1000  $\mu\text{L}$  51 % (v/v) TFA had been used, whereas now 500  $\mu\text{L}$  were applied to soak the filter paper and the membrane. Moreover, the chip transfer was conducted with a gold membrane that had been coated for 30 s. In an experiment discussed in Sect. 3.5.2, the Cy5-anti-HA conjugate had shown better fluorescence signals on these presumably more thickly coated membranes.



**Fig. 3.32** Synthesis of model peptides on the micro chip. **a, b** Alanine micro particles were deposited on each pixel electrode of the chip. Also the bond wires and connectors were covered with particles (particles appear *yellowish*). After a routine synthesis cycle, Fmoc-GGGYPYDVP-DYAGGG-OH was coupled to each of these pixel electrodes (not shown). **c, d** Subsequently, cysteine particles were deposited on selected pixel electrodes to form a defined pattern. **e** The particles were melted without spreading onto the uncovered pixels. Thus, cysteine was only attached to the peptides on the selected pixels

In Figs. 3.34 and 3.35 the first and the second imprint from a single micro chip are depicted. In accordance with the results of the fivefold transfer (see Sect. 3.4.3, Fig. 3.31), the first transfer was performed for 15 min, and the second for 20 min.



**Fig. 3.33** Blurred chip transfer onto gold-coated PVDF with 450 nm pore size. **a** Cysteine particle deposition pattern on the chip. **b** Fluorescence image obtained with the *GenePix 4000B* scanner after transfer and immunostaining with the Cy5-anti-HA antibody. **c** Close-up of the fluorescence pattern. The transfer was specific, but the pattern was partly blurred. Blurring was attributed to the pore size of the membrane and addition of too much transfer medium

Both experiments showed highly specific transfer of the cysteine-terminated peptides and clear fluorescence signals. Moreover, even peptides from the grid between the pixels are clearly transferred which indicates that the transfer succeeded in the  $\mu\text{m}$  range without any signs of lateral diffusion. A deposition of glycine particles on the grid was rare (see Fig. 3.32a, b), indicating that the approximately  $15\ \mu\text{m}$  wide grid must have been deposited with glycine in the melting step due to slight spreading of the particle mass (also see Fig. 1.8). However, the grid is inevitably contaminated with cysteine particles and thus every peptide on the grid is also equipped with a key molecule during the synthesis (see Fig. 3.32c).

In summary, a highly-specific and highly-resolved peptide transfer from the micro chip was possible if the 100 nm pore size membranes were used. The hydrophilic coating of these membranes (see Sect. 3.3.1) apparently caused no

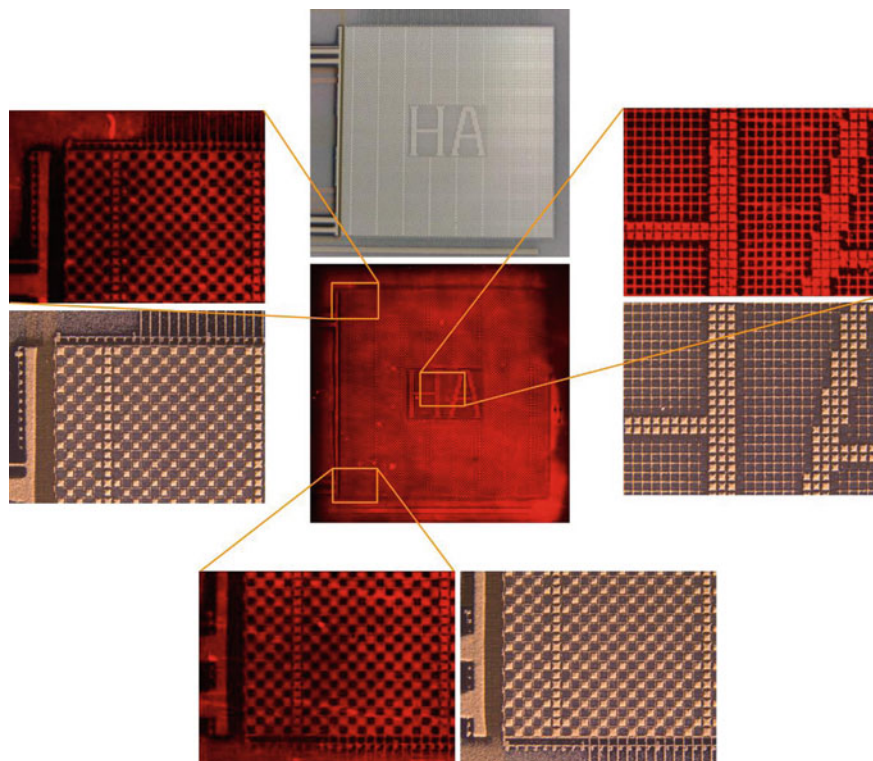


**Fig. 3.34** First imprint in the specific transfer of model peptides from a micro chip to a gold-coated membrane with 100 nm pore size. The immunostaining revealed highly-specific and highly-resolved transfer on the  $\mu\text{m}$ -scale. Even peptides from the grid between the pixel electrodes which also obtained a cysteine key in the synthesis were transferred without noticeable lateral diffusion. This demonstrated that the purification method is probably capable of purifying features in the sub- $\mu\text{m}$  scale. Peptides were stained with the Cy5-anti-HA antibody. The readout was performed with the *GenePix 4000B* scanner at 635 nm, whereby the membrane was glued to a microscopy slide. The corresponding cysteine particle deposition patterns are depicted to demonstrate the specificity and resolution of the transfer

problems in the transfer. The smaller pore size rather prevented blurring of the transferred pattern. Moreover, two high-quality transfers were achieved using the model peptide arrays, which, again, supports the feasibility of array replica production in the course of the purification.

The successful transfer demonstrates that the purification method, in principle, allows for the purification of arrays containing 10,000 individual features per  $\text{cm}^2$ . Furthermore, the transfer even of smaller features below 1  $\mu\text{m}$  in size seems to be possible without the risk of lateral diffusion (see Fig. 3.36).

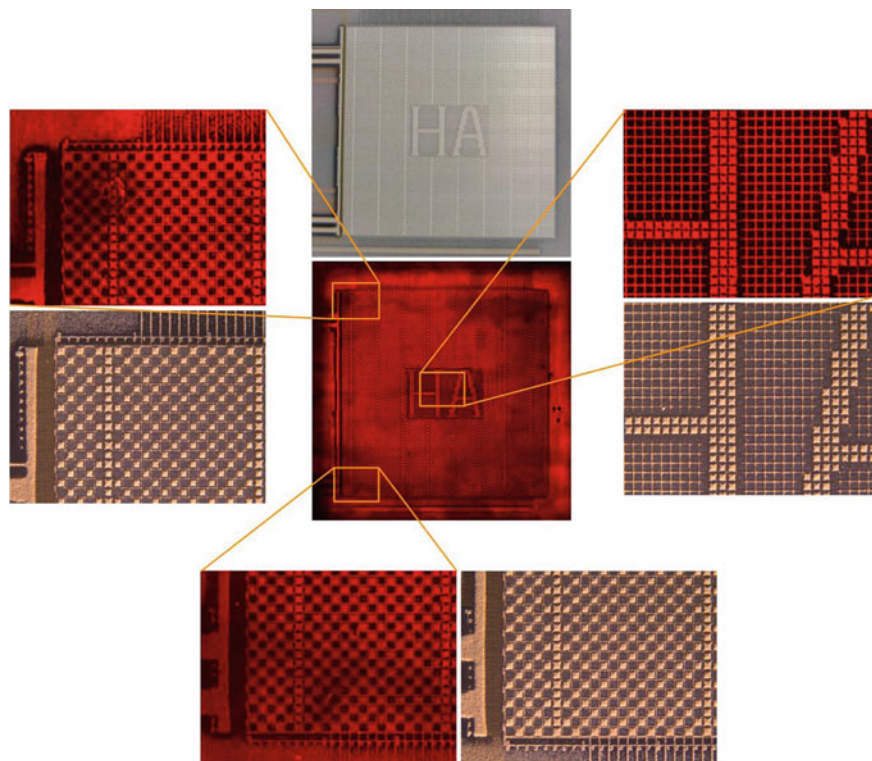


**Fig. 3.35** Second imprint in the specific transfer of model peptides from a micro chip to a gold-coated membrane with 100 nm pore size. A second transfer from the same microchip resulted in a comparable fluorescence pattern which supports the feasibility of peptide array replica production. The second transfer was performed for 20 min, whereas the first transfer had been conducted for 15 min. The readout was performed with the *GenePix 4000B* scanner at 635 nm, whereby the membrane was glued to a microscopy slide. The corresponding cysteine particle deposition patterns are depicted to demonstrate the specificity and resolution of the transfer

### 3.4.5 Purification of *in situ* Synthesized Peptide Arrays

To test the purification method with completely *in situ* synthesized peptide arrays instead of model peptides, a  $22 \times 21 \text{ cm}^2$  glass slide with the 10:90-PEGMA-co-PMMA-NH<sub>2</sub> coating was modified with the RAM linker. Subsequently, custom-designed peptide arrays were synthesized on this surface in the course of a routine peptide array synthesis at *PEPperPRINT GmbH*. Thereby the second generation laser printer (see Fig. 1.6) was applied.

The HA epitope used for the detection of the model peptides in the successful array transfers had been equipped with an *N*-terminal Gly<sub>3</sub> spacer (see Sect. 3.4.1 and Sect. 3.4.4). Here, the *in situ* synthesized peptides were elongated with an Ala<sub>2</sub> spacer before the specific cysteine pattern was printed in the last synthesis cycle



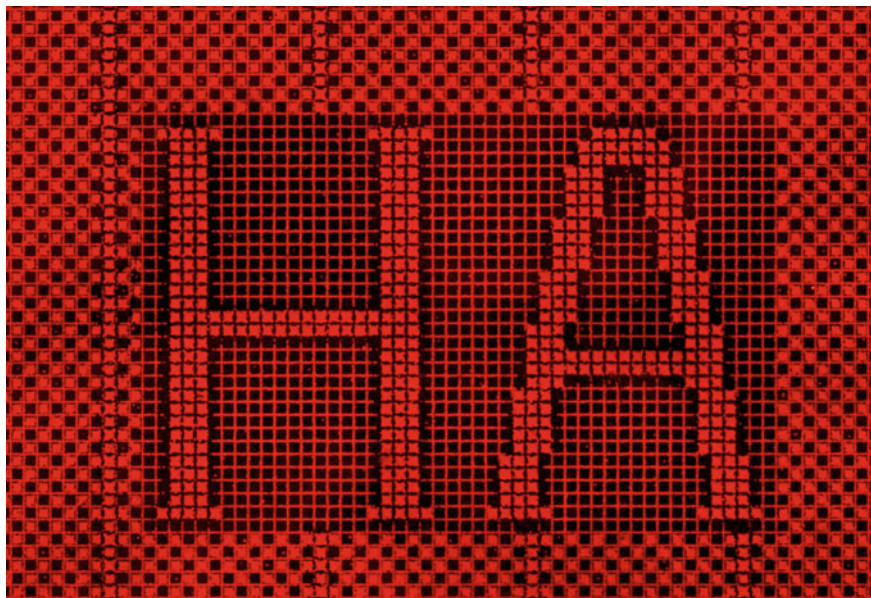


**Fig. 3.36** Close-up of the HA lettering of the second imprint. Even structures on the 15  $\mu\text{m}$  wide grid were transferred without lateral diffusion indicating that the transfer even of smaller features is possible

which meant saving one synthesis cycle (see Fig. 3.37a). A short spacer was assumed to be required to enable bulky proteins such as antibodies to reach the peptide on the membrane. At this point, all full-length peptides and synthesis fragments were still side-chain protected. The array purification was conducted in the same manner as the model peptide array purification. A receptor membrane with 100 nm pore size (20 s sputter time) was applied based on the good results in the high-resolution transfer using the micro chip (see Sect. 3.4.4). Figure 3.37 depicts the layout of an in situ synthesized test array and the corresponding fluorescence pattern obtained after immunostaining on the target membrane.

The test array contained two peptide epitopes: HA (YPYDVPDYA) and FLAG (DYKDDDDK). Only a selected pattern of these epitopes was elongated with a cysteine in the final printing step. Accordingly, the immunostaining after peptide transfer showed only the specific pattern of the cysteine-terminated peptides (Fig. 3.37b) which, in turn, indicated that the purification method could be applied to in situ synthesized arrays. However, compared to the intense HA staining, the FLAG staining showed very low fluorescence intensity. A lack in epitope-membrane distance due to the short *N*-terminal spacer length was assumed to hinder the anti-FLAG antibody in binding to the peptides. The spacer length is known to influence the antibody accessibility to immobilized peptides on gold surfaces [70]. On the other hand, a different quenching behaviour of the FluoProbes 752 dye ( $\lambda_{\text{ex}} = 748 \text{ nm}$ ,  $\lambda_{\text{em}} = 772 \text{ nm}$ ) in close proximity to the gold surface could also

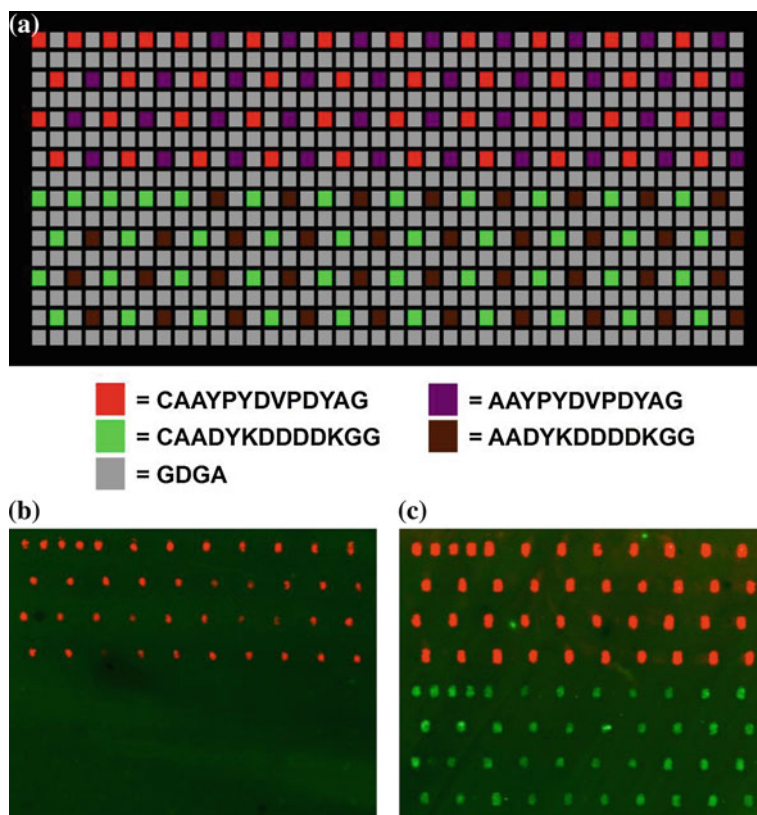


**Fig. 3.37** Layout and purification of an in situ synthesized peptide array. **a** The layout of the array contained a total of  $16 \times 40$  spots. Two peptide epitopes were printed in the depicted pattern whereby only selected spots (*red* and *green* squares) obtained an *N*-terminal cysteine (HA = YPYDVDPYA and FLAG = DYKDDDDK). Thus, reference epitopes without an *N*-terminal cysteine (*purple* and *brown* squares) were present in the same array. To achieve a wider spot to spot spacing in the given laser printer raster, a tetra peptide (GDGA, *grey* squares) was inserted. All peptides were synthesized on a standard support equipped with the RAM linker. **b** After transfer to a gold-coated PVDF membrane (20 s sputter time) immunostaining with the ATTO 680-anti-HA antibody (*red*) and FluoProbes 752-anti-FLAG (*green*) antibodies showed a specific transfer of the cysteine-terminated peptides. Compared to the intense HA staining the FLAG staining was almost not visible. **c** Blocking the membrane with PVP instead of *Rockland* blocking buffer before the immunostaining and overnight incubation with the FluoProbes 752-anti-FLAG solution noticeably increased the obtained fluorescence intensity for both epitopes

have contributed to the low fluorescence intensity in the immunostaining. In a second purification transfer which was conducted in parallel, the receptor membrane was blocked with 1 % (m/v) polyvinylpyrrolidone (PVP) instead of the routinely applied *Rockland* blocking buffer. The PVP had a weight average molar mass ( $M_w$ ) of around 40,000 g/mol which is rather low compared to the molecular weight of proteins in standard blocking buffers. Moreover, the incubation with

FluoProbes 752-anti-FLAG was conducted overnight, whereas the staining with ATTO 680-anti-HA was performed as before. The fluorescence scan showed an improved staining of both epitopes (Fig. 3.37c) which could be attributed to a better accessibility of the peptides in the absence of bulky blocking agents. However, these are preliminary findings and further studies will have to focus on optimizing the conditions in applications of the purified peptide arrays. In summary, the peptide array purification method proved to be applicable to in situ synthesized arrays reaffirming the results obtained with the model peptide arrays.

### 3.5 Important Parameters in the Transfer

The focus in the most recent work was placed on the development of a peptide array purification method and the proof-of-principle experiments. However, several parameters seemed to influence the quality of the array transfer and will need to be further optimized in the future. Therefore, the following chapter gives a brief overview of parameters which were considered to be crucial for the detection of peptides on the receptor membrane and the successful array purification.

#### 3.5.1 Blocking Agents

In the transfer of peptides from the model arrays (see Sect. 3.4.3), additional self-assembly of EG<sub>7</sub>-SH prior to routine blocking with *Rockland* blocking buffer led to an improvement in the immunostainings. The self-assembly of EG<sub>7</sub>-SH on the gold-coated membrane was routinely adopted into the peptide purification protocol and, therefore, further addressed in XPS. It was assumed that the EG<sub>7</sub>-SH helped to prevent nonspecific antibody adsorption and, therefore, decreased background in the immunostainings. Figure 3.38 shows a comparison of XP spectra measured on pieces of the same gold-coated PVDF membrane (20 s sputter time). The samples were treated with (A) EtOH (reference), (B) 2 mM EG<sub>7</sub>-SH in EtOH, (C) 2 mM poly(ethylene glycol) methylether thiol (PEG-SH, M<sub>n</sub> = 2,000) in EtOH, and (D) 1 % (m/v) PVP in water, at RT overnight. Besides the packing density, the arrangement of molecules, and the hydrophilicity of oligo(ethylene glycol) ether SAMs, the length of the EG chain is known to contribute to the protein repelling properties [71–73]. Therefore, the self-assembly of PEG-SH was considered to possibly render any further blocking of the membrane redundant.

Compared to the reference, the assembly of the two thiols (EG<sub>7</sub>-SH and PEG-SH) was indicated by an increase in O1 s and C1s signal intensities (see Fig. 3.38). Higher O1 s and C1s signals were detected for PEG-SH which could be caused by the longer EG chains of these molecules. The adsorption of PVP was indicated by an additional N1s signal. However, only low amounts of PVP were probably adsorbed because the signal in the C1s area was approximately in the same range

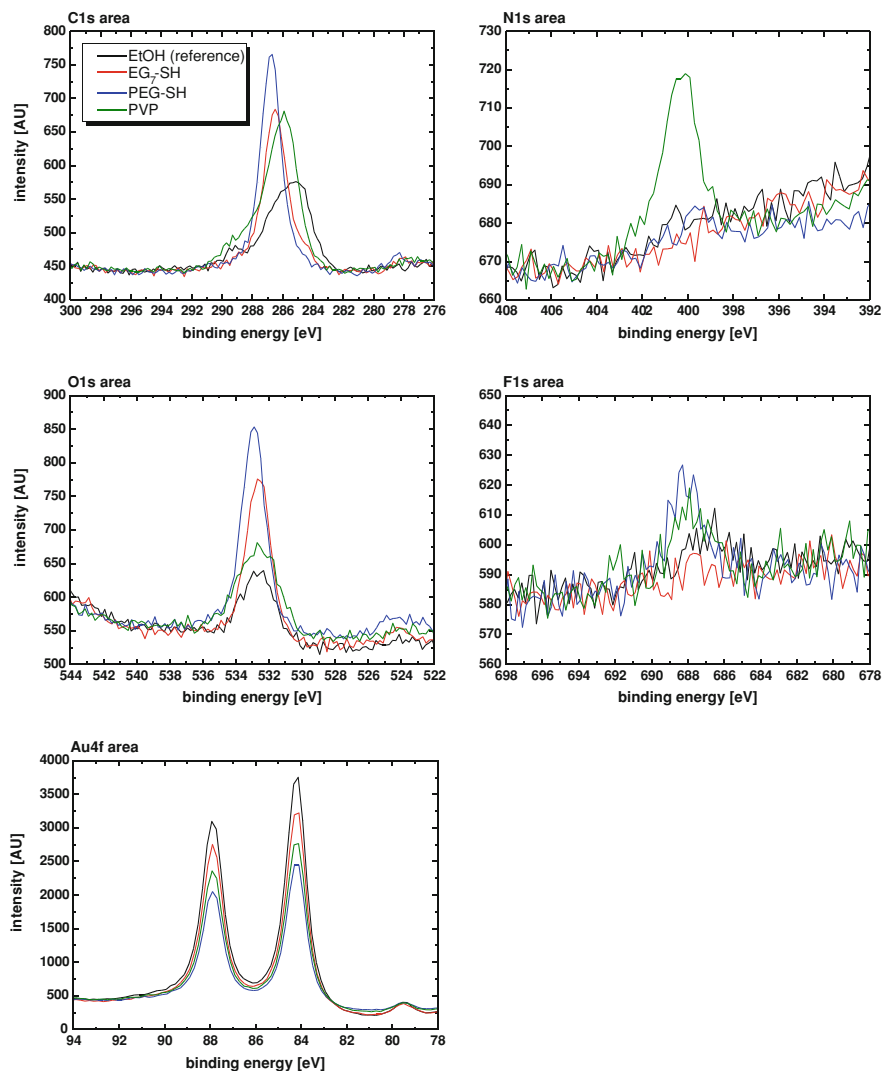


**Fig. 3.38** C1s, N1s, O1s, F1s, and Au4f areas of gold-coated membranes with different surface blocking. Self-assembly of the two EG-containing thiols was indicated by signals in the C1s and O1s areas, whereby the higher signal was detected for the longer EG chain in PEG-SH (*blue line*). PVP adsorption caused an additional peak in the N1s area (*green line*). In general, blocking attenuated the Au4f signals, whereby the lowest signal was obtained for the PEG-SH sample. Only weak F1s signals indicated a dense gold-coating of the membrane

as the signal for EG<sub>7</sub>-SH self-assembly. In the F1s area, only weak signals were detected which indicates that the gold coating presumably covered most of the underlying PVDF in the analysis volume (also see Sect. 3.3.2). The Au4f signals

were attenuated by the thiol self-assembly and the PVP adsorption, whereby the strongest decrease in signal intensity was detected for the PEG-SH sample.

Looking at the XP spectra, PEG-SH appears to yield the highest concentration of EG units on the membrane which could be connected with a higher resistance to protein adsorption. However, taking the higher number of EG units in PEG-SH (around 40–45) into account an even higher C1s and O1s was expected. Therefore, it can be assumed that EG<sub>7</sub>-SH is more densely packed than PEG-SH. Nevertheless, PEG-SH seemed to be an alternative to EG<sub>7</sub>-SH to achieve high protein resistance. However, a transfer experiment with an in situ synthesized array, which was conducted in parallel to the experiments described in Sect. 3.4.5, the immunostaining showed no fluorescence signals on the receptor membrane which was blocked with PEG-SH instead of EG<sub>7</sub>-SH. Therefore, it was assumed that the coating formed by PEG-SH either prevented the antibodies from reaching the epitopes or displaced the peptides from the surface. As a consequence, blocking of the membranes was continued with EG<sub>7</sub>-SH. EG<sub>7</sub>-SH interfered neither with the transferred peptides nor with the immunostaining. The exact blocking potential of the EG<sub>7</sub>-SH SAM on the gold-coated membrane in the presence of proteins was not further addressed in this work because the self-assembly was obviously successful and, as mentioned before, the protein-repelling properties of such oligo(ethylene glycol) ether SAMs are well-known [26, 73]. However, an interesting task in the future would be the self-assembly of different protein-repelling thiols on the receptor membrane to study the impact on the blocking potential.

Furthermore, replacement of *Rockland* blocking buffer with PVP seemed to provide better access for the antibodies if the spacer between epitope and cysteine was short. However, as mentioned above, these improvements have not been fully explored and will have to be further studied.

It must be mentioned that despite the specific transfer of in situ synthesized peptide arrays discussed in Sect. 3.4.5, also nonspecific transfer can occur. Figure 3.39 shows a transfer to a receptor membrane with 100 nm pores in which also the peptides without cysteine became visible in the immunostaining (*white* circles, also see Sect. 3.4.4, Fig. 3.37a). In this experiment, the surface had only been blocked with the EG<sub>7</sub>-SH. No additional *Rockland* buffer was applied which made it likely that also signals within the pores of the receptor membrane were detected. The lack in binding specificity was attributed to insufficient washing after the transfer and a defective gold coating in the depth of the pores. However, also the pore size of the receptor membrane could play a role in the efficient removal of nonspecifically adsorbed peptides and synthesis fragments from the membrane. Purification of in situ synthesized arrays with a resolution of 700–800 peptide spots per cm<sup>2</sup> probably does not require the 100 nm pore size membranes which may hamper the removal on nonspecifically adsorbed species. Instead, such in situ synthesized arrays could be transferred to the 450 nm membrane which had been successfully used with the laser-printed model peptide arrays (Sect. 3.4.3).

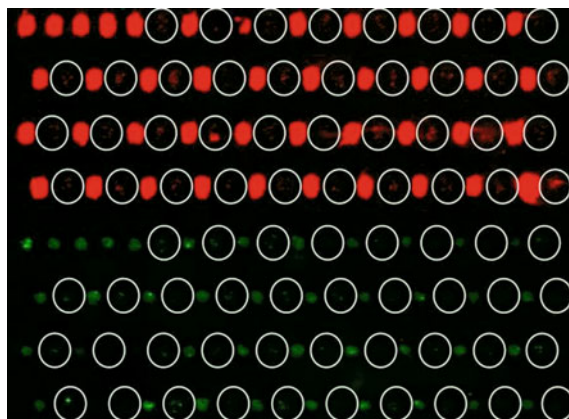


**Fig. 3.39** Nonspecific transfer of an in situ synthesized peptide array. The receptor membrane was only blocked with EG<sub>7</sub> thiol after the transfer. Nonspecific peptide transfer became visible by signals of the “control” peptide epitopes without an *N*-terminal cysteine (*white circles*). The nonspecific transfer was presumably caused by insufficient washing of the membrane after the transfer or a defective gold coating inside the membrane pores

### 3.5.2 Gold Thickness and Fluorescent Labels

In principle, a dense gold coating is favorable with regard to a specific peptide transfer and an efficient blocking using EG-thiols. As mentioned in [Sects. 3.4.3](#) and [3.4.4](#), the combination of gold thickness and fluorophore seems to affect the quality of the immunostaining. In general, the ATTO 680-anti-HA antibody, which was most frequently applied, showed good fluorescence signals if the membranes were sputter coated for 15–20 s corresponding to gold thicknesses between 22 and 47 nm on flat substrates (see [Sect. 3.3.2](#), [Table 3.3](#)). However, an experiment comparing the fluorescence of dyes on gold films of different thickness (20 and 30 s respectively) showed an interesting result. The array depicted in [Fig. 3.37](#) was additionally stained with the Cy3-anti-FLAG ( $\lambda_{\text{ex}} = 550 \text{ nm}$ ,  $\lambda_{\text{em}} = 570 \text{ nm}$ ) and Cy5-anti-HA ( $\lambda_{\text{ex}} = 643 \text{ nm}$ ,  $\lambda_{\text{em}} = 667 \text{ nm}$ ) antibodies. A new array transfer to a receptor membrane with 30 s gold coating was first stained with the ATTO 680-anti-HA and FluoProbes 752-anti-FLAG antibodies, then with the Cy3-anti-FLAG and Cy5-anti-HA antibodies. The readout was conducted with the *Odyssey Infrared Imager* (ATTO 680 and FluoProbes 752) and the *GenePix 4000B* scanner (Cy3 and Cy5). [Figure 3.40](#) shows a comparison of the fluorescence images.

The immunostainings showed that the ATTO 680-anti-HA and FluoProbes 752-anti-FLAG antibodies were clearly detectable on the 20 s gold-coated receptor membrane but not on the 30 s gold-coated membrane. Here, high background in the 800 nm channel (green) was visible which could be due to insufficient blocking. In contrast, the Cy5-anti-HA antibody in the *GenePix 4000B* scan

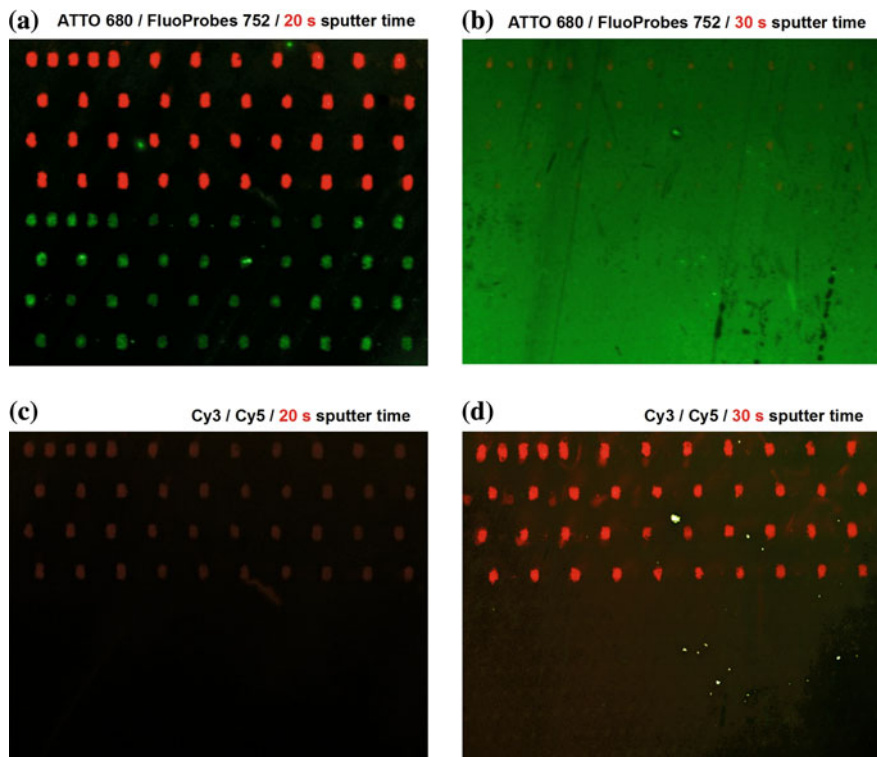


**Fig. 3.40** Comparison of dyes on 20 s (*left*) and 30 s (*right*) gold-coated membranes. **a,b** *Odyssey Infrared Imager* scans only showed clear signals on the receptor membrane which had been sputter coated for 20 s (ATTO 680-anti-HA and FluoProbes 752-anti-FLAG antibodies). The scan of the 30 s gold-coated membrane revealed a high background in the 800 nm channel (*green*) which could be due to insufficient blocking. **c,d** The *GenePix 4000B* scans revealed stronger signals of the Cy5-anti-HA antibody on the 30 s gold-coated receptor membrane. The Cy3-anti-FLAG antibody was not detected on either surface which could be due to a low accessibility, occupation of binding sites by the FluoProbes 752-anti-FLAG antibody, or quenching effects. The slightly visible “double signals” in **d** were caused by accidental shifting of the slide in the transfer

showed better signals on the 30 s gold-coated receptor membrane which is why this membrane was used in the high-resolution chip transfer (see [Sect. 3.4.4](#)).

In summary, an efficient immunostaining appears to depend on several parameters: In terms of background the thickness of the gold coating, the blocking agents, the pore size of the membrane, and thorough washing are important parameters. Regarding intense fluorescence signals, the choice of fluorophor, the accessibility of the antibody i.e. the length of the *N*-terminal spacer attached to the peptide, and the distance between fluorophor and surface most likely play a role. As mentioned above, quenching in proximity to gold-surfaces is a known phenomenon [66]. However, the gold thickness in the present work could only be

controlled via the sputter time. Variations in the gold thickness evidenced by slight color differences could not be avoided. To study the parameters summarized above, a more precise knowledge of the gold coating in terms of thickness and density inside the membrane pores would be required.

## References

1. I. Zubel, M. Kramkowska, *Sens. Actuators. A* **115**, 549–556 (2004)
2. I. Zubel, K. Rola, M. Kramkowska, *Sens. Actuators. A* **171**, 436–445 (2011)
3. C. Schirwitz, I. Block, K. König, A. Nesterov, S. Fernandez, T. Felgenhauer, K. Leibe, G. Torralba, M. Hausmann, V. Lindenstruth, V. Stadler, F. Breitling, F. R. Bischoff, *Curr. Protoc. Protein Sci.* 18.12.11–18.12.13 (2009). doi:[10.1002/0471140864.ps1802s57](https://doi.org/10.1002/0471140864.ps1802s57)
4. M. Beyer, I. Block, K. König, A. Nesterov, S. Fernandez, T. Felgenhauer, C. Schirwitz, K. Leibe, R. F. Bischoff, F. Breitling, V. Stadler, *Methods Mol. Biol.* **570**, 309–316 (2009)
5. V. Stadler, M. Beyer, K. König, A. Nesterov, G. Torralba, V. Lindenstruth, M. Hausmann, F.R. Bischoff, F. Breitling, *J. Proteome Res.* **6**, 3197–3202 (2007)
6. S. Tugulu, A. Arnold, I. Sielaff, K. Johnsson, H.A. Klok, *Biomacromolecules* **6**, 1602–1607 (2005)
7. T. Felgenhauer, V. Stadler, personal communication (2009)
8. D.M. Jones, A.A. Brown, W.T.S. Huck, *Langmuir* **18**, 1265–1269 (2002)
9. H. Liu, M. Li, Z.Y. Lu, Z.G. Zhang, C.C. Sun, *Macromolecules* **42**, 2863–2872 (2009)
10. V. Stadler, R. Kirmse, M. Beyer, F. Breitling, T. Ludwig, F.R. Bischoff, *Langmuir* **24**, 8151–8157 (2008)
11. S.M. Kimani, S.C. Moratti, *Macromol. Rapid Commun.* **27**, 1887–1893 (2006)
12. J.S. Wang, K. Matyjaszewski, *Macromolecules* **28**, 7901–7910 (1995)
13. A. Olivier, F. Meyer, J.M. Raquez, P. Damman, P. Dubois, *Prog. Polym. Sci.* **37**, 157–181 (2012)
14. S.M. Kimani, S.C. Moratti, *J. Polym. Sci. Part A: Polym. Chem.* **43**, 1588–1598 (2005)
15. A.K. Nanda, K. Matyjaszewski, *Macromolecules* **36**, 1487–1493 (2003)
16. D.M. Haddleton, S. Perrier, S.A.F. Bon, *Macromolecules* **33**, 8246–8251 (2000)
17. J. Striffler, *Effizienz spaltbarer Linker für die kombinatorische Peptidsynthese im Array-Format* Diploma thesis, University of Heidelberg, 2011
18. H. Bergenudd, G. Coullerez, M. Jonsson, E. Malmström, *Macromolecules* **42**, 3302–3308 (2009)
19. A. Ulman, *Chem. Rev.* **96**, 1533–1554 (1996)
20. T. P. Sullivan, W. T. S. Huck, *European J. Org Chem* **2003**, 17–29 (2003)
21. J.C. Love, L.A. Estroff, J.K. Kriebel, R.G. Nuzzo, G.M. Whitesides, *Chem. Rev.* **105**, 1103–1169 (2005)
22. T. Ast, N. Heine, L. Germeroth, J. Schneider-Mergener, H. Wenschuh, *Tetrahedron Lett.* **40**, 4317–4318 (1999)
23. J. Pehler, A. Brecht, R. Valiokas, B. Liedberg, G. Gauglitz, *Biosens. Bioelectron.* **15**, 473–481 (2000)
24. J.A.A. Sales, A.G.S. Prado, C. Airoidi, *Polyhedron* **21**, 2647–2651 (2002)
25. J. Mehne, G. Markovic, F. Pröll, N. Schweizer, S. Zorn, F. Schreiber, G. Gauglitz, *Anal. Bioanal. Chem.* **391**, 1783–1791 (2008)
26. K.L. Prime, G.M. Whitesides, *J. Am. Chem. Soc.* **115**, 10714–10721 (1993)
27. R.L.C. Wang, H.J. Kreuzer, M. Grunze, *J. Phys. Chem. B* **101**, 9767–9773 (1997)
28. R.L.C. Wang, H.J. Kreuzer, M. Grunze, *Phys. Chem. Chem. Phys.* **2**, 3613–3622 (2000)
29. S. Schilp, A. Rosenhahn, M.E. Pettitt, J. Bowen, M.E. Callow, J.A. Callow, M. Grunze, *Langmuir* **25**, 10077–10082 (2009)



30. I. Luzinov, D. Julthongpiput, A. Liebmann-Vinson, T. Cregger, M.D. Foster, V.V. Tsukruk, *Langmuir* **16**, 504–516 (2000)
31. A.K.Y. Wong, U.J. Krull, *Anal. Chem.* **383**, 187–200 (2005)
32. H.P. Wampler, D.Y. Zemlyanov, K. Lee, D.B. Janes, A. Ivanisevic, *Langmuir* **24**, 3164–3170 (2008)
33. A. Wang, H. Tang, T. Cao, S.O. Salley, K.Y.S. Ng, *J. Colloid Interface Sci.* **291**, 438–447 (2005)
34. H. Rink, *Tetrahedron Lett.* **28**, 3787–3790 (1987)
35. M.S. Bernatowicz, S.B. Daniels, H. Köster, *Tetrahedron Lett.* **30**, 4645–4648 (1989)
36. F. Guillier, D. Orain, M. Bradley, *Chem. Rev.* **100**, 2091–2157 (2000)
37. N. Jung, M. Wiehn, S. Bräse, in ed by S. Bräse, V. Balzani, A. Meijere, K. N. Houk, J. M. Lehn, H. Kessler, S. V. Ley, S. L. Schreiber, *Top. Curr. Chem.* **278**, 1–88 (2007)
38. V. Stadler, T. Felgenhauer, M. Beyer, S. Fernandez, K. Leibe, S. Güttler, M. Gröning, K. König, G. Torralba, M. Hausmann, V. Lindenstruth, A. Nesterov, I. Block, R. Pipkorn, A. Poustka, F.R. Bischoff, F. Breitling, *Angew. Chem. Int. Ed.* **47**, 7132–7135 (2008)
39. M. Beyer, Entwicklung und Anwendung neuartiger Trägeroberflächen zur kombinatorischen Peptidsynthese mit Aminosäure-Tonerpartikeln, Ph.D. thesis, University of Heidelberg, 2005
40. I. Block, Herstellung und Anwendung von hochkomplexen Peptidbibliotheken, Ph.D. thesis, University of Heidelberg, 2009
41. F. Stieber, U. Grether, H. Waldmann, *Angew. Chem. Int. Ed.* **38**, 1073–1077 (1999)
42. F. Berst, A.B. Holmes, M. Ladlow, *Org. Biomol. Chem.* **1**, 1711–1719 (2003)
43. S. Hoffmann, R. Frank, *Tetrahedron Lett.* **35**, 7763–7766 (1994)
44. M. Beyer, T. Felgenhauer, F.R. Bischoff, F. Breitling, V. Stadler, *Biomaterials* **27**, 3505–3514 (2006)
45. C. Peters, H. Waldmann, *J. Org. Chem.* **68**, 6053–6055 (2003)
46. M. Gude, J. Ryf, P.D. White, *Let. Pept. Sci.* **9**, 203–206 (2002)
47. M. Beyer, personal communication (2008)
48. R. Volkmer, *ChemBioChem* **10**, 1431–1442 (2009)
49. K. Hilpert, D.F.H. Winkler, R.E.W. Hancock, *Nat. Protoc.* **2**, 1333–1349 (2007)
50. R. J. Pounder, M. J. Stanford, P. Brooks, S. P. Richards, A. P. Dove, *Chem. Commun.* 5158–5160 (2008)
51. C.E. Hoyle, C.N. Bowman, *Angew. Chem. Int. Ed.* **49**, 1540–1573 (2010)
52. A. Holmberg, A. Blomstergren, O. Nord, M. Lukacs, J. Lundeberg, M. Uhlén, *Electrophoresis* **26**, 501–510 (2005)
53. J.A. Camarero, B.J. Hackel, J.J. De Yoreo, A.R. Mitchell, *J. Org. Chem.* **69**, 4145–4151 (2004)
54. F. Liu, N.A. Hashim, Y. Liu, M.R.M. Abed, K. Li, *J. Membr. Sci.* **375**, 1–27 (2011)
55. D. T. Clark, W. J. Feast, D. Kilcast, W. K. R. Musgrave, *J. Polym. Sci. Part A-1 Polym. Chem.* **11**, 389–411 (1973)
56. Millipore Technical Support, personal communication, (2012)
57. N. Singh, S.M. Husson, B. Zdyrko, I. Luzinov, *J. Membr. Sci.* **262**, 81–90 (2005)
58. Y. Chang, C.Y. Ko, Y.J. Shih, D. Quémener, A. Deratani, T.C. Wei, D.M. Wang, J.Y. Lai, *J. Membr. Sci.* **345**, 160–169 (2009)
59. T.H. Young, H.H. Chang, D.J. Lin, L.P. Cheng, *J. Membr. Sci.* **350**, 32–41 (2010)
60. C. Duschl, A.F. Sévin-Landais, H. Vogel, *Biophys. J.* **70**, 1985–1995 (1996)
61. H.J. Himmel, A. Terfort, C. Wöll, *J. Am. Chem. Soc.* **120**, 12069–12074 (1998)
62. A. Isidro-Llobet, M. Álvarez, F. Albericio, *Chem. Rev.* **109**, 2455–2504 (2009)
63. R.S. Garigipati, *Tetrahedron Lett.* **38**, 6807–6810 (1997)
64. T. Pohl, personal communication, (2011)
65. F. Breitling, C. Schirwitz, T. Felgenhauer, I. Block, V. Stadler, R. Bischoff, in *Antibody Engineering*, ed. by R. Kontermann, S. Dübel (Springer, Berlin, 2010), pp. 573–589. doi:10.1007/978-3-642-01144-3\_36

66. R. R. Chance, A. H. Miller, A. Prock, R. Silbey, Fluorescence and energy transfer near interfaces: the complete and quantitative description of the Eu<sup>3+</sup>/mirror systems, *Chem. Phys.* **63**, 1589 (1975)
67. M. Beyer, A. Nesterov, I. Block, K. König, T. Felgenhauer, S. Fernandez, K. Leibe, G. Torralba, M. Hausmann, U. Trunk, V. Lindenstruth, F.R. Bischoff, V. Stadler, F. Breitling, *Sci.* **318**, 1888 (2007)
68. K. König, I. Block, A. Nesterov, G. Torralba, S. Fernandez, T. Felgenhauer, K. Leibe, C. Schirwitz, F. Löffler, F. Painke, J. Wagner, U. Trunk, F.R. Bischoff, F. Breitling, V. Stadler, M. Hausmann, V. Lindenstruth, *Sens. Actuators. B* **147**, 418–427 (2010)
69. F. Löffler, J. Wagner, K. König, F. Märkle, S. Fernandez, C. Schirwitz, G. Torralba, M. Hausmann, V. Lindenstruth, F.R. Bischoff, F. Breitling, A. Nesterov, *Aerosol. Sci. Tech.* **45**, 65–74 (2011)
70. G.J. Wegner, H.J. Lee, R.M. Corn, *Anal. Chem.* **74**, 5161–5168 (2002)
71. J.H. Lee, H.B. Lee, J.D. Andrade, *Prog. Polym. Sci. (Oxford)* **20**, 1043–1079 (1995)
72. I. Szleifer, *Biophys. J.* **72**, 595–612 (1997)
73. S. Herrwerth, W. Eck, S. Reinhardt, M. Grunze, *J. Am. Chem. Soc.* **125**, 9359–9366 (2003)
74. <http://www.millipore.com/catalogue/item/ipvh00010>. Accessed 19 Jan 2012
75. <http://www.millipore.com/catalogue/item/vvlp09050>. Accessed 19 Jan 2012

# Chapter 4

## Conclusion

### 4.1 Conclusion

The aim of the present work was to develop a purification method for combinatorially synthesized peptide arrays. This goal was achieved by transferring the peptide array to a second solid support whereby only full-length peptides were able to re-bind via an N-terminal cysteine. In general, the method is compatible with standard micro-particle based solid phase peptide synthesis (mpSPPS) and only few additional steps are required to allow for peptide purification: The solid support was equipped with a standard acid-labile linker, the RAM linker, which could be cleaved after the peptide synthesis in the course of the side-chain deprotection using TFA. Coupling and cleavage of the RAM linker proved to be easily achieved in the peptide array synthesis, whereas the implementation of the physiologically cleavable HBA linker was not successful. Furthermore, an N-terminal cysteine was added to the peptides in the last synthesis step. Due to the protecting group strategy and routine acylation steps, only full-length peptides should obtain this “key”-sequence which was implicitly required for the purification effect in the transfer. The transfer of entire arrays was achieved by using flexible PVDF membranes which could be soaked with the required TFA medium and brought into close contact with the synthesis support. According to the developed method, the peptide array is simply placed on top of such a piece of TFA-soaked membrane in order to simultaneously initiate the transfer the entire array as well as the cleavage of side-chain protecting groups. To allow for the specific transfer of only the cysteine-terminated peptides, the membranes were additionally coated with a thin gold-layer. Peptides with the N-terminal cysteine could, thus, rebind across a thiol-gold bond which was found to be compatible with the TFA-acidic conditions. Specific transfer of peptide arrays could be demonstrated down to a resolution of 10,000 peptide spots per cm<sup>2</sup>. Even at such high-resolutions the array quality was not diminished by lateral diffusion suggesting that arrays of even higher resolution could be purified by this method in the future.

## 4.2 Outlook

In principle, the purification method can be directly applied to obtain high-quality and high-complexity peptide arrays. Moreover, the method is not limited to peptide arrays synthesized by the micro particle-based approach but could also be used to purify arrays synthesized by the SPOT technique.

To further optimize the method with respect to the desired application of the peptide arrays, several tasks remain. First of all, an automation of the transfer process would be favorable: Although the described technique was applicable for the highly-resolved arrays on micro chips, an automation of the process would reduce the risk of shifting of the support. Moreover, the gold-coating of the membrane is the key requisite for the purification effect in the transfer of peptides because it allows for a specific re-binding of full-length array members. The gold-coating was applied by sputter coating and, thus, the film thickness could only be estimated by the sputter time and the resulting color of the gold membrane. The sputter time is a good parameter when flat substrates are coated, but for porous membranes a more detailed analysis of the gold thickness in the depth of the structure is required. In the present work, sputter times between 15 and 30 s corresponding to an approximate gold thickness of 22–47 nm on flat substrates showed good transfer results. However, nonspecific transfer could also occur which was assumed to be an effect of inhomogeneous coating in the depth of the membrane pores. Furthermore, the effect of the gold coating on the fluorescence of standard fluorophores has to be further studied. In typical applications of peptide arrays, analytes are labelled with a fluorophore to detect interaction with the array. The presence of a gold surface can lead to fluorescence quenching rendering this detection method inefficient. Therefore, a more detailed understanding of the fluorescence behaviour in correlation to the gold thickness on a membrane is desired. In this context, also the length of spacer sequences at the N-terminus of the peptides is assumed to have a considerable impact. The distance of the binding site to the surface determines whether the peptide is accessible to the analyte molecules and whether the fluorescence of the dye can be quenched.

Another task in the future will be the homogenization of the peptide amount per synthesis spot in the array. As described in the introduction, the amount per spot is strictly dependent on the synthesis efficiency which, in turn, depends on the target sequence. If there is always an excess of full-length peptides relative to the number of specific binding sites on the receptor membrane, the transfer method could also be used to balance the amount of peptides per spot.

Although some parameters have yet to be further investigated, the method already yields high-quality peptide arrays in a fast and simple manner. The technique can be applied to any peptide array synthesized according to the N<sup>z</sup>-Fmoc strategy and it allows for one-step purification of entire peptide libraries. Thus, this work paved the way for the routine production of high-purity and high-density peptide arrays. Such arrays can help to advance the field of genomics and biomedical research in the future.

# Chapter 5

## Materials and Methods

### 5.1 Devices and Measuring Parameters

#### 5.1.1 UV/Vis Spectrometry

UV/Vis spectra were measured with the *SmartSpec Plus* spectrometer (*Bio-Rad Laboratories*, Munich/Germany). For the measurements disposable UV cuvettes (*neoLab GmbH*, Heidelberg/Germany) with a transparency between 220 and 900 nm were applied. To determine DGs according to the PDFA method (see [Sect. 2.3.1](#)) the respective surface was typically covered with a defined volume of 20 % (v/v) piperidine in DMF. After 20 min incubation time at least two 100  $\mu$ L samples of the solution were pipetted into UV cuvettes and directly measured at 301 nm. The DG was calculated based on the extinction (see [Sect. 2.3.1](#), Eq. 2.1).

#### 5.1.2 Ellipsometry

Film thicknesses were measured with the M-44 multiple wavelength ellipsometer (*J. A. Woollam Co. Inc.*, Lincoln, NE/USA). The samples were aligned at a nominal incidence angle of  $75^\circ$  to the surface normal. SAM and polymer layer thicknesses were determined using the appendant *WVASE* software and a single CAUCHY model layer [1]. Clean Si(100) wafers kept in air are usually covered with a 21–25 Å thin SiO<sub>2</sub> layer [2, 3] on which SAMs of organo-silanes can be assembled as an anchor group for polymers (see [Sect. 2.2.2](#)). The thickness of the polymer coating in such multilayered systems was determined by measuring the sample against a UV-cleaned reference wafer (silicon bulk + silicon oxide). Assuming homogeneous molecular packing (silicon bulk + silicon oxide + organic layer) the CAUCHY model was used to fit the thicknesses of the organic layers (see [Sect. 2.3.2](#), Eq. 2.7).

### 5.1.3 Scanning Electron Microscopy

The device was a *LEO 1530 Scanning Electron Microscope (Carl Zeiss SMT AG, Oberkochen/Germany)*. SEM images were taken with support by Hacı Osman GÜVENÇ.

### 5.1.4 X-ray Photoelectron Spectroscopy

The instrument used was a MAX 200 with a LHS 12 spectrometer (*Leybold–Heraeus GmbH, Hanau/Germany*) equipped with an Al  $K_{\alpha}$  and a Mg  $K_{\alpha}$  X-ray source (respective energies: 1486.6 and 1253.6 eV) and a Specs EA200 multi-channeltron detector. Measurements were performed with either Al or Mg anode using the standard parameters displayed in Table 5.1. Dependent on the type of material shifts in the peak position occurred. For example, peaks in the spectra of pristine PVDF membranes were shifted by up to +11 eV due to charging effects. Therefore, start and end energy were adapted to the peak position and the shape of the peak in the narrow scans. First an overview spectrum was measured: In case, a shift of more than 1 eV from the expected peak position was observed, the parameters for both start and end energy were adapted to the shift and the peak shape, respectively.

All spectra were subsequently normalized with a device specific transmission function because the sensitivity of the detector is dependent on the energy region. The spectra were then processed in the *Microcal Origin 3.78* software (*Microcal Software Inc., Northampton, MA/USA*) with the appendant peak fitting module. All spectra measured on silicon wafers or glass substrates were normalized to the alkylic C1s signal at 284.6 eV. Spectra of PVDF membranes were normalized to the CH<sub>2</sub> signal at 286.3 eV [4], whereas spectra measured on gold-coated membranes were normalized to the Au4f <sub>7/2</sub> signal at 84.21 eV [5].

Integration for the quantitative analysis of the signals was also performed with the *Origin* peak fitting module. A SHIRLEY baseline subtraction [6] taking a

**Table 5.1** Standard parameters for XPS measurements

Orbital	Start energy (eV)	End energy (eV)	Step width (meV)	Dwell time (ms)	Pass energy (eV)	Scans
Overview	1000	−4.8	400	10	96	3
Au4f	108	63	200	40	48	20
Br3p	200	174	200	250	48	20
C1s	302	273	200	100	48	20
F1s	706	676	200	40	48	20
N1s	410	390	200	250	48	20
O1s	541	521	200	40	48	20
Si2p	110	89	200	100	48	20

**Table 5.2** Ionization cross-sections and attenuation lengths for atomic orbitals in spectra measured with the Al anode (X-ray photon energy: 1486.6 eV)

Orbital	$\sigma_A(E_b)$ [7]	$\lambda_A(E_b)$ [Å]
C1s	1.00	24.0
N1s	1.80	21.5
O1s	3.08	20.3
F1s	4.43	19.7

discontinuity at the respective peak maximum into account was conducted prior to integration. The cross-sections and attenuation lengths used for quantitative analyses according to Eq. 2.12 (see Sect. 2.3.4) are listed in Table 5.2. Measurements for quantitative analyses were performed using the Al anode.

### 5.1.5 Sputter Coating

Membranes were sputter-coated using the *MED 020 Modular High Vacuum Coating System (Bal-Tec AG (Leica Microsystems), Wetzlar/Germany)* in the group of Prof. Dr. SPATZ (University of Heidelberg/Germany). Fitted pieces of *Immobilon-P* and *Durapore* membranes, respectively, were arranged on the sample holder. The device was evacuated to less than  $2 \times 10^{-4}$  mbar and the argon pressure was set to  $5 \times 10^{-2}$  mbar. Sputter coating with gold was executed at 60 mA for 15–35 s. Gold-coated surfaces were stored under argon atmosphere.

### 5.1.6 Fluorescence Scans

Fluorescence scans were either performed with the *Odyssey Infrared Imager (LICOR Biosciences, Lincoln, NE/USA)* or the *GenePix 4000B Microarray Scanner (Molecular Devices, Sunnyvale, CA/USA)*.

#### 5.1.6.1 Odyssey Infrared Imager

The *Odyssey Infrared Imager* is equipped with two solid state laser simultaneously providing light excitation at 685 and 785 nm. Accordingly, the Odyssey was used to scan samples stained with the ATTO 680, ATTO 700, IRDye 700DX, IR-Dye 800CW, and FluoProbes 752 dyes. To ensure good contact between the membranes and scanner plate the membranes were weighted with a low fluorescence glass plate (*Sigma-Aldrich GmbH, Steinheim/Germany*). The *Odyssey Infrared Imager* was routinely set to 21  $\mu\text{m}$  resolution and a detector intensity of 6.0. Image brightness, contrast, and color were adjusted in the *Odyssey Application Software 3.0* (V. 3.0.21). To compare the fluorescence intensity measured on

different membranes, the membranes were always scanned in one run and the entire image was adjusted. Quantitative analyses were performed with the *GenePix Pro 6.0 Acquisition and Analysis Software*. The images were imported and the automated *irregular feature recognition* was used to obtain the background-corrected mean fluorescence intensity of all spots in an array.

### 5.1.6.2 GenePix 4000B Microarray Scanner

The *GenePix 4000B* scanner is a microscopy slide scanner equipped with two solid state lasers providing simultaneous light excitation at 532 and 635 nm. The scanner was applied to scan samples labelled with the Cy3 and Cy5 dyes. To scan pieces of glass slides or membranes the samples had to be glued to microscopy slides using *Spray Mount (3 M Deutschland GmbH, Neuss/Germany)* so that the samples could be fixed in the sample holder. Image acquisition was performed with the *GenePix Pro 6.0 Acquisition and Analysis Software*. The scanner was set to a resolution of 5  $\mu\text{m}$ , 33 % scan power, and photo multiplier tube (PMT) values of 500–700 depending on the fluorescence intensity in a pre-scan. Furthermore, the focus offset was adjusted for best acuity.

### 5.1.7 Spotting Robot

The peptide arrays were spotted by Christian SCHMIDT (DKFZ) using the *BioChip Arrayer (PerkinElmer Life Sciences, Boston, MA/USA)* with a single *PiezoTip*. The volume per spot was set to 0.5 nL. Each peptide solution was prepared in filtered phosphate buffer (pH 7.0, 7 mM) and filled in *Small Volume 384 Well Plates (Greiner Bio-One GmbH, Frickenhausen/Germany)*.

### 5.1.8 Equipment for the Micro Chip-Based Synthesis

The setup for the micro chip-based peptide array synthesis consisted of custom-built *coupling chambers* with two gas valves, custom-built *washing chambers*, and Teflon *shields*. The design of this special equipment is described elsewhere in more detail [8]. Moreover, circuit boards and bonding wires designed at the *Kirchhoff Institute for Physics (University of Heidelberg, Germany)* and manufactured at *Würrth Elektronik GmbH & Co KG (Niedernhall/Germany)* were used.



## 5.2 Materials

### 5.2.1 Chemicals and Solvents

Py (99+ %, *Acros Organics*) and DyLight 680-streptavidin (*Pierce Protein Research Products*) were obtained from *Thermo Fisher Scientific* (Geel/Belgium). KOH (p.a.) and DCM ( $\geq 99.8$  %, anhydrous) were purchased from *Applichem GmbH* (Darmstadt/Germany). DMF (peptide grade) and TFA (99.9 %) were purchased from *Biosolve BV* (Valkenswaard/Netherlands). To obtain anhydrous DMF for large scale reactions the DMF was dried over molecular sieve (4 Å) purchased from *Carl Roth GmbH* (Karlsruhe/Germany). Si(100) wafers were obtained from *Georg-Albert PVD GmbH* (Silz/Germany). Fmoc- $\beta$ -alanine (99.4 %) was purchased from *Iris Biotech GmbH* (Marktredwitz/Germany). KCl (99.5 %) and PVP ( $M_w = 40,000$  g/mol) were obtained from *Merck KGaA* (Darmstadt/Germany). DATT ( $\geq 98$  %), HBTU, MMA ( $\geq 99$  %), PMDETA ( $\geq 98$  %), TEG-MME ( $\geq 97$  %), and the RAM linker were obtained from *Merck Schuchardt OHG* (Hohenbrunn/Germany). *Durapore* filters (0.1  $\mu\text{m}$  pore size, 90 mm in diameter) and *Immobilon-P* membranes (0.45  $\mu\text{m}$  pore size) were purchased from *Millipore Corporation* (*Merck KGaA*, Darmstadt/Germany). HOBt (anhydrous) was obtained from *Molekula Ltd.* (Dorset/UK). DMSO ( $\geq 99.8$  %),  $\text{Ac}_2\text{O}$  ( $\geq 99$  %),  $\text{KH}_2\text{PO}_4$  ( $\geq 99$  %),  $\text{NaH}_2\text{PO}_4 \cdot 2\text{H}_2\text{O}$  ( $\geq 98$  %), and toluene ( $\geq 99.5$  %) were purchased from *Carl Roth GmbH* (Karlsruhe/Germany). Circular filter papers (3 hw) were obtained from *Sartorius AG* (Göttingen/Germany).

(3-Aminopropyl)triethoxy silane ( $\geq 98$  %), 2-propanol (p.a.), 3-GPS ( $\geq 98$  %), acetone (p.a.),  $\beta$ -mercaptoethanol ( $\geq 99$  %),  $\text{Cu}(\text{OAc})_2$  (98 %),  $\text{CuCl}$  ( $\geq 99$  %), DCM (p.a.), DIC (99 %), DIPEA ( $\geq 98$  %), DMF (anhydrous, 99.8 %, used for small scale reactions), EG7-SH ( $\geq 95$  %), EtOH (p.a.), HBA linker ( $\geq 95$  %), MeOH (p.a.), NaCl ( $\geq 99$  %), NBS (99 %), hexane (anhydrous, 95 %), NMI ( $> 99$  %), *N*-propylamine ( $\geq 99$  %), PEGMA ( $M_n \approx 360$  g/mol), PEG-SH ( $M_n \approx 2,000$  g/mol), piperidine (99 %), PTES ( $\geq 98$  %), PVA ( $\geq 98$  %), SMCC ( $\geq 98$  %), TFAA ( $\geq 99$  %), triethylamine ( $\geq 99.5$  %), TWEEN 20, and  $\alpha$ -bromoisobutryl bromide (98 %) were obtained from *Sigma-Aldrich GmbH* (Steinheim/Germany). All chemicals and solvents were used without further purification.

Nitrogen (5.0, P200) and argon (5.0, P200) were purchased from *Guttr-off GmbH* (Wertheim-Reicholzheim/Germany). For washing steps and buffers solely Milli-Q-filtered water (*Millipore Corporation*, *Merck KGaA*, Darmstadt/Germany, resistivity  $\sim 18.2$  M $\Omega\text{cm}$ ) was used.

### 5.2.2 Micro Chips

“Peptide Chip 5” was designed at the *Kirchhoff Institute for Physics* (University of Heidelberg, Germany) and produced at *ON Semiconductor* (Phoenix, AZ/USA).

### 5.2.3 Amino Acid Micro Particles

Amino acid micro particles were produced by Dr. Simon FERNANDEZ and Daniela RAMBOW at the German Cancer Research Center (DKFZ, Heidelberg/Germany). Compounds for the toner production were obtained from the following companies: Fmoc-protected and Opfp-activated amino acids (*Sigma-Aldrich GmbH*, Steinheim/Germany, and *Merck KGaA*, Darmstadt/Germany), polymer resin (SLEC PLT 7552, *Sekisui GmbH*, Düsseldorf/Germany), pyrazolone orange (*ABCR GmbH*, Karlsruhe/Germany), and *Aerosil* silica nano particles (*Aerosil 812*, hydrophobic, *Evonik Degussa GmbH*, Essen/Germany). For more detailed information on the composition and production of the particles reference is made to the literature [9, 10].

### 5.2.4 Pre-Synthesized Peptides

All pre-synthesized peptides were produced by Dr. Rüdiger PIPKORN and Mario KOCH in the *Genomics & Proteomics Core Facility* (German Cancer Research Center (DKFZ), Heidelberg/Germany).

### 5.2.5 Buffers and Antibodies

#### 5.2.5.1 Phosphate Buffers

Phosphate buffers were prepared with equimolar solutions of  $\text{KH}_2\text{PO}_4$  and  $\text{Na}_2\text{HPO}_4 \cdot 2\text{H}_2\text{O}$ . The two solutions were mixed in a respective ratio to obtain the desired pH. If required, additional 0.05 % (v/v) TWEEN 20 were added.

#### 5.2.5.2 PBS-T

0.15 M phosphate buffer saline (PBS) containing additional 0.05 % (v/v) TWEEN 20 (PBS-T) was freshly prepared before use. 8.00 g NaCl (137.0 mmol), 0.20 g KCl (2.7 mmol), 1.44 g  $\text{Na}_2\text{HPO}_4 \cdot 2\text{H}_2\text{O}$  (8.1 mmol), and 0.20 g  $\text{KH}_2\text{PO}_4$  (1.5 mmol) were solved in water. The solution was adjusted to pH 7.4 with HCl and then filled up to 1 L. After filtration 500  $\mu\text{L}$  TWEEN 20 were added under constant stirring.

#### 5.2.5.3 Rockland buffer

*Rockland Blocking Buffer for Fluorescent Western-Blotting* (Rockland buffer) was obtained from *Rockland Immunochemicals Inc.* (Gilbertsville, PA/USA) and used as received.

### 5.2.5.4 Antibodies

The monoclonal mouse-anti-HA 12CA5 IgG antibody (anti-HA) was obtained from Dr. Gerd MOLDENHAUER (German Cancer Research Center (DKFZ), Heidelberg/Germany). The monoclonal mouse-anti-FLAG M2 IgG antibody (anti-FLAG) was purchased from *Sigma-Aldrich GmbH* (Steinheim/Germany). Fluorescent labels were attached by Jürgen KRETSCHMER (German Cancer Research Center (DKFZ), Heidelberg/Germany) using commercial labeling kits and the respective protocols which were recommended by the manufacturers. Labeling kits for the ATTO 680 and ATTO 700 dyes were obtained from *ATTO-TEC GmbH* (Siegen/Germany). Labeling kits for the *Lightning-Link* Cy3 and Cy5 dyes and the FluoProbes 752 dye were purchased from *Innova Biosciences Ltd.* (Cambridge/UK). The IRDye 700DX labelling kit was obtained from *LI-COR Biosciences* (Lincoln, NE/USA).

## 5.3 Methods

### 5.3.1 Preparation of Synthesis Surfaces

In the present work, different solid supports with different formats were equipped with synthesis coatings. The derivatization of microchips ( $2 \times 2 \text{ cm}^2$ ) and Si(100) wafers was routinely performed in petri dishes ( $V \approx 50 \text{ mL}$ ). Microscopy slides were treated in batches of 40 slides in custom-built Teflon containers ( $V \approx 200 \text{ mL}$ , also see Sect. 3.1.3, Fig. 3.22). The  $22 \times 21 \text{ cm}^2$  glass slides used in the laser printer were coated in batches of 14 slides in custom-built glass containers ( $V \approx 2.5 \text{ L}$ , also see Sect. 3.1.3, Fig. 3.23). To keep oxygen- or moisture-sensitive reactions under inert gas atmosphere the respective containers were placed in a desiccator. The desiccator was typically brought to inert gas atmosphere before and after addition of the reaction mixture by evacuating and flooding with argon up to three times. Additional desiccant (*Silica Gel, Carl Roth GmbH, Karlsruhe/Germany*) was applied for moisture-sensitive reactions. For silanization and siA-TRP two different containers were applied to avoid coating of the container.

#### 5.3.1.1 Cleaning and Activation

Glass surfaces were cleaned and activated by overnight treatment with 1 M KOH in 2-propanol. The surfaces were intensively washed with water, rinsed with acetone, and then dried in a stream of air. After heating to  $110 \text{ }^\circ\text{C}$  for 30 min, the surfaces were allowed to cool to RT under inert gas atmosphere.

Micro chip surfaces and Si(100) wafers were activated by UV irradiation for 1 h in air. UV irradiation was generated with a 150 W mercury vapour lamp

(Heraeus Noblelight GmbH, Hanau/Germany, model TQ 150, purchased from UV-Consulting Peschl, Mainz/Germany). The surface was placed in about 4 cm distance from the lamp. Si(100) wafers were treated for 2 h, whereby the wafer was slightly disarranged each 30 min to evenly irradiate the entire surface. After cooling to RT activated surfaces were directly silanized.

### 5.3.1.2 Synthesis of the Bromine Silane

2-Bromo-*N*-(3-triethoxysilyl propyl) isobutyramide (bromine silane) was synthesized according to the following protocol: 2.77 mL TEA (20 mmol, 2.024 g) and 4.68 mL APTES (20 mmol, 4.427 g) were solved in anhydrous DCM (70 mL) in a nitrogen flask and cooled to  $-80$  °C. Subsequently, a solution of 2.47 mL  $\alpha$ -bromoisobutyryl bromide (20 mmol, 4.598 g) in anhydrous dichloromethane (30 mL) was added dropwise under constant stirring. After warming to room temperature, the solvent was removed under reduced pressure. The residue was dissolved in anhydrous hexane (50 mL) and stirred for 30 min. Precipitates were filtered from the solution under inert gas atmosphere using a fritted funnel with a sintered glass disc (fine pore size). Then the solution was concentrated under reduced pressure. The remaining brownish oil was distilled under vacuum. The product is colorless oil.  $^1\text{H-NMR}$  (300 MHz,  $\text{CDCl}_3$ ):  $\delta = 0.63$  (t,  $^3\text{J} = 7.5$  Hz, 2H), 1.19 (m, 9H), 1.65 (m, 2H), 1.91 (s, 6H), 3.23 (m, 2H), 3.75 (m, 6H), 6.85 ppm (s(br), 1H);  $^{13}\text{C-NMR}$  (75 MHz,  $\text{CDCl}_3$ ):  $\delta = 7.75, 18.28, 22.69, 32.62, 42.59, 58.46, 63.33, 171.86$  ppm.

### 5.3.1.3 Self-Assembly of the Bromine Silane

A solution of 2 mM bromine silane and 8 mM PTES in anhydrous DCM was prepared and directly added to the activated dry surfaces. The surfaces were left to react overnight under argon atmosphere. Subsequently, the DCM was stepwise replaced with ethanol. The surfaces were washed three times for 5 min each with ethanol, two times for 2 min each with acetone, dried in a stream of compressed air, and then baked in a pre-heated oven at 110 °C for 2 h. After cooling to RT the slides were either directly coated by siATRP or stored at 4 °C under argon atmosphere.

### 5.3.1.4 siATRP for 10:90-PEGMA-co-PMMA Coatings

10:90-PEGMA-co-PMMA films were grafted on the silanized surfaces according to the following protocol: 2.88 mL PEGMA (8.75 mmol, 3.17 g), 8.38 mL MMA (78.75 mmol, 7.89 g), 91  $\mu\text{L}$  PMDETA (0.44 mmol, 76 mg) and 620  $\mu\text{L}$  TEG-MME (3.96 mmol, 650 mg) were mixed in 37 mL DMSO in a nitrogen flask. The solution was degassed by evacuating the flask and floating it with argon three

times. 44 mg CuCl (0.44 mmol) were added in argon counter stream. The solution was stirred until the copper was completely dissolved. Meanwhile, the container with the surfaces was brought to inert gas atmosphere in a desiccator. The solution was then quickly added to the surfaces. The desiccator was thoroughly evacuated and flooded with argon three times. The polymerization was left to react for 20 h at RT. Subsequently, the surfaces were washed five times for 5 min each with DMSO, two times for 5 min each with MeOH, and two times for 10 min each with water. After rinsing with acetone, the surfaces were blown dry in a stream of compressed air and stored at 4 °C under argon atmosphere.

For polymerizations on microscopy slides or laser printer glass slides the reaction was up-scaled to the required volume. A piece of silanized Si(100) was added to the reaction as a reference to determine the respective film thickness via ellipsometry, if the siATRP was conducted on glass.

#### 5.3.1.5 Coupling of Fmoc- $\beta$ -Alanine

To couple Fmoc- $\beta$ -alanine to the 10:90-PEGMA-co-PMMA-OH coatings, a solution of 0.1 M Fmoc- $\beta$ -alanine in anhydrous DMF was prepared in a nitrogen flask. 1.2 eq DIC (0.12 M) was added and the solution was stirred for 5 min. Subsequently, 2 eq NMI (0.2 M) was added. The solution was directly added to the surfaces. The respective container was placed in a desiccator and brought to inert gas atmosphere. The surfaces were left to react overnight. Afterwards the surfaces were washed three times for 5 min each with DMF. To cap residual hydroxyl groups, the slides were directly incubated in a solution of 10 % (v/v) Ac<sub>2</sub>O, 20 % (v/v) DIPEA, and 70 % (v/v) DMF overnight. After washing five times for 5 min each with DMF and two times for 2 min each with MeOH the surfaces were dried in a stream of compressed air. Before further use, the Fmoc protecting groups were cleaved by incubating the surfaces in a solution of 20 % (v/v) piperidine in DMF for 20 min. The Fmoc cleavage was followed by washing three times for 5 min each with DMF and two times for 3 min each with MeOH. For the peptide synthesis, the whole procedure was repeated up to two times to sequentially couple  $\beta$ -alanine residues as a spacer to the surface. Derivatized surfaces were stored at 4 °C under argon atmosphere.

#### 5.3.1.6 AEG<sub>3</sub> SAMs

##### *Assembly from Solution*

A solution of 30 mM 3-GPS in anhydrous DCM was prepared and added to the activated dry surfaces. The surfaces were left to react overnight in a desiccator under argon atmosphere. Subsequently, the surfaces were washed three times for 2 min each with DCM. A solution of 20 % (v/v) DATT in anhydrous DMF was directly added to the surfaces without drying. The surfaces were allowed to react

overnight (or 24 h). Then, the samples were washed five times for 5 min each with DMF, two times for 3 min each with MeOH, rinsed with acetone, and dried in a stream of compressed air. AEG<sub>3</sub>-coated surfaces were stored at 4 °C under argon atmosphere.

### *Sandwich-Technique*

The 3-GPS SAM could also be self-assembled on microscopy slides by pipetting 50  $\mu$ L pure 3-GPS on an activated dry microscopy slide. The slide was covered with another microscopy slide and left to react for 2 h in a desiccator under argon atmosphere. Subsequently, the slides were separated and treated as described above.

## **5.3.2 Coupling of Cleavable Linkers**

### **5.3.2.1 Coupling of the HBA Linker**

To couple the HBA linker a solution of 0.2 M Fmoc-HBA in anhydrous DMF was prepared. The same volume of a solution of 0.2 M PyBOP and 0.2 M HOBT in anhydrous was added. The solution was mixed for 5 min. Subsequently, 0.2 M DIPEA were added. The amino-terminated surfaces were placed in an appropriate container, brought to argon atmosphere in a desiccator, and directly covered with the freshly prepared solution. A micro chip was usually covered with 500  $\mu$ L inside a washing chamber, whereas microscopy slides were placed in a petri dish and covered with 1 mL of the solution each. After overnight incubation the surfaces were directly treated with a solution of 10 % (v/v) PVA, 20 % (v/v) DIPEA, and 70 % (v/v) DMF for 30 min. The surfaces were washed three times for 5 min each with DMF, two times for 3 min each with acetone, and then dried in a stream of compressed air. The surfaces were either stored at 4 °C under argon atmosphere or deprotected for the first amino acid coupling. To cleave the Fmoc protecting group, the surfaces were rocked in a solution of 20 % (v/v) piperidine in DMF for 30 min, followed by washing three times for 5 min each with DMF, two times for 3 min each with MeOH, and drying in a stream of compressed air.

### **5.3.2.2 Coupling of the RAM Linker**

To couple the RAM linker to 10:90-PEGMA-co-PMMA-NH<sub>2</sub> films a 0.1 M solution of Fmoc-RAM in anhydrous DMF was prepared in a nitrogen flask. 1.2 eq DIC (0.12 M) was added and the solution was stirred for 5 min. Subsequently, 2 eq NMI (0.2 M) was added. The surfaces were placed in an appropriate container and brought to argon atmosphere in a desiccator. The solution was added

and the desiccator was again evacuated and flooded with argon three times. Microscopy slides were usually coated in batches of 40 slides in a Teflon container, whereas micro chips were covered with 500  $\mu\text{L}$  inside a washing chamber. After overnight incubation, the surfaces were treated with a solution of 10 % (v/v)  $\text{Ac}_2\text{O}$ , 20 % (v/v) DIPEA, and 70 % (v/v) DMF for 30 min. The surfaces were washed three times for 5 min each with DMF, two times for 3 min each with acetone, and then dried in a stream of compressed air. The surfaces were either stored at 4  $^\circ\text{C}$  under argon atmosphere or deprotected for the first amino acid coupling. To cleave the Fmoc protecting group, the surfaces were rocked in a solution of 20 % (v/v) piperidine in DMF for 30 min, followed by washing three times for 5 min each with DMF, two times for 3 min each with MeOH, and drying in a stream of compressed air.

### ***5.3.3 Coupling of SMCC and Spotting***

A solution of 10 mM SMCC in anhydrous DMF was prepared. Slides bearing the HBA linker were placed in a petri dish, brought to argon atmosphere in a desiccator, and directly covered with 1 mL of the SMCC solution each. After overnight incubation under argon atmosphere the surfaces were washed three times for 5 min each with DMF, two times for 2 min each with MeOH, and then dried in a stream of compressed air. The slides were either stored at 4  $^\circ\text{C}$  under argon atmosphere or directly incubated in phosphate buffer (pH 7.0, 7 mM) for 30 min before spotting.

After the peptide spotting, the slides were allowed to react for additional 30 min and then rocked for 30 min in a solution of 50 mM  $\beta$ -mercaptoethanol in phosphate buffer (pH 7.0, 7 mM). The slides were washed three times for 5 min each in phosphate buffer, two times for 5 min each in EtOH, and then dried in a stream of compressed air.

### ***5.3.4 Cleavage of the HBA Linker***

#### **5.3.4.1 Standard Cleavage**

To destabilize the HBA linker a solution of 10 mM NBS and 16 mM py in anhydrous DCM was prepared. The samples were placed in a petri dish and brought to argon atmosphere in a desiccator. Subsequently, the solution was added and the desiccator was gently rocked for 10 min. The surfaces were washed three times for 2 min each with anhydrous DCM and then dried in a stream of argon. The surfaces were either directly incubated in phosphate buffer (pH 8.0, 0.07 M, 0.05 % (v/v) TWEEN 20) to cleave the linker or stored at 4  $^\circ\text{C}$  under argon atmosphere.

### 5.3.4.2 Alternative Cleavage

In the cleavage of spotted peptide arrays, four literature-known cleavage agents were tested [11, 12]. Based on an estimated amount of 5 nmol HBA per array, the following reactions were conducted (also see Sect. 3.2.3):

- (a) A reference array was rocked in DCM for 2 h in air.
- (b) An array was rocked in 1 mL of a solution of 2.5 mM Cu(OAc)<sub>2</sub> in *N*-propylamine for 2 h in air.
- (c) An array was rocked in 1 mL of a solution of 10 mM NBS and 10 mM py in DCM for 45 min. Subsequently, the array was rocked in MeOH overnight.
- (d) An array was rocked in 1 mL of a solution of 15 mM NBS and 50 mM py in DCM for 10 min. Subsequently, the array was rocked in phosphate buffer (pH 8.0, 0.07 M, 0.05 % (v/v) TWEEN 20) overnight.
- (e) An array was rocked in 1 mL of a solution of 2.5 M Cu(OAc)<sub>2</sub> in *N*-propylamine for 2 h in air.

All samples were additionally washed two times for 2 min each with the respective solvent, two times for 2 min each with MeOH, and then dried in a stream of compressed air. Sample D was washed with water instead of MeOH to remove residual buffer salts.

### 5.3.5 Micro Particle-Based Peptide Synthesis

Micro particles containing the Opfp-activated and Fmoc-protected amino acids were selectively addressed onto the linker-modified surfaces either using the laser printer [9] or the micro chip technique [8, 10, 13]. The arrays on microscopy slides (see Sect. 3.4.1, Fig. 3.46) were printed by Dr. Thomas FELGENHAUER (*PEPper-PRINT GmbH*, Heidelberg/Germany) according to established protocols [9] using the prototype of the laser printer. The peptide synthesis on the 22 × 21 cm<sup>2</sup> glass slides was commissioned to the company *PEPperPRINT GmbH* (Heidelberg/Germany) [14]. In the micro chip approach, the particle deposition on “Peptide Chip 5” was conducted by Felix LÖFFLER according to the published protocol [13]. After each particle deposition step, the deposition pattern was checked. Then, the solid supports were transferred into a pre-heated oven and allowed to react at 90 °C for 90 min under nitrogen atmosphere. After cooling to room temperature, unreacted amino groups were directly capped with 10 % (v/v) Ac<sub>2</sub>O, 20 % (v/v) DIPEA, and 70 % (v/v) DMF: Microscopy glass slides were rocked in an excess of this mixture for 30 min, whereas micro chips were first treated for 5 min, then for additional 20 min with newly added solution. Subsequently, the surfaces were washed two times for 5 min each with DMF and 5 min with acetone. The surfaces were either stored at 4 °C under argon atmosphere or directly deprotected for the next coupling cycle. To cleave the Fmoc protecting group, the microscopy slides



were rocked in a solution of 20 % (v/v) piperidine in DMF for 20 min. Micro chips were equally treated with for 30 min. Subsequently, the surfaces were washed three times for 5 min each with DMF, two times for 3 min each with MeOH, and then blown dry in a stream of compressed air. The next particle deposition was performed or a pre-synthesized peptide was coupled from solution as described in the next protocol.

### ***5.3.6 Coupling of Peptides from Solution***

To couple the pre-synthesized HA epitope (Fmoc-NH-GGGYPYDVPDYAGGG-OH) to arrays of glycine and alanine spots, respectively, a solution of 1 mM peptide in anhydrous DMF was prepared. The same volume of a solution of 10 mM HOBt and 10 mM HBTU was added. The solution was mixed for 5 min. Subsequently, 10 mM DIPEA were added. The surface was placed in an appropriate container, brought to argon atmosphere in a desiccator, and directly covered with the freshly prepared solution. A micro chip was usually covered with 500  $\mu$ L inside a washing chamber, whereas microscopy slides were placed in a petri dish and covered with 1 mL of the solution each. After overnight incubation the surfaces were directly treated with a solution of 10 % (v/v)  $\text{Ac}_2\text{O}$ , 20 % (v/v) DIPEA, and 70 % (v/v) DMF for 30 min. The surfaces were washed three times for 5 min each with DMF, two times for 3 min each with acetone, and then dried in a stream of compressed air. To cleave the Fmoc protecting group, the surfaces were rocked in a solution of 20 % (v/v) piperidine in DMF for 30 min, followed by washing three times for 5 min each with DMF, two times for 3 min each with MeOH, and drying. Subsequently, the cysteine pattern was applied as described in the previous protocol.

### ***5.3.7 Peptide Array Transfer and Purification***

A piece of gold-coated PVDF was placed on top of a circular filter paper inside a petri dish (also see Sect. 3.4.2, Fig. 3.47). Filter paper and membrane were soaked with 1000  $\mu$ L (500  $\mu$ L) 50 % (v/v) TFA in toluene. The array was immediately placed on the membrane face down, weighted, and left for the desired transfer time (10–45 min). After the transfer membrane and array were carefully separated. The membrane was directly incubated in a solution 50 % (v/v) TFA and steadily rocked to completely cleave the side-chain protecting groups. Subsequently, the samples were washed five times for 5 min each with toluene, two times for 2 min each with DCM, one time for 2 min in EtOH, and then dried or immediately incubated in the respective blocking solution.

### 5.3.8 *Blocking with EG<sub>7</sub>-SH and PEG-SH*

After the transfer and subsequent washing steps, the gold-coated membranes were immersed in a 2 mM solution of EG<sub>7</sub>-SH (or PEG-SH) in EtOH. The membranes were incubated for 24 h, washed five times for 2 min each with EtOH, and then 2 times for 2 min each with water. Subsequently, the membranes were either directly immunostained or additionally blocked.

### 5.3.9 *Blocking Before Immunostaining*

To block the samples before the immunostaining either *Rockland* buffer or a solution of 1 % (m/v) PVP in PBS-T was used. The membranes were rocked in this solution for 60 min, washed in PBS-T for 5 min, and then directly immersed in the staining solution.

### 5.3.10 *Immunostaining*

A 1:1000 dilution of the respective antibody (IRDye 700DX-anti-HA, ATTO 680-anti-HA, ATTO 700-anti-HA, Cy5-anti-HA, FluoProbes 752-anti-FLAG, or Cy3-anti-FLAG antibody) in 5 mL PBS-T with additional 0.1 % (v/v) *Rockland* buffer was freshly prepared before the immunostaining. The surfaces were rocked in this solution for 60 min (or overnight), washed five times for 5 min each with PBS-T, and then two times for 2 min each with water to remove buffer salts. Before the scan the surfaces were carefully dried in a stream of compressed air.

### 5.3.11 *Staining with the Biotin/Streptavidin System*

Before the staining with the biotin/streptavidin system the surfaces were blocked with *Rockland* buffer for 60 min. A 1:10,000 dilution of DyLight 680-streptavidin in PBS-T was freshly prepared. The surfaces were rocked in this solution for 60 min, washed five times for 5 min each with PBS-T, and then two times for 2 min each with water to remove buffer salts. Before the scan the surfaces were carefully dried in a stream of compressed air.

## References

1. A.L. Cauchy, *Bull. Sci. Mathé.* **14**, 6–10 (1830)
2. K. Vedam, *Thin Solid Films* **313–314**, 1–9 (1998)
3. H. Fujiwara, *Spectroscopic Ellipsometry: Principles and Applications* (Wiley, West Sussex, 2007)
4. D.T. Clark, W.J. Feast, D. Kilcast, W.K.R. Musgrave, *J. Polym. Sci. Part A-1 Polym. Chem.* **11**, 389–411 (1973)
5. N.H. Turner, A.M. Single, *Surf. Interface Anal.* **15**, 215–222 (1990)
6. D.A. Shirley, *Phys. Rev. B* **5**, 4709–4714 (1972)
7. J.H. Scofield, *J. Electron Spectrosc. Relat. Phenom.* **8**, 129–137 (1976)
8. C. Schirwitz, I. Block, K. König, A. Nesterov, S. Fernandez, T. Felgenhauer, K. Leibe, G. Torralba, M. Hausmann, V. Lindenstruth, V. Stadler, F. Breitling, F. R. Bischoff, *Curr. Protoc. Protein Sci.* 18.12.11–18.12.13 (2009). doi:[10.1002/0471140864.ps1802s57](https://doi.org/10.1002/0471140864.ps1802s57)
9. V. Stadler, T. Felgenhauer, M. Beyer, S. Fernandez, K. Leibe, S. Güttler, M. Gröning, K. König, G. Torralba, M. Hausmann, V. Lindenstruth, A. Nesterov, I. Block, R. Pipkorn, A. Poustka, F.R. Bischoff, F. Breitling, *Angew. Chem. Int. Ed.* **47**, 7132–7135 (2008)
10. M. Beyer, A. Nesterov, I. Block, K. König, T. Felgenhauer, S. Fernandez, K. Leibe, G. Torralba, M. Hausmann, U. Trunk, V. Lindenstruth, F.R. Bischoff, V. Stadler, F. Breitling, *Science* **318**, 1888 (2007)
11. F. Stieber, U. Grether, H. Waldmann, *Angew. Chem. Int. Ed.* **38**, 1073–1077 (1999)
12. J.A. Camarero, B.J. Hackel, J.J. De Yoreo, A.R. Mitchell, *J. Org. Chem.* **69**, 4145–4151 (2004)
13. F. Löffler, J. Wagner, K. König, F. Märkle, S. Fernandez, C. Schirwitz, G. Torralba, M. Hausmann, V. Lindenstruth, F.R. Bischoff, F. Breitling, A. Nesterov, *Aerosol. Sci. Tech.* **45**, 65–74 (2011)
14. [www.pepperprint.com](http://www.pepperprint.com) Accessed 28 Jan 2012

# Appendix

## Abbreviations

% (m/m)	Mass fraction
% (m/v)	Mass per volume fraction
% (n/n)	Mole fraction
% (v/v)	Volume fraction
Ac	Acetyl moiety
Ac <sub>2</sub> O	Acetic anhydride
AEG <sub>3</sub> SAM	Amino-terminated SAM with an intramolecular EG <sub>3</sub> spacer
AES	AUGER electron spectroscopy
ATRP	Atom transfer radical polymerization
AU	Average unit
AUC	Area under the curve (in XPS)
BSE	Back scattered electron
Boc	<i>tert</i> butoxycarbonyl moiety
Bn	Benzyl moiety
Bromine silane	2-bromo- <i>N</i> -(3-triethoxysilyl propyl) isobutyramide
CMOS	Complementary metal oxide semiconductor
DATT	1,13-diamino-4,7,10-trioxatridecane
DCC	<i>N,N'</i> -dicyclohexylcarbodiimide
DCM	Dichloromethane
DG	Derivatization grade
DIC	<i>N,N'</i> -diisopropylcarbodiimide
DIPEA	<i>N,N</i> -diisopropylethylamine
DMF	<i>N,N</i> -dimethylformamide
DMSO	Dimethyl sulfoxide
DNA	Deoxyribonucleic acid
EDTA	Ethylenediaminetetraacetic acid
e.g.	[Latin] <i>exempli gratia</i> , for example
EG <sub>7</sub> -SH	<i>O</i> -(2-mercaptoethyl)- <i>O'</i> -methylhexaethyleneglycol
eq	Equivalent(s)
Et	Ethyl moiety
EtOH	Ethanol
EWG	Electron withdrawing group

ESCA	Electron spectroscopy for chemical analysis
Fmoc	9-fluorenylmethoxycarbonyl (protecting group)
3-GPS	3-(glycidyl)oxypropyl trimethosysilane
HATU	2-(7-Aza-1H-benzotriazole-1-yl)-1,1,3,3-tetramethyluronium hexafluorophosphate
HBA	4-hydrazinobenzoic acid
HBTU	2-(1H-benzotriazole-1-yl)-1,1,3,3-tetramethyluronium hexafluorophosphate
HOAt	1-hydroxy-7-aza-benzotriazol
HOBt	1-hydroxybenzotriazol
HPLC	High pressure liquid chromatography
h	Hour(s)
i.e.	[Latin] <i>id est</i> , which means/meaning
$\lambda_{em}$	Emission wavelength
$\lambda_{ex}$	Excitation wavelength
LED	Light emitting diode
Me	Methyl moiety
MeCN	Acetonitrile
MEHQ	Monomethyl ether hydroquinone, 4-methoxyphenol
MeOH	Methanol
MEK	Methylethylketone
min	Minute(s)
MMA	methylmethacrylate
$M_n$	Number average molar mass
$M_w$	Weight average molar mass
mpSPPS	Micro particle-based solid phase peptide synthesis
NMI	<i>N</i> -methylimidazole
OPC	Organic photoconductor (drum)
Opfp	Orthopentafluorophenyl moiety
p.a.	Per analysis (quality grade for chemicals and solvents)
Pbf	2,2,4,6,7-pentamethyl-2,3-dihydrobenzofuran-5-sulfonyl (protecting group)
PBS-T	Phosphate buffer saline with additional TWEEN 20
PCR	Primary charge roller
PDFA	Piperidinedibenzofulvene adduct
PEG	Poly(ethylene glycol)
PEGMA	Poly(ethylene glycol) methacrylate
10:90-PEGMA-co-PMMA	Graft copolymer film consisting of 10 % (n/n) PEGMA and 90 % (n/n) PMMA
PEG-NH <sub>2</sub>	Poly(ethylene glycol), amino terminated
PEG-OH	Poly(ethylene glycol), hydroxy terminated
PEG-SH	Poly(ethylene glycol) methylether thiol
PG	Protecting group

Ph	Phenyl
piranha solution	Mixture of 30 % (v/v) H <sub>2</sub> O <sub>2</sub> (30 % aqueous solution) and 70 % (v/v) H <sub>2</sub> SO <sub>4</sub>
PMDETA	1,1,4,7,7-pentamethyldiethylenetriamine
ppm	Parts per million
PS	Polystyrene
PTES	<i>N</i> -propyl triethoxysilane
PTFE	Polytetrafluoroethylene
PVA	Pivalic anhydride
PVDF	Polyvinylidene fluoride
PVP	Polyvinylpyrrolidone
PyBOP	Benzotriazole-1-yl-oxy-tripyrrolidinophosphonium hexafluorophosphate
RAM	RINK amide (linker), <i>p</i> -[( <i>R,S</i> )- $\alpha$ -[1-(9H-Fluoren-9-yl)-methoxyformamido]-2,4-dimethoxybenzyl]- phenoxy-acetic acid
RT	Room temperature (here 23 °C)
s	Second(s)
SAM	Self-assembled monolayer
SE	Secondary electron
SEM	Scanning electron microscopy (microscope)
siATRP	Surface-initiated atom transfer radical polymerization
SIMS	Secondary ion mass spectrometry
SMCC	Succinimidyl-trans-4-( <i>N</i> -maleimidylmethyl)cyclohexane-1-carboxylate
SPPS	Solid phase peptide synthesis
TEGMME	tri(ethylene glycol) monomethyl ether
<i>t</i> Bu	<i>tert</i> butyl moiety
TAMRA	5(6)-carboxytetramethyl rhodamine
TFA	Trifluoroacetic acid
TFAA	Trifluoroacetic acid anhydride
TFAc	Trifluoroacetyl
TFFH	1,1,3,3-tetramethylfluoro formamidinium hexafluorophosphate
THF	Tetrahydrofuran
TIBS	Triisobutyl silane
T <sub>m</sub>	Melting point
Trt	Trityl moiety
TWEEN 20	Polyoxyethylensorbitan monolaurate (surfactant)
UPS	Ultra-violet photoelectron spectroscopy
UV	Ultra-violet
VASE	Variable angle spectroscopic ellipsometry
XPS	X-ray photoelectron spectroscopy

# Amino Acid Codes

---

Ala	A	Alanine	Leu	L	Leucine
Arg	R	Arginine	Lys	K	Lysine
Asn	N	Asparagine	Met	M	Methionine
Asp	D	Aspartic acid	Phe	F	Phenylalanine
Cys	C	Cysteine	Pro	P	Proline
Gln	Q	Glutamine	Ser	S	Serine
Glu	E	Glutamic acid	Thr	T	Threonine
Gly	G	Glycine	Trp	W	Tryptophan
His	H	Histidine	Tyr	Y	Tyrosine
Ile	I	Isoleucine	Val	V	Valine

---

## Funding

This work was supported by:

The *Helmholtz International Graduate School for Cancer Research (International Ph.D. Program)* at the German Cancer Research Center (DKFZ);

The *Max-Buchner Research Foundation* (project number 2834);

The EU FP7 project PEPLASER

(Land Baden-Württemberg, project number 720.830-5-177);

and by contract research “*Methoden für die Lebenswissenschaften*” of the *Baden-Württemberg Stiftung*.



# Curriculum Vitae

Dr. *rer. nat.* Christopher Schirwitz

\* September 3, 1982, in Göttingen, Germany

---

## Postdoctoral Studies

- Since 04/2013 Postdoc with PD Dr. F. Breitling at the Karlsruhe Institute of Technology (KIT), Institute of Microstructure Technology (IMT), Eggenstein-Leopoldshafen, Germany
- 04/2012–03/2013 Postdoc with Dr. J. D. Hoheisel at the DKFZ, Department of Functional Genome Analysis, Heidelberg, Germany

## Doctoral Studies

- 05/2008–03/2012 Ph.D. studies in Physical Chemistry with Prof. (apl.) Dr. R. Dahint, University of Heidelberg, Department of Applied Physical Chemistry, Germany

## Studies

- 04/2003–03/2008 Studies in Chemistry, University of Marburg, Germany

- 08/2002–05/2003 **Civil Service** in Münster, Germany

- 1993–2002 **Schooling** in Münster, Germany

## Stipends and Awards

- 12/2012 *Viktor Meyer Award* for excellent Ph.D. work, *Curtius Foundation*, University of Heidelberg, Germany
- 10/2010 Travel grant of the Graduate Academy, University of Heidelberg
- 07/2009–06/2011 Research fellowship of the *Max-Buchner Foundation*, project number: 2834
- 08/2008–07/2011 Ph.D. stipend of the *Helmholtz International Graduate School for Cancer Research*

## Complete List of Publications

- [1] C. Schirwitz, F. F. Löffler, T. Felgenhauer, V. Stadler, A. Nesterov-Müller, R. Dahint, F. Breitling and F. R. Bischoff, Purification of High-complexity Peptide Microarrays by Spatially Resolved Array Transfer to Gold-coated Membranes, *Advanced Materials* **2013**, 25, 1598–1602
- [2] J. Wagner, F. Löffler, T. Förtsch, C. Schirwitz, S. Fernandez, H. Hinkers, H. F. Arlinghaus, F. Painke, K. König, F. R. Bischoff, A. Nesterov-Müller, F. Breitling, M. Hausmann and V. Lindenstruth, Image Processing Quality Analysis for Particle Based Peptide Array Production on a Microchip, *In-Tech* **2012**

---

(continued)

(continued)

- 
- [3] C. Schirwitz, F. F. Löffler, T. Felgenhauer, V. Stadler, F. Breitling and F. R. Bischoff, Sensing immune responses with customized peptide microarrays, *Biointerphases* 2012, 7, 47
- [4] F. Löffler, C. Schirwitz, J. Wagner, K. König, F. Märkle, G. Torralba, M. Hausmann, F. R. Bischoff, A. Nesterov-Müller and F. Breitling, Biomolecule Arrays Using Functional Combinatorial Particle Patterning on Microchips, *Advanced Functional Materials* **2012**, 22, 2503–2508
- [5] R. Schmidt, J. Jacak, C. Schirwitz, V. Stadler, G. Michel, N. Marmé, G. J. Schütz, J. D. Hoheisel and J. P. Knemeyer, Single-molecule detection on a protein-array assay platform for the exposure of a tuberculosis antigen, *Journal of Proteome Research* **2011**, 10, 1316–1322
- [6] F. Löffler, J. Wagner, K. König, F. Märkle, S. Fernandez, C. Schirwitz, G. Torralba, M. Hausmann, V. Lindenstruth, F. R. Bischoff, F. Breitling and A. Nesterov, High-precision combinatorial deposition of micro particle patterns on a microelectronic chip, *Aerosol Science and Technology* **2011**, 45, 65–74
- [7] F. Breitling, F. Löffler, C. Schirwitz, Y. C. Cheng, F. Märkle, K. König, T. Felgenhauer, E. Dörsam, F. R. Bischoff and A. Nesterov, Alternative setups for automated peptide synthesis, *Mini-Reviews in Organic Chemistry* **2011**, 8, 121–131
- [8] A. Nesterov, E. Dörsam, Y. C. Cheng, C. Schirwitz, F. Märkle, F. Löffler, K. König, V. Stadler, R. Bischoff and F. Breitling, Small Molecule Microarrays: Peptide arrays with a chip, *Methods in molecular biology*, Humana Press (New York, NY, USA), **2010**, 669, 109–124
- [9] K. König, I. Block, A. Nesterov, G. Torralba, S. Fernandez, T. Felgenhauer, K. Leibe, C. Schirwitz, F. Löffler, F. Painke, J. Wagner, U. Trunk, F. R. Bischoff, F. Breitling, V. Stadler, M. Hausmann and V. Lindenstruth, Programmable high voltage CMOS chips for particle-based high-density combinatorial peptide synthesis, *Sensors and Actuators, B: Chemical* **2010**, 147, 418–427
- [10] T. Felgenhauer, C. Schirwitz and F. Breitling, Peptide Synthesis, *Ullmann's Encyclopedia of Industrial Chemistry*, Wiley-VCH (Weinheim, Germany), **2010**
- [11] F. Breitling, C. Schirwitz, T. Felgenhauer, I. Block, V. Stadler and R. Bischoff, Epitope Mapping by Printed Peptide Libraries, *Antibody Engineering*, Springer (Berlin/Heidelberg, Germany), **2010**, Part V, 573–589
- [12] C. Schirwitz, I. Block, K. König, A. Nesterov, S. Fernandez, T. Felgenhauer, K. Leibe, G. Torralba, M. Hausmann, V. Lindenstruth, V. Stadler, F. Breitling and F. R. Bischoff, Combinatorial peptide synthesis on a microchip, *Current Protocols in Protein Science* **2009**, 18.12.11–18.12.13
- [13] M. Beyer, I. Block, K. König, A. Nesterov, S. Fernandez, T. Felgenhauer, C. Schirwitz, K. Leibe, R. F. Bischoff, F. Breitling and V. Stadler, Peptide Microarrays: A novel combinatorial approach to high-density peptide arrays, *Methods in Molecular Biology*, Humana Press (New York, NY, USA), **2009**, 570, 309–316
-